THE DELAMINATION THEORY OF WEAR

MASSACHUSETTS INSTITUTE OF TECHNOLOGY

PREPARED FOR
OFFICE OF NAVAL RESEARCH
ADVANCED RESEARCH PROJECTS AGENCY

SEPTEMBER 1974

Unclassified

SECURITY CLASSIFICATION OF THIS PAGE (When Data Entered)

REPORT DOCUMENTATION PAGE		READ INSTRUCTIONS BEFORE COMPLETING FORM
1. REPORT NUMBER	2. GOVT ACCESSION NO.	3. RECIPIENT'S CATALOG NUMBER AD/A-003583
4. TITLE (and Subtitle) The Delamination Theory of Wear Progress Report		5. TYPE OF REPORT & PERIOD COVERED Annual May 1973 - June 1974
		6. PERFORMING ORG. REPORT NUMBER
7. AUTHOR(s) Nam P. Suh, Said Jahanmir, Ernest P. Abrahamson		8. CONTRACT OR GRANT NUMBER(s) N00014-67-A-0204-0080 NR 229-011
9. PERFORMING ORGANIZATION NAME AND ADDRESS Materials Processing Laboratory Department of Mechanical Engineering		10. PROGRAM ELEMENT, PROJECT, TASK AREA & WORK UNIT NUMBERS 000000#4D10
11. CONTROLLING OFFICE NAME AND ADDRESS Department of the Navy Office of Naval Research Arlington, Virginia 22217 N00014		12. REPORT DATE September 1974
		13. NUMBER OF PAGES 155
14. MONITORING AGENCY NAME & ADDRESS(if different from Controlling Office) Office of Naval Research, MIT, Resid. Repres. E19-62B 77 Massachusetts Avenue Cambridge, Massachusetts 02139 (N66017)		15. SECURITY CLASS. (of this report) Unclassified
		15a. DECLASSIFICATION/DOWNGRADING SCHEDULE

16. DISTRIBUTION STATEMENT (of this Report)

The distribution of this document is unlimited.

17. DISTRIBUTION STATEMENT (of the abstract entered in Block 20, if different from Report)

PRICES SUBJECT TO CHANGE

18. SUPPLEMENTARY NOTES

19. KEY WORDS (Continue on reverse side if necessary and identify by block number)

sliding, wear particles, strain gradient, deformation, void formation/ crack propagation, delamination, iron, steel, copper, soft coatings.

20. ABSTRACT (Continue on reverse side if necessary and identify by block number)

The delamination theory of wear and the supporting experimental evidence are presented. The theory provides an alternative explanation for the wear of metals sliding at low speeds to that hitherto provided by "adhesion" theories. The theory is valid when there is no significant temperature rise at the surface to induce any phase transformation and thermally activated diffusion of elements. It is shown that at low

DD FORM 1 JAN 73 1473 EDITION OF 1 NOV 65 IS OBSOLETE S/N 0102-014-6601

(continuation of Block 20)

sliding speed the wear of metals occurs by subsurface deformation which induces void and crack nucleation and subsequent crack propagation parallel to the surface. The cracks eventually propagate to the surface producing thin wear sheets. This phenomenon has been observed on a variety of metals from soft cadmium to fully hardened AISI 4340 steel.

Preliminary results indicate that the weight loss is not linearly proportional to the sliding distance. Initially wear particles are generated at a rapid rate by the fatigue fracture of the deformed original asperties. This high wear rate regime is then followed by a regime of a low weight loss while the subsurface crack nucleation and propagation takes place. When the crack reaches a critical length and propagates to the surface, delamination begins and the wear becomes catastrophic.

The delamination theory of wear predicts that the best method of preventing wear is to use a material without large second phase particles or inclusions. For example, annealed zone refined iron has 1/3 the wear rate of AISI 1020 steel, although its hardness is only a third of that of the latter. Another prediction of the theory is that a thin layer of a soft metal on a hard substrate should reduce the wear rate because the dislocations are not stable in the thin layer. It is shown that a 0.1 μm cadmium coating on both contacting surfaces of AISI 1018 steel reduces wear by three orders of magnitude over the unplated steel. This coating is effective in an inert atmosphere, inert oil, but not effective in an oxidizing atmosphere. When the cadmium coating is thicker than 0.1 μm, the wear rate is high because the dislocations are stable in the thicker layer and delamination occurs within the cadmium coating.

THE DELAMINATION THEORY OF WEAR

Progress Report
to
The Advanced Research Project Agency, DOD
Contract No. N00014-67-A-0204-0080
NR 229-011

Nam P. Suh

Said Jahanmir

Ernest P. Abrahamson, II

Materials Processing Laboratory
Department of Mechanical Engineering
Massachusetts Institute of Technology
Cambridge, MA 02139

September 1974

Approved for public release; distribution unlimited.

ABSTRACT

The delamination theory of wear and the supporting experimental evidence are presented. The theory provides an alternative explanation for the wear of metals sliding at low speeds to that hitherto provided by "adhesion" theories. The theory is valid when there is no significant temperature rise at the surface to induce any phase transformation and thermally activated diffusion of elements. It is shown that at low sliding speed the wear of metals occurs by subsurface deformation which induces void and crack nucleation and subsequent crack propagation parallel to the surface. The cracks eventually propagate to the surface producing thin wear sheets. This phenomenon has been observed on a variety of metals from soft cadmium to fully hardened AISI 4340 steel.

Preliminary results indicate that the weight loss is not linearly proportional to the sliding distance. Initially wear particles are generated at a rapid rate by the fatigue fracture of the deformed original asperties. This high wear rate regime is then followed by a regime of a low weight loss while the subsurface crack nucleation and propagation takes place. When the crack reaches a critical length and propagates to the surface, delamination begins and the wear becomes catastrophic.

The delamination theory of wear predicts that the best method of preventing wear is to use a material without large second phase particles or inclusions. For example, annealed zone refined iron has 1/3 the wear rate of AISI 1020 steel, although its hardness is only a third of that of the latter. Another prediction of the theory is that a thin layer of a soft metal on a hard

substrate should reduce the wear rate because the dislocations are not stable in the thin layer. It is shown that a 0.1 μm cadmium coating on both contacting surfaces of AISI 1018 steel reduces wear by three orders of magnitude over the unplated steel. This coating is effective in an inert atmosphere, inert oil, but not effective in an oxidizing atmosphere. When the cadmium coating is thicker than 0.1 μm, the wear rate is high because the dislocations are stable in the thicker layer and delamination occurs within the cadmium coating.

ACKNOWLEDGMENT

This research was supported by The Advanced Research Projects Agency of the Department of Defense and was monitored by ONR under Contract No. N00014-67-A-0204-0080. The authors wish to express their appreciation to Dr. Edward Van Reuth and Lt. Richard Miller.

The authors are grateful to Prof. F. A. McClintock of M.I.T. and Dr. V. C. Westcott of Trans-Sonics, Inc. for their valuable discussion and critisisms of this work.

Table of Contents

Table of Contents (Cont.)

List of Figures

List of Figures

List of Tables

Chapter 1

INTRODUCTION

According to the COSMAT report of the national Acacemy of Science, one of the most important areas for future research in materials is the wear of metals [1]*. This finding is not surprising since many machine components become unusable due to sliding wear. Yet there is no theoretical basis on which to design the surface metallurgically. The sliding wear of metals has been investigated extensively in the past three decades and various wear mechanisms have been considered: adhesive, abrasive, diffusive, corrosive, fatigue, and fretting wear. The existance of abrasive, diffusive and corrosive wear mechanisms has been established reasonably firmly. However, the mechanisms of adhesive, fatigue and fretting wear are not clearly understood. The findings are inconsistent in many cases and the theories which have been advanced are not based on the known physics and physical metallurgy of the materials. In 1973, considering these variables, Suh introduced the delamination theory of wear for metals sliding at low speeds [2].

This report contains the delamination theory of wear and the experimental evidence for this theory which has been investigated at MIT over the past year. Based on the theory, a number of predictions have been made on wear phenomena such as the existance of subsurface cracks, the shape of the wear particles, the effect of metallurgical variables and the design of wear resistant surfaces. All these predictions have been supported by experimental results [3-8]**, and are included in this report. The remaining task is

*The numbers in the brackets designate the references of page.

**A list of these papers is included in Appendix E.

the quantitative prediction of the wear rate based on basic material properties.

Chapter 2

ADHESION THEORIES OF WEAR AND CHARACTERISTICS OF WEARING SURFACES

A) A Critical Review of Adhesion Theories of Wear

Prior to the introduction of the delamination theory of wear by Suh [2], the friction and wear behavior of metals under low speed sliding conditions had been explained in terms of the adhesion theory of wear. Although there are many different mathematical models of this theory, the basic tenet of the theories is the same. According to the adhesion theory, the friction and wear behavior of metals is controlled by the adhesion of contacting asperities. The purpose of this review is to discuss the main features of several adhesion models and compare them with experimental results.

The simplest and oldest adhesion model for wear was that advanced by Archard [9]. This theory postulates that when asperities come into contact and adhere strongly to each other, the subsequent separation occurs in the bulk of the weaker asperity in a single action. This process is assumed to create a particle from the softer surface which adheres to the harder surface. When these transferred particles become free, loose wear particles are formed and wear, observed as weight loss, is assumed to occur. According to Archard's model, if all the junctions have the same diameter and if the real area of contact is given by the normal load L divided by hardness H, the total volume of the material removed during sliding through a distance S, is given by

$$V=K\frac{LS}{3H} \quad , \tag{1}$$

where K is a wear constant which gives the probability that a wear particle will be formed from an asperity junction. Archard's theory assumes that the wear particles are hemispherical and their size is of the order of asperity contact, and that the deformation is confined to a region near the asperity contact. It also implies that hardness is the most important criterion, because it controls the real area of contact, and that softer metals wear faster than harder ones. It will be shown later that the experimentally determined wear process is not necessarily consistent with these assumptions and implications.

The adhesional theory of friction [10] makes the same basic assumption as the adhesion theory of wear, i.e., the two contacting asperities adhere to each other. If the average shear strength of a junction is τ, the tangential frictional force F is given by

$$F=\tau A_r=\frac{\tau L}{H} \quad , \tag{2}$$

where A_r is the real area of contact. The coefficient of friction, μ, is approximately 1/6, if it is assumed that H is about six times τ, the shear strength of the softer metal. This value is much lower than those measured in air and an order of magnitude smaller than those measured in vacuum.

Green [11] refined the adhesional theory of friction by assuming the asperities to be rigid-perfectly plastic and using slip line fields which satisfy the displacement field and equilibrium. This model yields coefficients of friction which agree with experimentally observed values better

th' the Archard model. Green showed that junctions grow during sliding as a result of the applied shear force, but the normal load carried by the junctions does not increase correspondingly, in fact usually becoming tensile during separation. This theory also predicts, as Archard's model implied, that the plastic deformation is confined to the region near the asperities.

Gupta and Cook [12,13] extended Green's model by considering the possibility that some of the junctions are weak and some strong. The strong junctions are assumed to adhere and shear in a manner similar to those predicted by Green, while the weak junctions are assumed to slide over each other inducing plastic deformation in the asperity of the softer metal. This model predicts that when the normal load is increased, the number of asperity junctions increases by the 0.91 power of normal load while the area of each individual junction grows only by the 0.09 power. Although this model explains how the real area of contact can be larger than L/H and relates μ to the nature of the asperity junctions, it is still based on the assumption that the deformation occurs at the asperities.

Rabinowicz [14] advanced an adhesion theory of friction which includes the role of the surface energy on adhesion. He showed that the real area of contact is larger than L/H due to the change in the surface energy when two asperities adhere to each other. Rabinowicz's theory predicts that when the ratio of the surface energy to hardness is large, the coefficient of friction increases because the real area of contact increases. Again,

in this model the attention is at the asperity junction.

In all of the above mentioned models, the basic assumptions are:

(1) the mechanical flow strength of the asperities are the same as the bulk,

(2) the deformation is confined to a region close to the asperity contact,

(3) the asperities will maintain their general shape rather than being smeared and worn.

These theories imply that the size of the wear particles is likely to be of the order of asperity contacts. They neglect the microstructural effects, the possible variations in the properties of metals near the surface, and elasto-plastic nature of metals. Although deformation may be confined to the asperities if the normal distance between two sliding surfaces is fixed rather than the normal load, this situation rarely exists in real sliding conditions. Normally, the separation between two surfaces is governed by the normal load. Consequently, the zone deformed plastically by the applied load will follow the stress field existing in an elasto-plastic solid, as is qualitatively illustrated in Fig. 2.1 [15]. This extends much deeper into the surface, rather than being confined to the asperities.

B) Characteristics of Worn Surfaces and Subsurfaces

A number of experimental results, which have been obtained since the introduction of the delamination theory of wear, contradict the basic assumptions and implications of the adhesion theories. These experimental

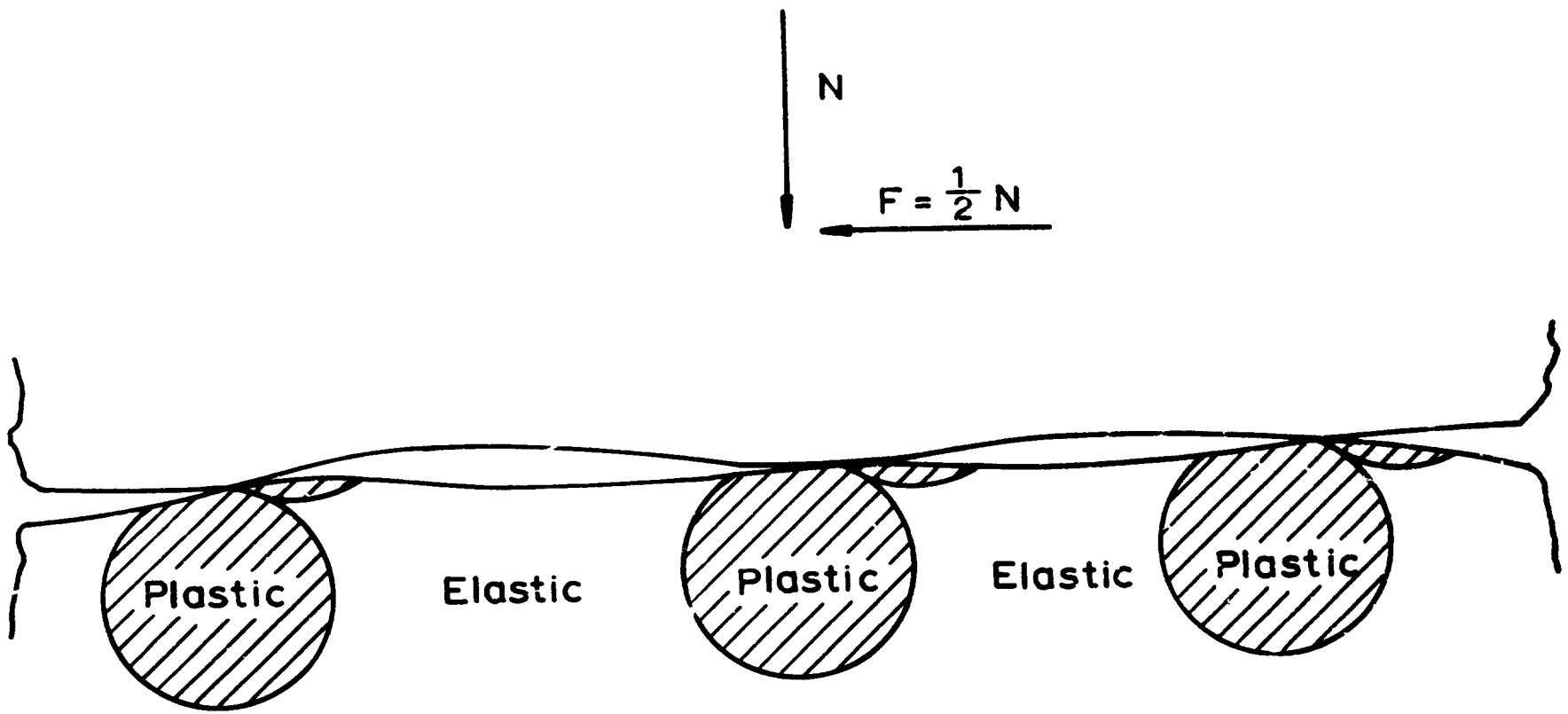

Figure 2.1 Elastic-plastic stress distribution due to normal and tangential forces near a surface in sliding contact.

results will be reviewed here briefly.

All worn surfaces show large plastic deformation and strain gradients when the speciman is sectioned perpendicular to the worn surface and etched, as shown in Fig. 2.2. It was shown [3] that the depth of the plastically deformed zone increases gradually during the early stages of the wear process, and eventually reaches a steady state value. The deformation shown in the micrograph can be measured quantitatively to determine the equivalent plastic strain as a function of the distance from the surface using the technique developed by Dautzenberg and Zaat [16]. Agustsson [17] determined the equivalent plastic strain in annealed AISI 1020 steel and annealed copper. The results are shown in Figs. 2.3 and 2.4, which show that the equivalent plastic strains at the worn surfaces of steel and copper exceed 16 and >100 (by extrapolation), respectively. The plastic strain extends to a depth of 40 μm in steel and 100 μm in copper. These plastic strains are <u>much</u> larger than fracture strains found in normal bulk deformation of metals. It is clear that the metal at the surface behaves differently from the bulk.

There is little evidence that the original asperities remain as asperities after a slider moves over the surface. SEM micrographs show that the wear track becomes <u>very</u> smooth after a slider has made several passes, in Fig. 2.5, it appears that the asperities are completely smeared over the surface and the wear track is plowed by the hard asperities on the mating surface. The micrograph shows a typical portion of the wear track in the early stages of sliding and there is no obvious indication of adhesion or transfer of particles from the other contacting surface.

Figure 2.2 Subsurface deformation in AISI 1020 steel under a load of 2.25 kg after 54m sliding in argon.

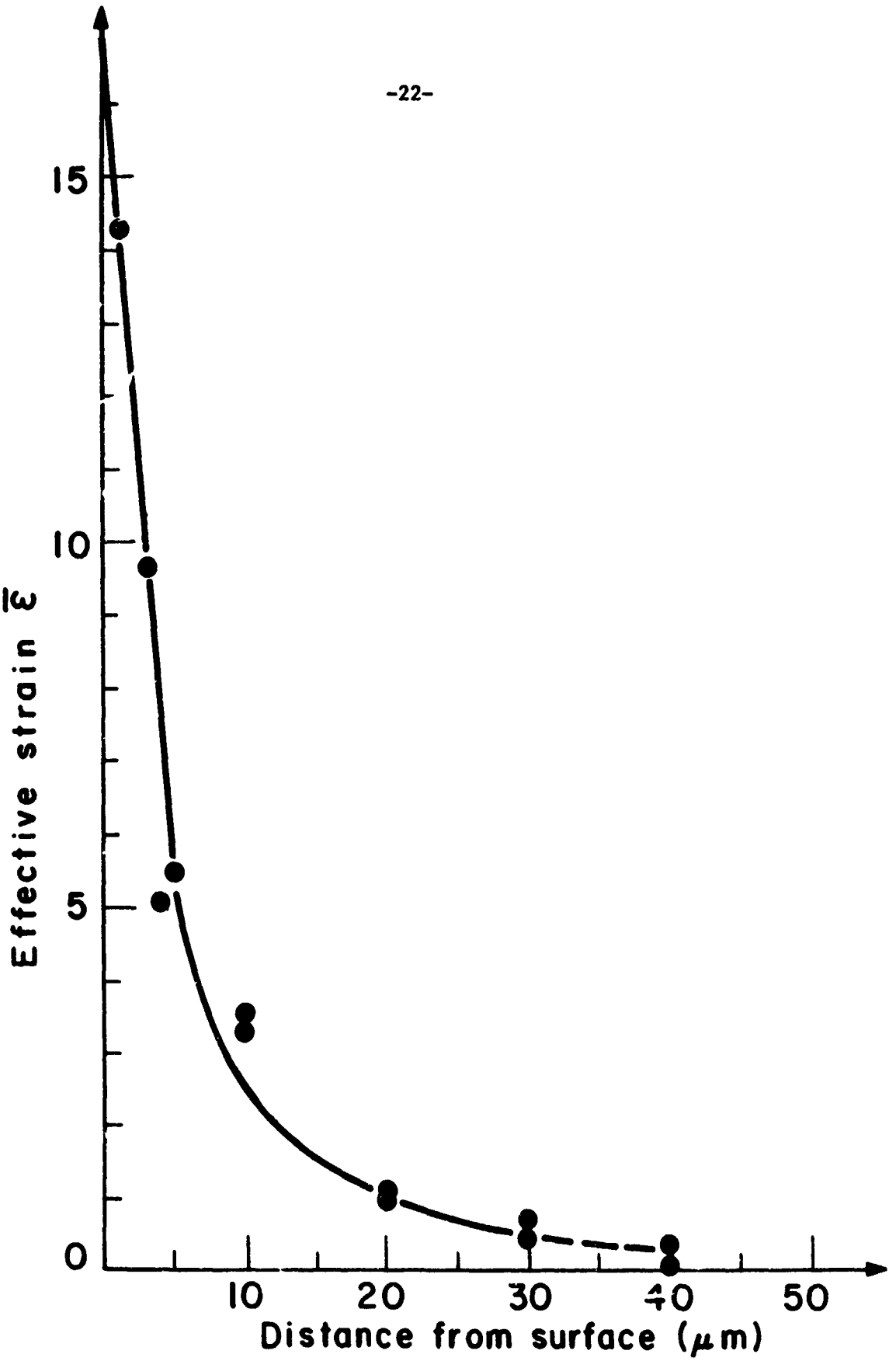

Figure 2.3 Strain-field at the subsurface of worn AISI 1020 steel under a load of 2.1 kg after 180m sliding in argon.

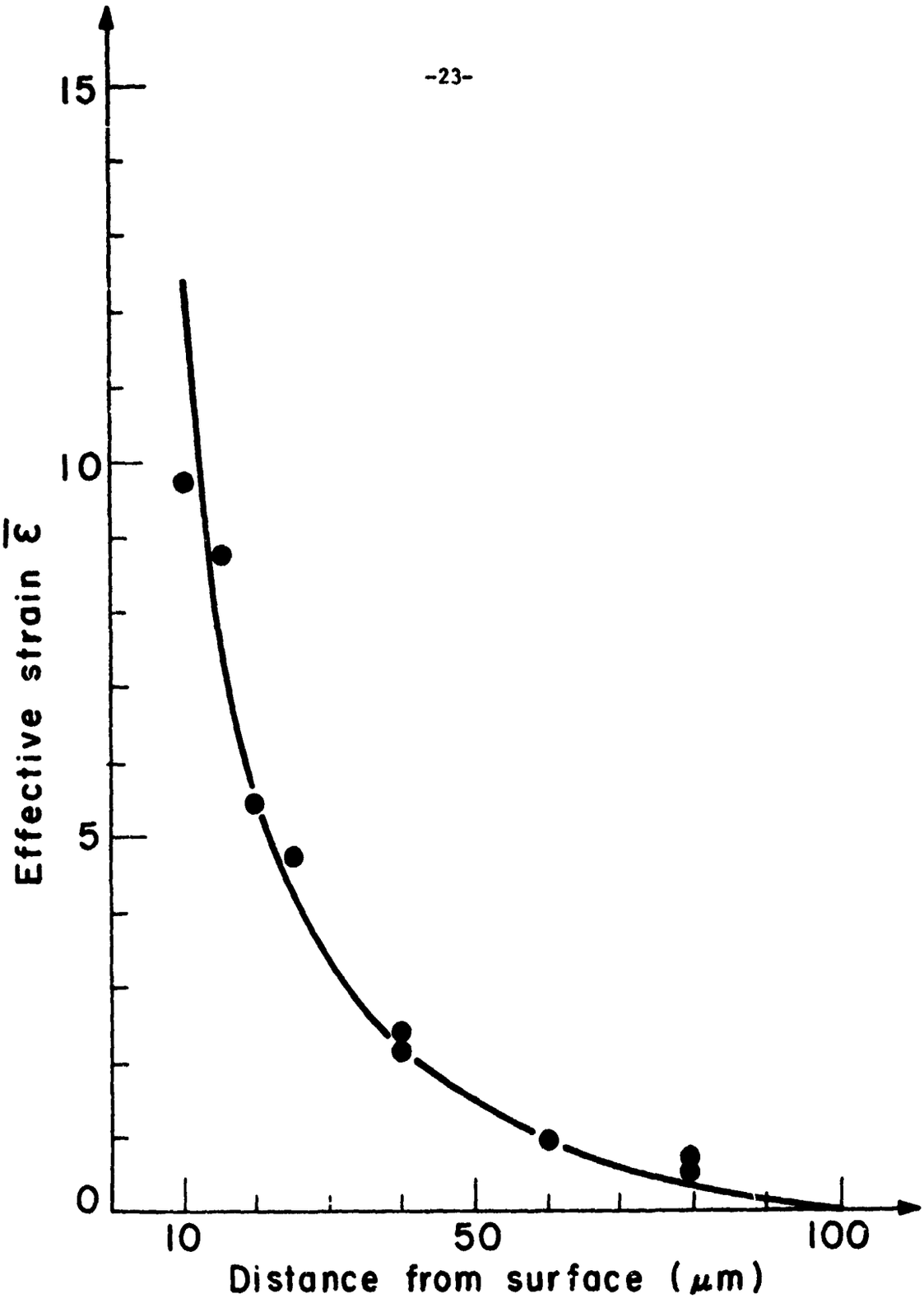

Figure 2.4 Strain-field at the subsurface of worn 99.5% purity, copper under a load of 2.1 kg after 68m sliding in argon.

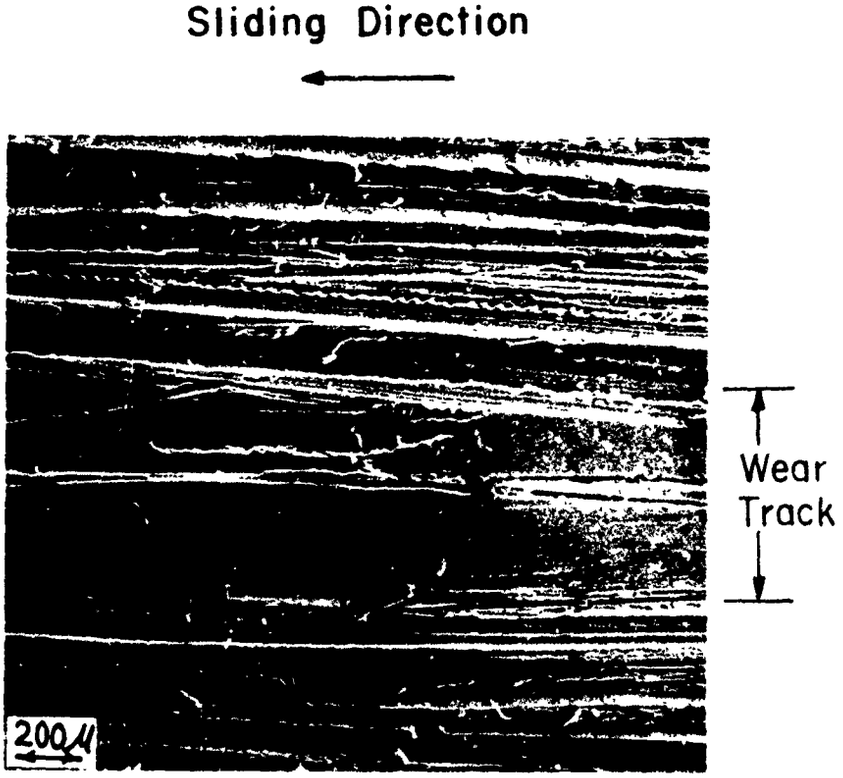

Figure 2.5 Wear track of annealed OFHC copper after 30 cm of sliding against an AISI 52100 steel pin under a load of 250 gm, in air.

Now there is concrete proof that the majority of the wear particles are in the form of thin sheets whose length is one or two orders of magnitude longer than the size of the asperity contact. The aspect ratio of these particles is much larger than 10 [4-6].

The flow stress of the metal near the surface is not the same as the bulk flow stress both before and after the wear tests. In the absence of any phase transformation associated with thermal effects at very high sliding speeds, the immediate surface layer is softer than the subsurface below it [18]. The flow stress gradient in f.c.c. metals can be determined approximately through hardness tests by varying the indentation load. Such measurements were made by Savitskii [19] with f.c.c. metals. In that study the hardness of the original aluminum samples was 20 kg/mm^2. After wear testing, the maximum microhardness observed was 33 kg/mm^2 at a depth of 10 to 15 μm from the surface as shown in Fig. 2.6. This decreased to 18 kg/mm^2 at the wear track. These experimental results are limited to f.c.c. and h.c.p. metals. In the case of b.c.c. metals the soft layer is so thin (estimated to be of the order of 100 Å) that the hardness gradient can not be measured by this technique.

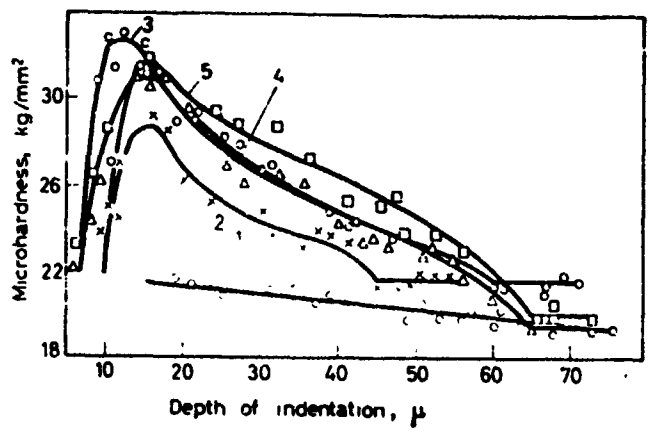

Figure 2.6 Variation of microhardness with depth for aluminium after sliding at different pressures [19] P (kg/cm^2) : 1,0; 2,64; 3,74; 4,94; 5,112.

Chapter 3

THE DELAMINATION THEORY OF WEAR

As discussed in Chapter 1, wear of metals is a complex phenomenon. No one theory can explain all the observed wear mechanisms, therefore it is necessary to define the limitations and applicability of a given theory. In this chapter we will review the delamination theory of wear. This explains the mechanism of wear when two metal surfaces are sliding at relatively low speeds. At present, the theory does not cover sliding at high speeds where other variables are present due to thermal effects. An effort is being made to extend the theory to this latter case, but it will not be covered in this report.

The wear mechanism considered in this chapter is based on dislocation theory and the plastic deformation and fracture of metals near a surface. Although a wear equation is developed to show that this theory can predict the phenomenological aspect of wear, the primary emphasis of the chapter is on the qualitative explanation of all the observed phenomena. It is clear that the theory needs to be refined further, both theoretically and experimentally, if a more precise quantitative prediction of wear phenomena based on this theory is to be made. However, the delamination theory of wear can be extremely useful in providing qualitative insights and answers to wear problems, as illustrated by the large number of supporting evidence given in this report.

A) The Delamination Theory of Wear

The delamination theory of wear is based on the following reasoning:

a) During wear, dislocations are generated in the material due to the plastic deformation of the surface by the slider. If an oxide layer is present it is broken by the passage of the slider thus exposing a fresh clean surface. This then allows those dislocations nearly parallel to the surface to be eliminated due to the action of the image force. Consequently, the material at and very near the surface does not have a high dislocation density.

b) With continued sliding there will be pile-ups of dislocations at finite distance from the surface. In time, this will lead to the formation of voids, which will be enhanced if the material contains a hard second phase for dislocations to pile against.

c) Voids can also form by gross plastic flow of the matrix around large hard particles.

d) With time, the voids will coalesce, either by their growth or by shearing of the metal. The end result is a crack parallel to the wear surface.

e) When this crack reaches a critical length (dependent upon the material), the material between the crack and the surface will shear, producing a sheet-like particle.

1) Behavior of Dislocations Near a Surface

Consider the surface of metal B just after slider A has moved over it (Fig. 3.1). The surface exposed at this time must be reasonably "clean" without a continuous, hard, coherent surface layer. During the sliding process, many dislocations are generated in the contacting metals due to the

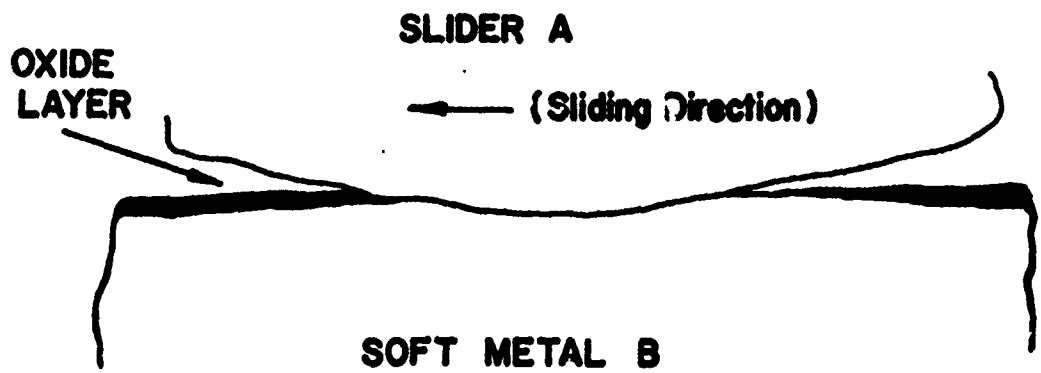

Figure 3.1 The surface of metal B as slider A moves over it.

general plastic and microplastic deformation of the asperities, with a greater number of dislocations being generated in the softer metal. Among the dislocations generated, some of those which are closely parallel to the surface and located within a finite distance from the surface may disappear as soon as the free surface is exposed due to the image force* acting on these dislocations. This will be the case unless the dislocations are constrained by strong nodal points within the lattice. Therefore, the dislocation density near the surface is always less than the dislocation density away from the surface. This means that the very surface layer cold-works less than the sub-surface and thus is able to undergo relatively larger plastic deformation.

The thickness of the low dislocation density zone of the surface layer depends on the surface energy of the metal and the magnitude of the drag stress acting on the dislocations. The surface energy affects the thickness of this zone because the total surface area changes when dislocations emerge at the surface. The drag stress is the stress that needs to be overcome for dislocations to move in an infinite solid. This drag stress will be referred to as the dislocation friction stress so as to be consistant with the definitions used in dislocation theory. This friction stress depends on the Peierls stress, the internal stresses created by other dislocations and substitutional and interstitial atoms, the nodal spacing of dislocations, and the distribution and properties of any secondary

*"Image force" acting on a dislocation is simply a convenient way of considering stresses and interactions near a stress-free surface. The force arises due to the existance of the stress-free surface.

phase particles. The friction stress has been measured for a limited number of metals. As shown in the Appendix B, the maximum thickness of this layer is about 1/10 micron in the case of 3% silicon iron and about 10 to 20 microns in the case of well annealed pure copper. In commercial grade metals this layer is expected to be much thinner due to inherently higher friction stresses. In general, this layer will be thicker for f.c.c. metals than for b.c.c. metals.

When a hard slider with a high elastic modulus comes in contact with a soft metal with a low elastic modulus, the interface boundary condition demands that the dislocation existing in the softer metal experience forces which repel them from the surface. If these dislocations do not encounter an obstacle which is strong enough to stop their motion, they will be driven into the softer material, strain hardening the sub-surface layer.

2) Crack and Wear Sheet Formation

As the dislocation density builds up at the sub-surface layer, cracks and voids can form by a number of different mechanisms [20]. The rate of void formation may be increased when there are hard particles present in the metal, since the motion of the mobile dislocations generated by the applied load may be blocked by the particles. When these hard particles are stronger than the cohesive strength of the matrix, cracks and voids can be nucleated under the stress of dislocation pile-ups [21-23]. Small cracks can also form when these hard particles break up under the dislocation pile-up stress. Voids can also be created during plastic deformation by the decohesion of the matrix-particle interface and by plastic flow of the matrix around a

hard particle [24]. Crack formation around hard particles is likely to be one of the most important mechanisms of void formation, since in most commercial grade metals there are many hard particles such as oxides, borides, carbides and nitrides.

The formation of cracks and voids at the subsurface does not guarantee the formation of wear particles. Loose particles can form only when these cracks and voids join together so that the strength of the subsurface layer is less than the shear stress applied at the interface between the slider and the surface. These cracks and voids link together due to the plastic deformation by three different mechanisms: growth of voids, crack propagation, and the plastic shear deformation of the metal between the voids [25]. Joining of voids by shear deformation is schematically illustrated in Fig. 3.2.

If the amplitude of the shear deformation is very small, a large number of cracks must be created before a loose particle can form. Therefore, in the absence of large shear deformation along a given direction, wear particles may not form until additional cracks are nucleated. This is the reason that fretting wear decreases with decreasing displacement amplitude when the amplitude is below a critical value.* This critical amplitude must be determined by the spacing of the holes and cracks which in turn depends on the hard particle density and surface topography.

---

* In the past this phenomenon has been explained in terms of the elastic deformation of the asperities. However, because of the normal stress at each asperity, it is likely that the equivalent stress has reached the yield stress at localized contact points.

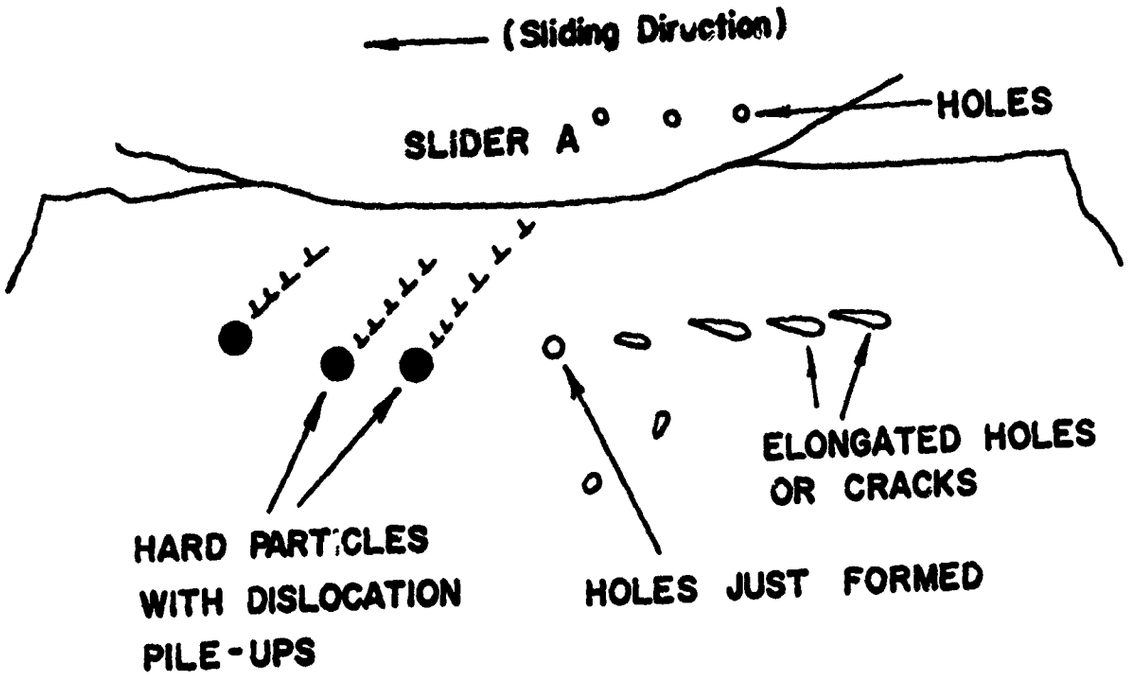

Figure 3.2 The process of wear particle formation by the shear deformation of voids.

The foregoing reasoning indicates that the wear particles formed may be in the form of thin sheets rather than spherical particles, especially if the particles are formed by the linking of cracks through shear deformation. Furthermore, in hard metals, the wear sheet is likely to be thinner than in softer metals because of the larger friction stress in the former.

Once these sheet-like wear particles become loose, some of them may assume curvatures, long thin sheets assuming helical shapes (in the form of screw threads), because of the residual stress existing in the sheets. The residual stress is primarily generated by the non-uniform distribution of dislocations across the sheet thickness.

The mechanism of wear particle formation discussed in this section does not exclude the possibility that some wear particles will not be sheets. The particles, which come loose when the material between voids undergoes cleavage fracture, may not be sheets. However, the number of these particles is expected to be less than the number of wear sheet particles.

3) Particle Size and Formation of Round Particles

After these wear sheets are created, some of them may be entrapped between the two sliding surfaces. These trapped particles may either be rolled into a spherical shape , broken into small pieces or remain the same, depending on the material properties of the loose particles and the sliding conditions. When the metal is relatively brittle, the delaminated sheets may break into pieces and form many small wear particles, since these sheets may have regions of high stress concentration due to the presence of

sharp cracks and inclusions. On the other hand, the sheets of a ductile metal may remain intact or simply roll into a large particle. As it will be shown in a later section, this is indeed the case. Metals such as zinc, lead and cadmium form thick wear particles in comparison to metals with high flow stresses such as steel. This situation is further accentuated by the fact that these ductile metals also have low friction stress, producing a thicker low dislocation zone which increases the degree of plowing and the amplitude of the compressive stress near the hard asperity and soft metal contact.

4) Wear of the Hard Surface

This theory also explains why the surface of a hard metal sliding against a soft metal, e.g., steel against copper, must wear. This can be explained in terms of micro-plasticity and the dislocation pile-up process. Although the overall contact stress may be less than the bulk yield stress of the harder metal, the stress at contacting asperities may be high enough for the localized generation of dislocations and pile-up of dislocations at hard obstacles. When a sufficient number of these dislocations pile-up, cracks may form in the harder metal. However, the crack nucleation rate is low because its friction stress and the cohesive strength are both high. Furthermore, because of the extremely small plastic shear deformation of the surface, a large number of cracks must be nucleated before a loose particle can form. Therefore, the wear rate of the harder metal is much lower than that of the softer metal.

5) Deformation of the Surface Layer

The deformation of the surface may be accomplished by the adhesion between asperities, as described by the adhesion theory of friction, or it may result from the "plowing" of the surfaces by asperities on the harder body. This plowing action may be enhanced if a soft layer exists on the material. When there is a flow stress gradient near the surface, such as that shown in Fig. 2.6, the normal load exerted by the asperities of the harder metal can not be supported by the very surface layer with the lowest flow stress. Therefore, the asperities of the harder material may sink farther into the softer material, increasing the shear stress required for tangential motion. This explains why the classical adhesion mechanism between the asperities cannot account for the large tangential load transmitted, especially in a vacuum or in an inert atmosphere. In fact it is interesting to note that the coefficient of friction predicted by the adhesion theory is farther off from the experimental results when tests are done in an inert atmosphere, although the experimental conditions more closely approximate the assumptions made by the adhesion theory. It is important to emphasize that if the "plowing" mechanism is operative, adhesion is not necessary for wear, although the presence of adhesion accelerates the wear rate.

B) Experimental Evidence for the Delamination Theory of Wear

A large number of experiments have been performed using more than a dozen metallurgically different materials. They included "inclusion and void-free" b.c.c. metals to f.c.c. metals. Both cold-worked and annealed

metals have been tested. The slider (AISI 52100 steel) was much harder than the specimens in most cases, but experiments were also performed with sliders and specimens made of the same metal. The experimental arrangements for the wear tests were the typical cyliner-on-cylinder type and the reciprocal pin-on-flat type. The tests were performed in argon atmosphere to reduce oxidation and accelerate the wear process. All tests were carried out at room temperature without any lubrication. A more complete description of the materials and the experimental procedure may be found in Appendices C and D respectively.

1) Subsurface Void and Crack Formation

As sliding commences, a surface layer of the sliding metals will be subjected to plastic deformation. This deformation is caused by the shear stress which arises at the contact due to adhesion and "plowing". The large plastic deformation observed must be built up in increments. The degree of plastic deformation in one increment is limited by the elastoplastic boundary existing near the plastically deformed contact zone. It has been observed that the depth of deformation increases with sliding distance and eventually reaches a steady state value.

Intense plastic deformation at the deformed layer nucleates voids around inclusions and hard second phase particles by matrix/particle separation, as shown in Fig. 3.3*. The micrographs show the formation of cracks around

---

* For the experimental conditions please refer to table 1 on page 89 for the test number given in the figure captions.

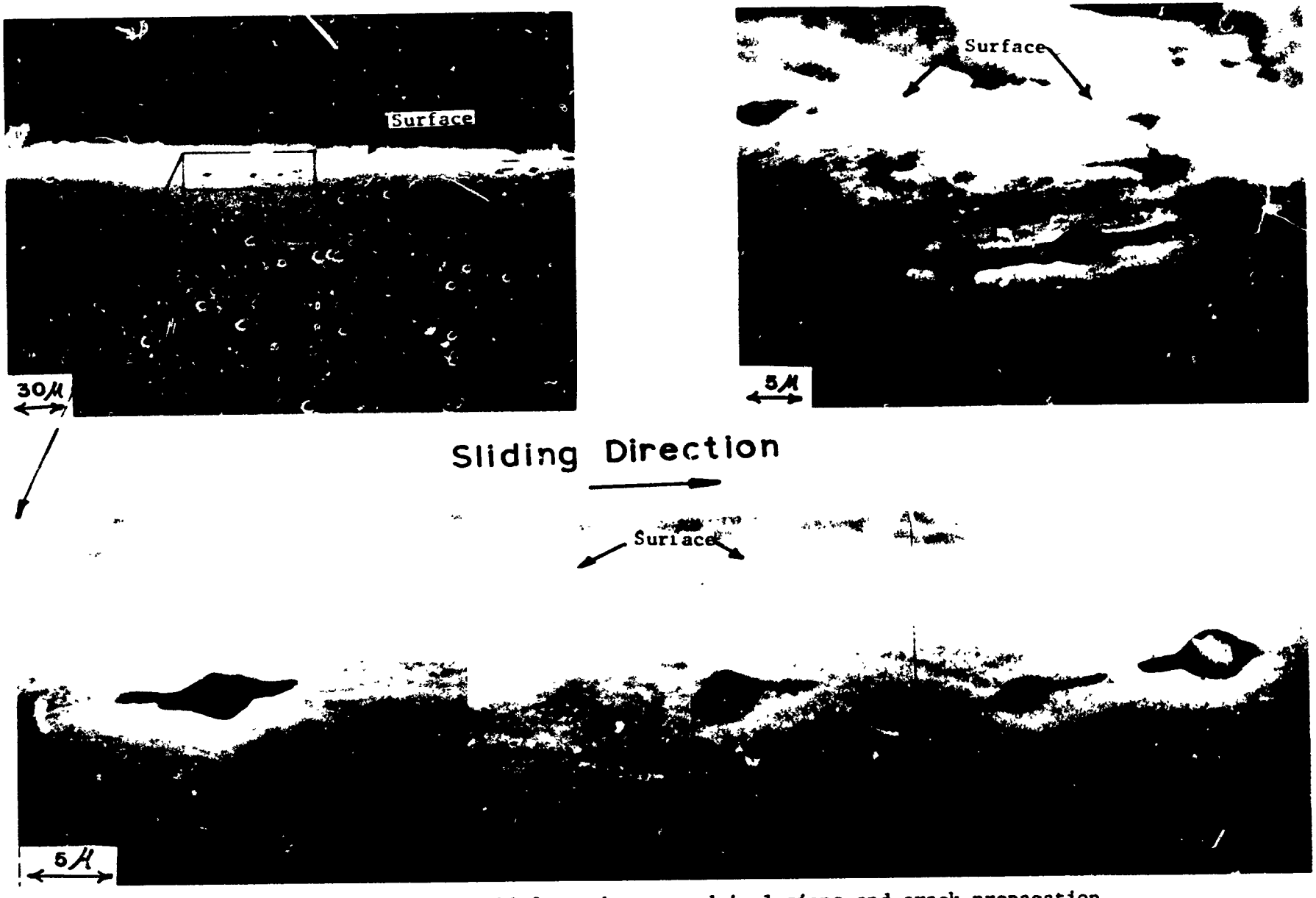

Figure 3.3 Void formation around inclusions and crack propagation from these voids near the surface in annealed Fe-1.3% Mo (Test No. 21).

(a)

(b)

Figure 3.4 Subsurface deformation, void elongation and crack fromation in steel
a) Doped AISI 1020 steel (Test No. 41)
b) Commercial AISI 1020 steel (Test No. 43)

the inclusions in Fe-1.3% Mo. It is noted that continued deformation has started to link up the voids near the surface into small cracks which are parallel to the wear track. The process eventually produces long subsurface cracks which are still parallel to the surface.

The subsurface void and crack formation in AISI 1020 steel is shown in Fig. 3.4. The deformed subsurface, parallel to the sliding direction (Fig. 3.4. a) indicates that most of the voids are associated with the carbide particles. Absence of carbides from some voids can be attributed to carbide pull-out during polishing.

The subsurface voids are elongated by further plastic deformation and usually they are directed along the shear deformation lines as can be observed in Fig. 3.4 a. These enlarged voids will then coalesce to form longer cracks fairly parallel to the deformation direction, i.e. parallel to the sliding direction, c.f. Fig. 3.4 b. In this micrograph, which was obtained from commercial AISI 1020 steel, a series of long parallel subsurface cracks are observed. This specimen had many internal voids as shown in the figure. It should be noted that only the subsurface voids have been elongated and joined to form longer cracks.

A swirling pattern of deformation and cracking is sometimes noted on steel tested under reciprocating geometry (Fig. 3.5). This may explain the spherical shaped wear particles observed under reciprocating types of wear. Additionally, it will be noted that there are two cracks running on differnt planes which eventually would have generated large wear particles. Subsurface voids and cracks also form in metals without hard second phase or inclusions [3], but the mechanism of void nucleation in these metals has not

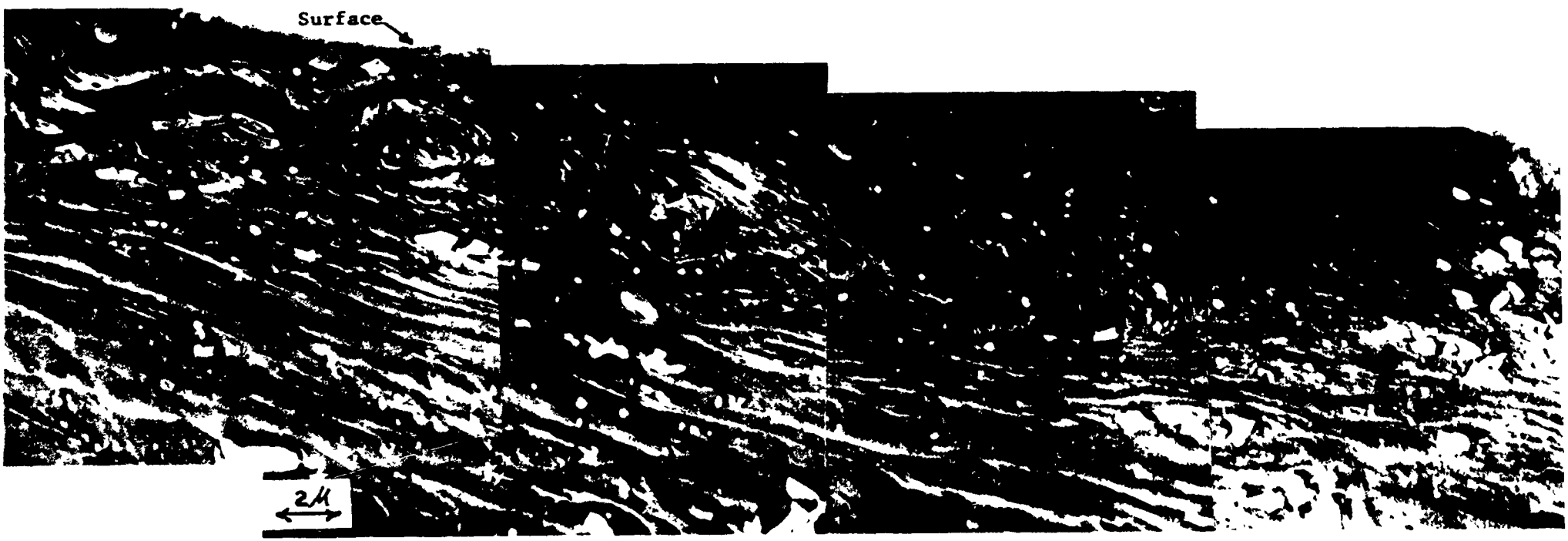

Figure 3.5 Subsurface deforamtion pattern in doped AISI 1020 steel (Test No. 33). Note the swirling pattern and large particles formed due to non-coplanar crack propagation.

been determined experimentally. These voids join to form long subsurface cracks, as shown in Figs. 3.6 and 3.7. The micrograph in Fig. 3.6 shows a 50 μm crack parallel to the surface which is approximately 3 μm below the sliding surface of a Fe-500 ppm W solid solution specimen.

Fig. 3.7 shows a long subsurface crack and some shorter cracks which have not yet joined together in an OFHC copper specimen. A higher magnification of the section revealed a large number of voids. Void concentration increases as the surface is approached, although in the copper there are no inclusions easily identifiable at this magnification.

2) Wear Sheet Formation

As deformation proceeds, the subsurface cracks advance to the free surface by shear of the material between the cracks and the surface. Fig. 3.8, which is a micrograph of the wear track of OFHC copper, shows one such crack which has reached the wear surface. The relatively smooth wear track with parallel furrows in the sliding direction is further evidence for the "plowing" mechanism discussed earlier.

The smooth wear track of this specimen together with a low wear rate, indicates that the rate of delamination is slow (light wear). The wear sheets were detached from the surface only in selected areas and occasionally cracks similar to that shown in Fig. 3.8 or shorter cracks perpendicular to the wear track were observed, as shown in Fig. 3.9.

Further sliding will advance the cracks to the surface of all portions of the crack front (opposite to the sliding direction). Figures 3.10 and

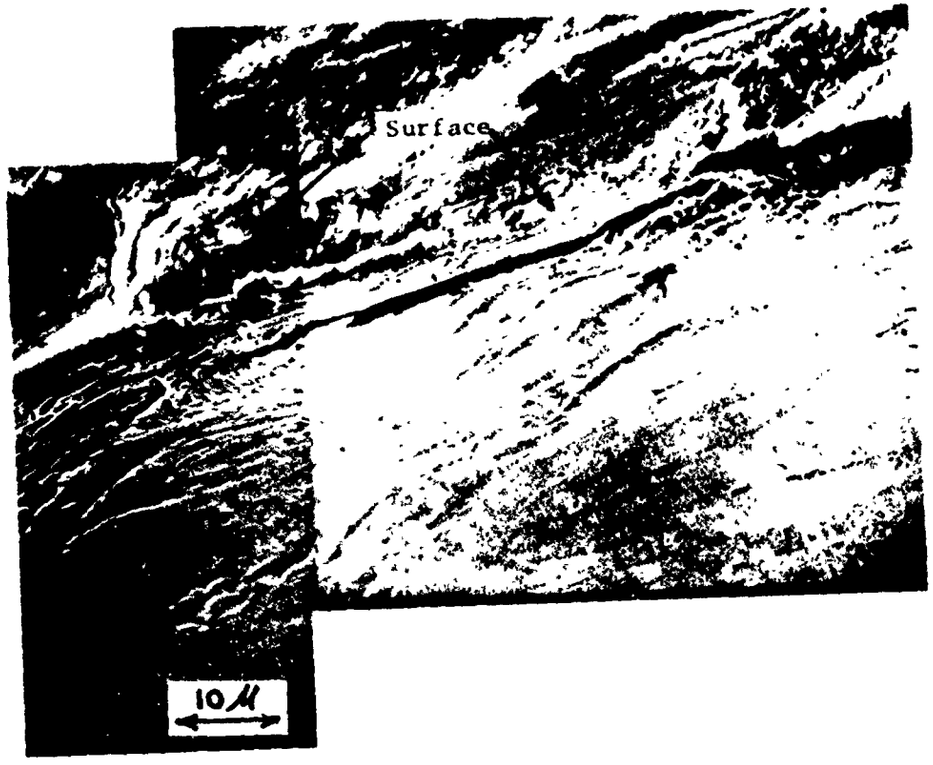

Figure 3.6 Subsurface deformation and crack formatin in iron solid solution (Test No. 8).

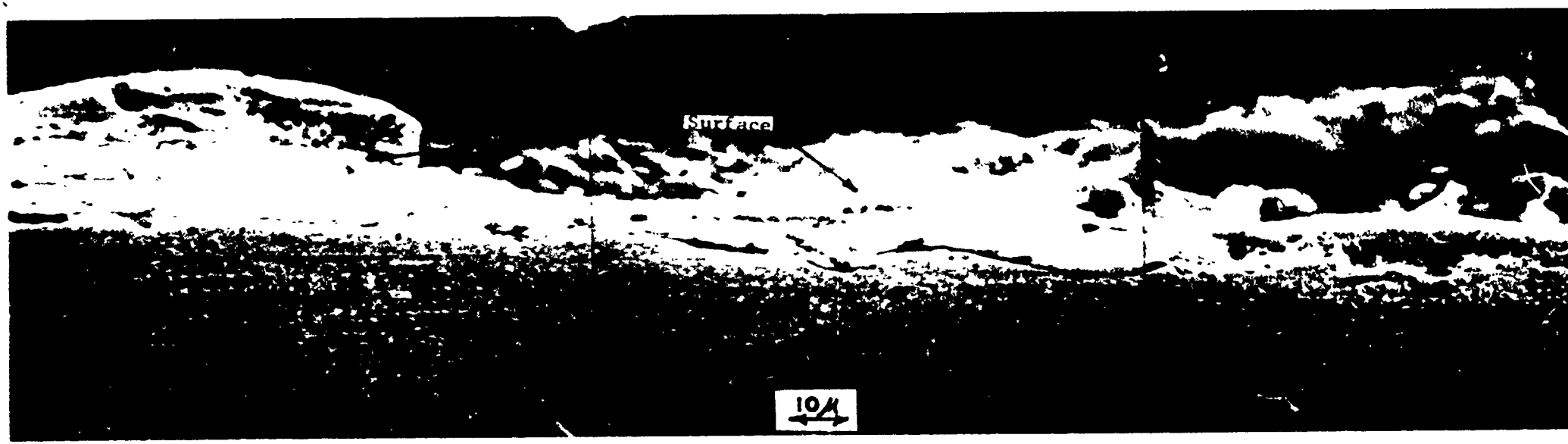

Figure 3.7 Void and crack formation in annealed OFHC copper (Test No. 52).

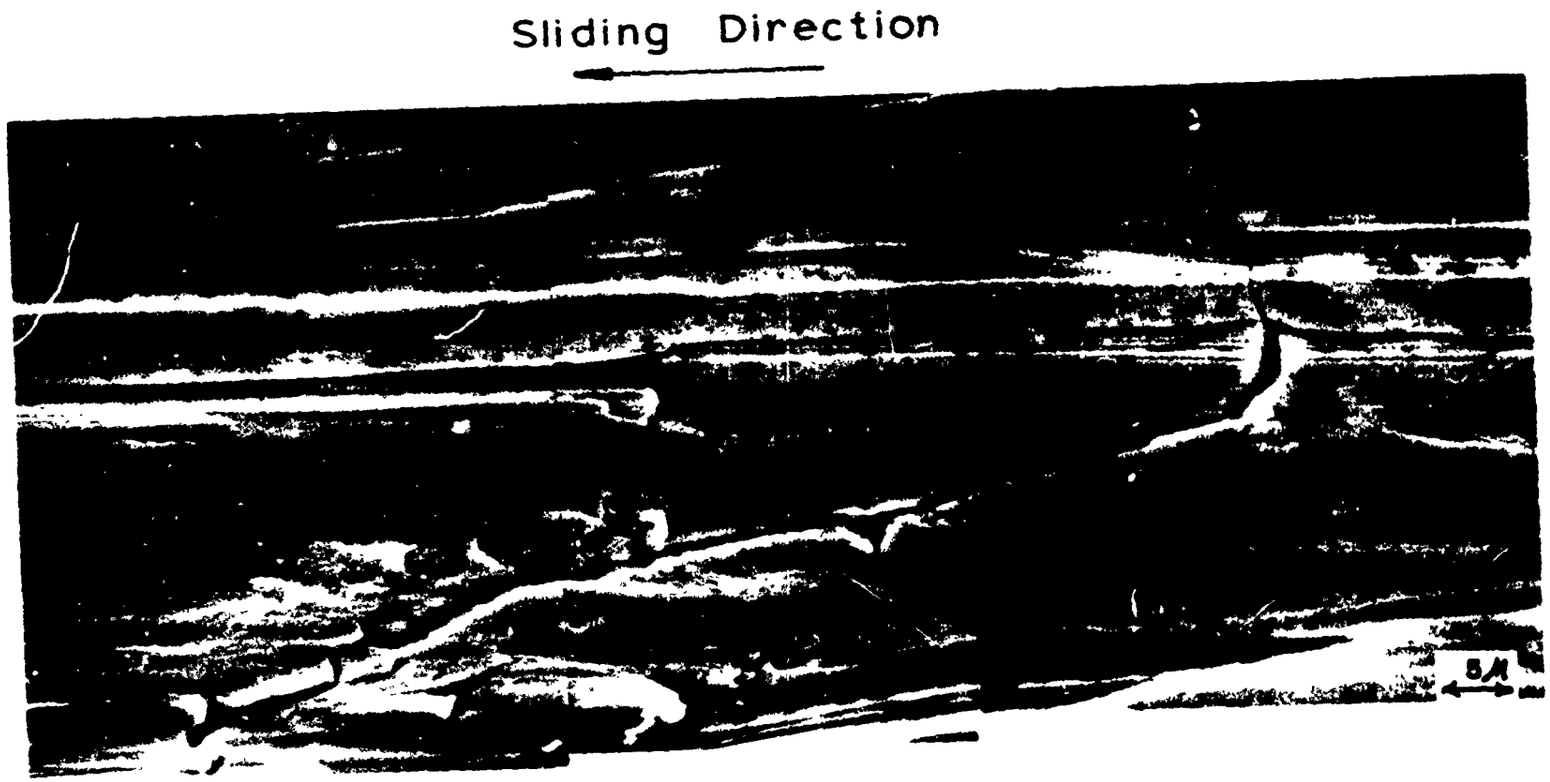

Figure 3.8 Wear sheet formation at the wear track of OFHC copper (Test No. 51).

(a)

Sliding Direction

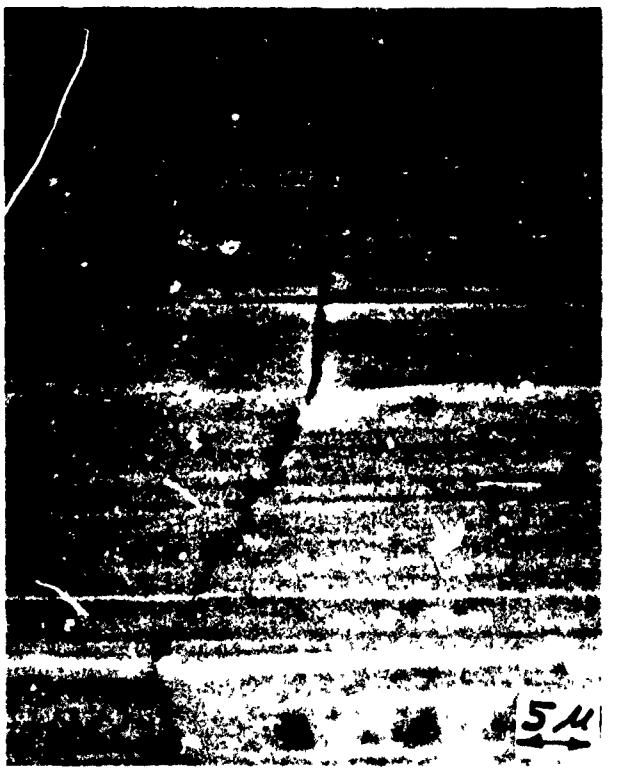

(b)

Figure 3.9 Wear track of OFHC copper (Test No. 51).
a) Wear sheet formation
b) Crack perpendicular to the sliding direction

3.11 show this behavior for Fe-8800 ppm W and Fe-2.7% Mo respectively. These micrographs indicate that the wear sheets have been lifted slightly from the surface since the cracks have just reached the surface.

The wear sheet will lift further from the plane of the surface due to the residual stress and strain in the sheet or due to the repeated loading. This is dramatically shown in Fig. 3.12 for Fe-4000 ppm W. The sheet in this photograph is only attached ot the wear surface at the left end. Another example of this stage in wear sheet formation is evident in Fig. 3.13.

Since the maximum bending moment is at the left end of the sheet, where it is still in contact with the worn surface, a crack will develop at this position. This type of crack is observed in Fig. 3.13. Another example of this crack, which eventaully detaches the sheet from the surface, may be seen in Fig. 3.14. It should be emphasized here that the ductility plays a major role in wear sheet detachment, since the crack formation by the bending action of the sheet will be enhanced in less ductile metals.

It is interesting to note that all of the wear sheets shown in the micrographs of Figs. 3.8 to 3.14 have dimensions of 70-120 μm in length, 60-100 μm in width and only 1-10 μm in thickness. This clearly contradicts the adhesive model of wear which claims that the measured wear particle thickness is about one third of the length [14]. It is quite conceivable that after the wear sheets are separated from the surface, they will fracture to many smaller fragments.

The wear sheets which have been presented so far were observed on the wear tracks of pure materials, i.e. pure iron, iron-tungsten solid solutions

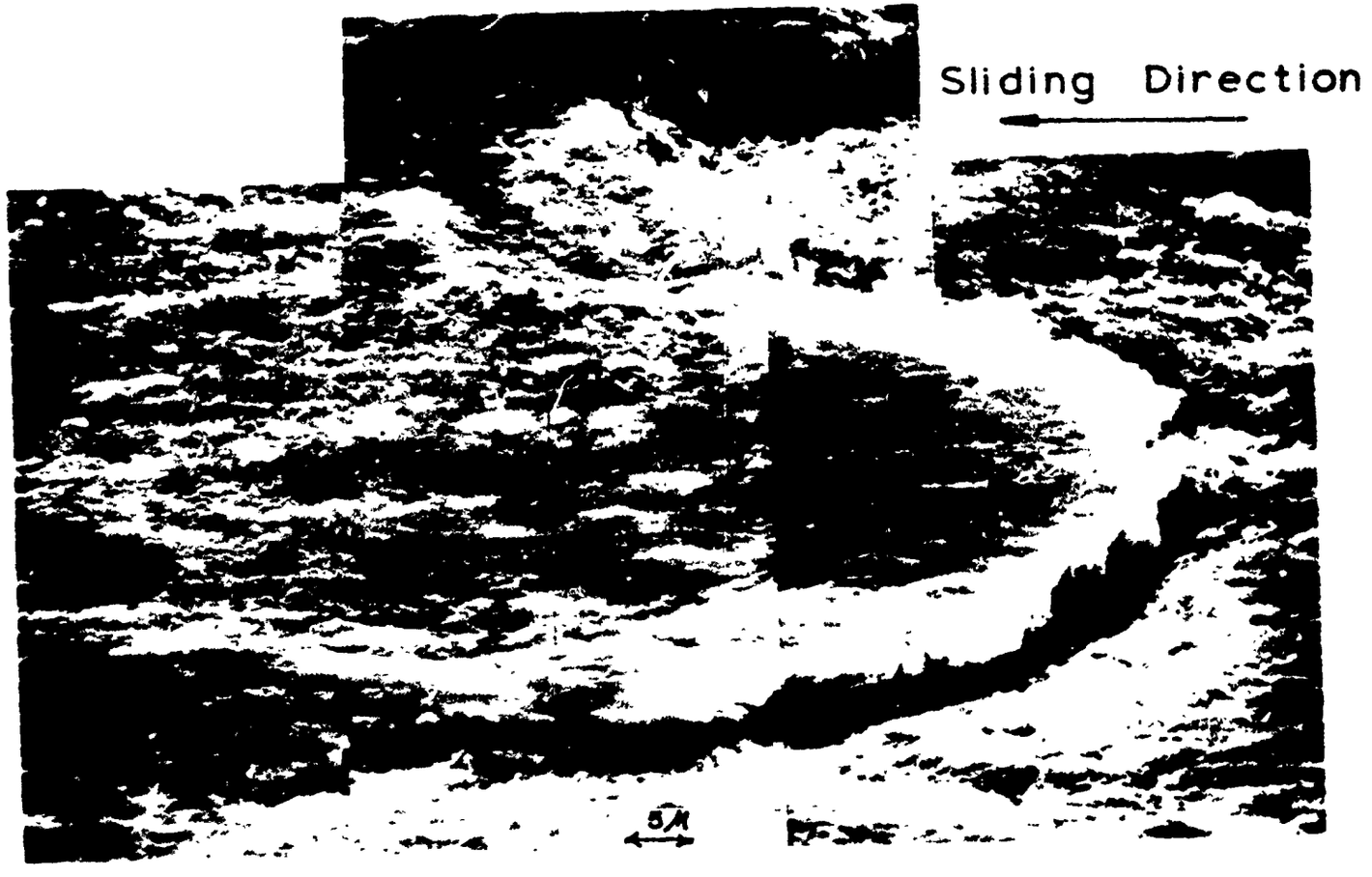

Figure 3.10 Wear sheet on the wear track of iron solid solution (Test No. 18).

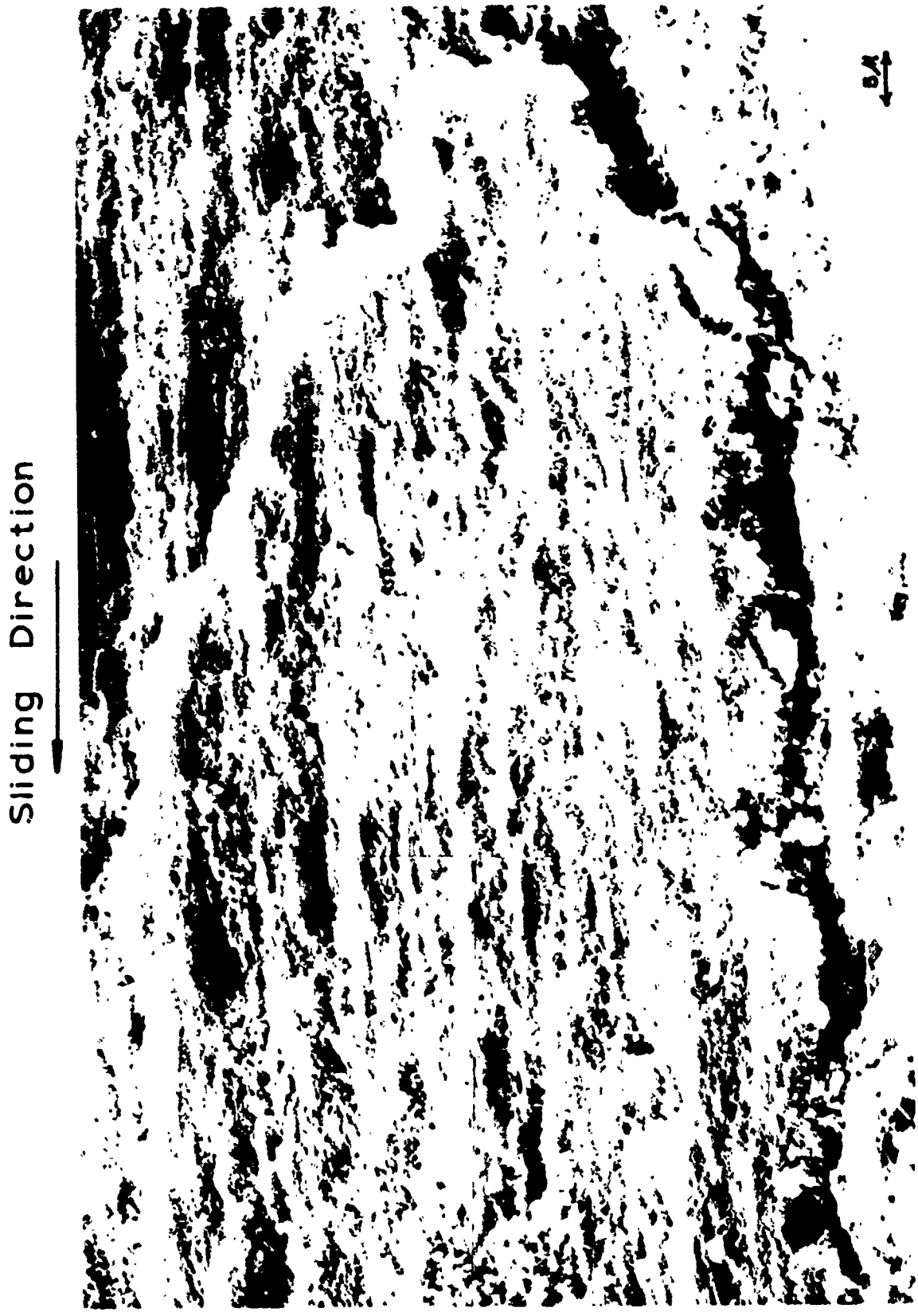

Figure 3.11 Wear sheet on the wear track of iron solid solution (Test No. 22).

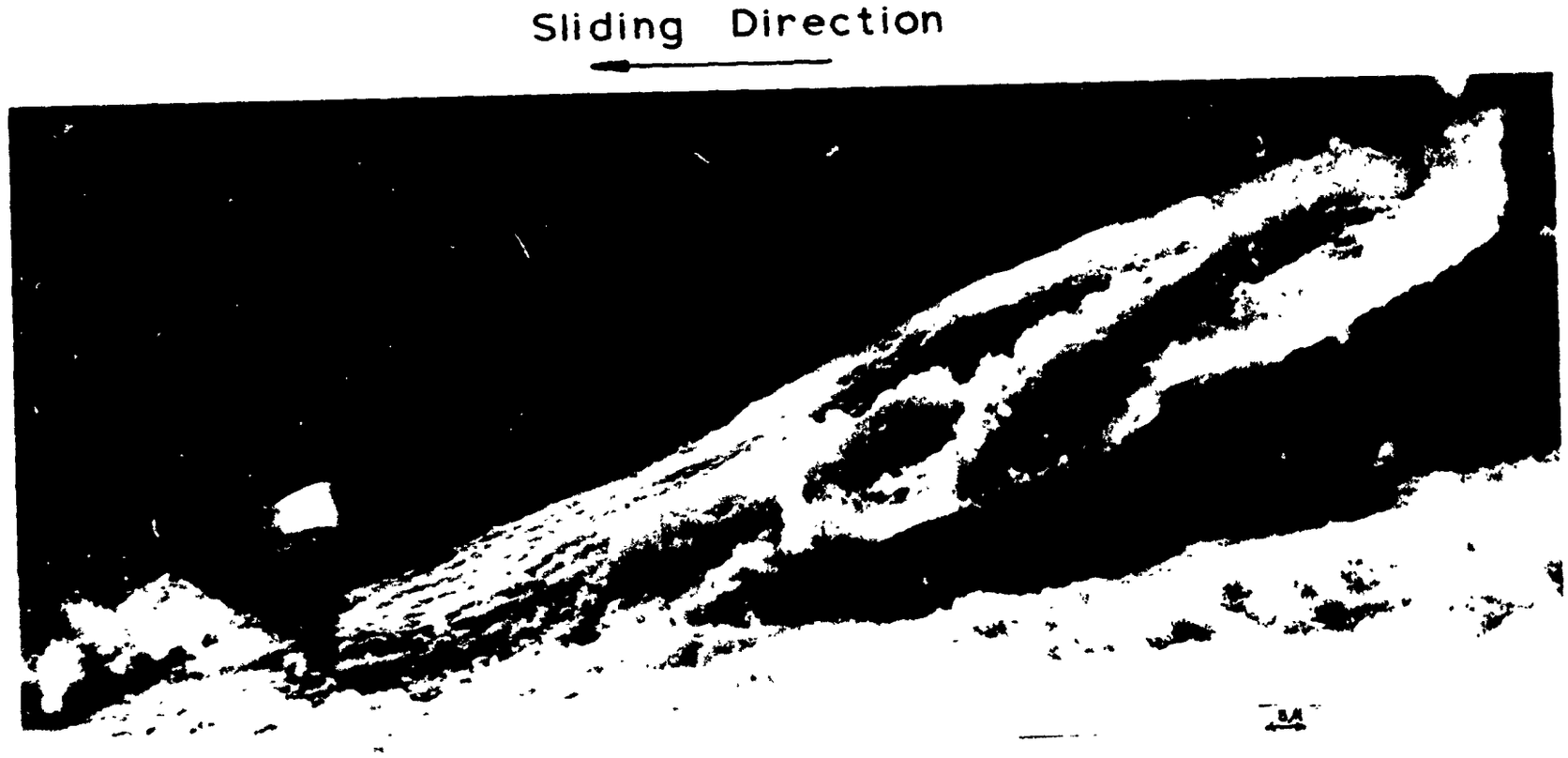

Figure 3.12 Wear sheet lifting from the worn surface of iron solid solution (Test No. 13).

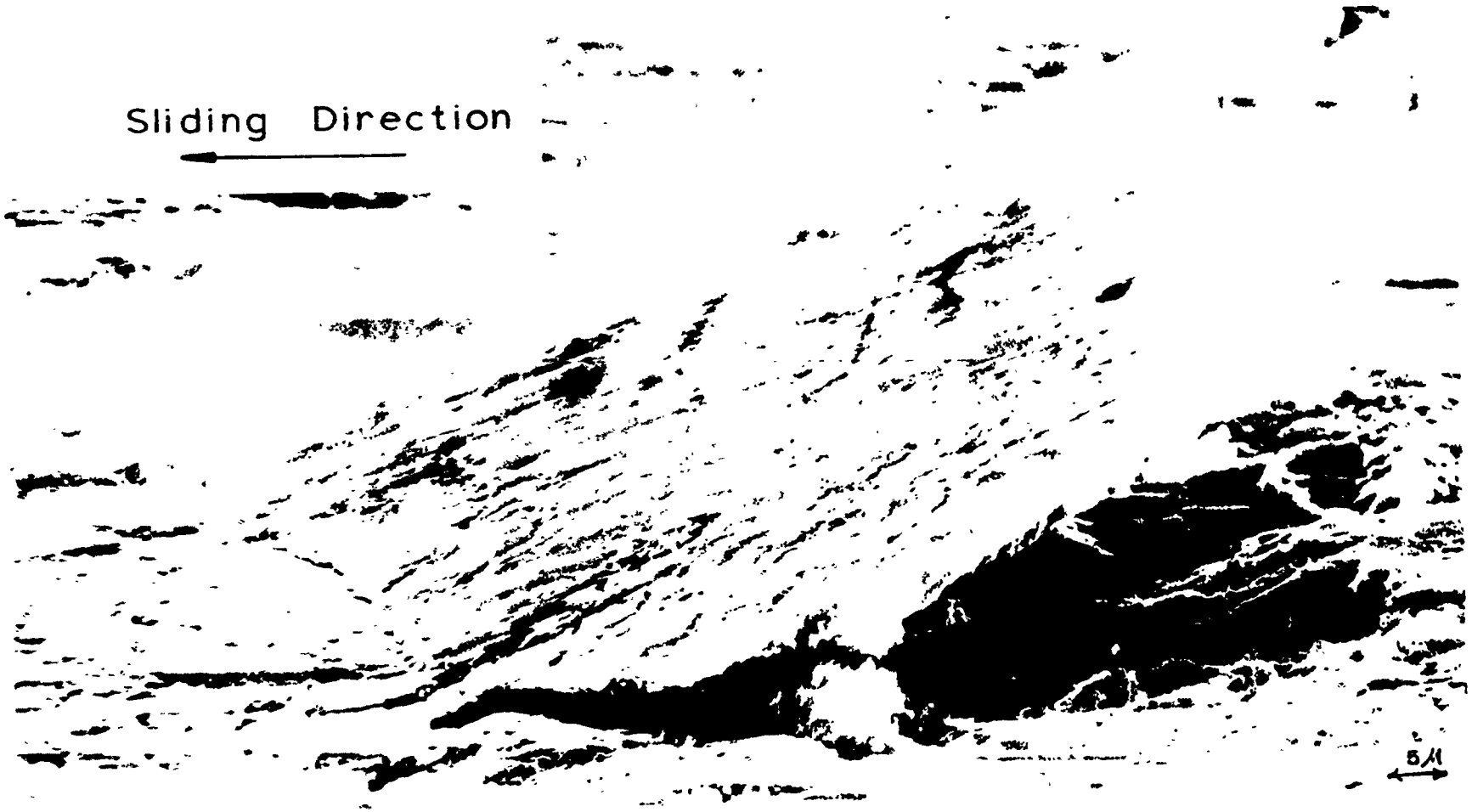

Figure 3.13 Wear sheet on the worn surface of iron solid solution (Test No. 1[illegible])

Figure 3.14 Wear sheet formation in iron solid solution (Test No. 18).

and OFHC copper. Examination of the wear tracks of steel specimens revealed only a few attached wear sheets, c.f. Fig. 3.15. However, there were many wear craters indicating that delamination had occurred. Fig. 3.15 indicates that the wear sheets in steel are 40 μm long and 20 μm wide.

The size of the wear sheets does not correlate with Hertzian stress analysis based on a sphere contacting a flat surface. Hertzian analysis predicts that under the 5 pound load used in the tests, the contact diameter will be 200 μm and the maximum shear stress will occur at a depth of 50 μm from the surface. This indicates that the critical position where sub-surface voids and cracks are developed is not the predicted point of maximum shear stress. The similarity between the elastic contact size and the lateral dimensions of the wear sheet is misleading. The actual width of the wear track was much larger than 200 μm , and scanning electron microscopic observations showed that many wear sheets may be present across the wear track.

The micrograph in Fig. 3.14 shows the surface topography of the top of the wear sheet as well as the underside of the sheet. The top surface is relatively smooth with parallel furrows in the sliding direction. This surface topography and other similar evidence; i.e. Figs. 3.8, 3.9, and 3.13, lend support to the "plowing" concept, which attributes the shear stress at the sliding surface to plowing of the soft surface layer of the specimen as well as by some degree of adhesion of the sliding surfaces.

It was discussed earlier that the subsurface cracks form by the process of void coalescence in ductile metals, resembling ductile fracture.

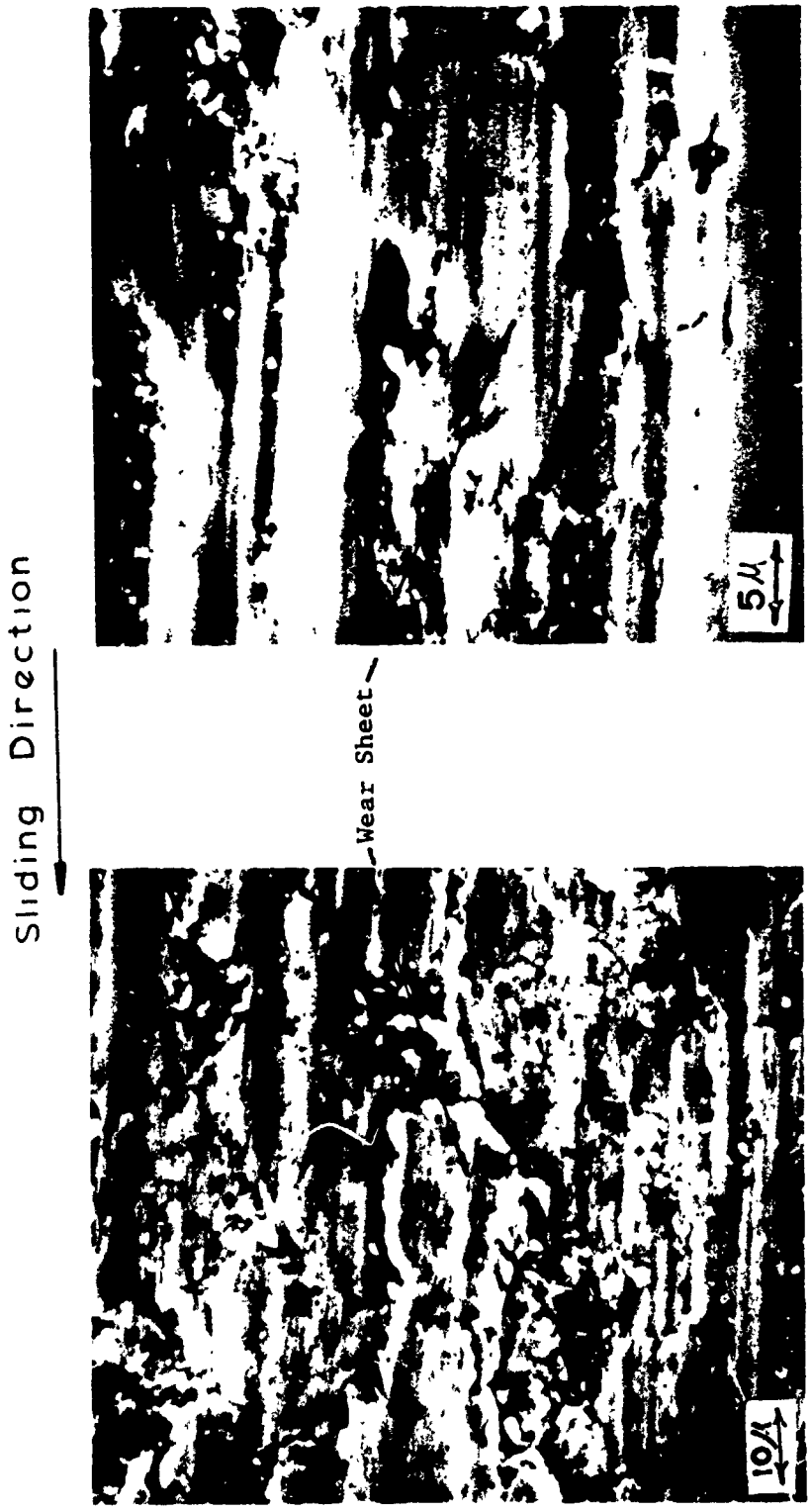

Figure 3.15 Wear sheet on the wear track of steel (Test No. 43).

Therefore, one would expect that the surface topography beneath the wear sheets to be similar to ductile fracture surfaces. This fact is evident in Fig. 3.14 and more clearly in Fig. 3.15, which show a wear sheet has been separated from, but still attached at one end to the surface of pure iron. This sheet appears to be much brighter than the surrounding area because it rests at a large angle to the surface; and the electron beam is reflected from the sheet at a higher intensity than from the wear surface. A section of this micrograph is magnified in Fig. 3.15 b to show shear dimples below the sheet. This resembles ductile fracture where shear dimples are caused by rupture of material between the voids [26].

Fig. 3.16 c, which was obtained from the same specimen, but at a region where a wear sheet had been detached from the wear track, shows the shear dimples very clearly. Therefore, one may expect to observe the shear dimples on the wear track, at the regions where the sheets have been separated, if the slider has not passed over that area.

The examination of the wear surface of Fe-2.7% Mo, showed that the shear dimples formed in this material were very similar to those formed in the pure iron. However, the size of the dimples appeared to be smaller. The observations indicated that wear sheet formation mechanism may be the same in solid solutions and in pure metals.

The ductile fracture patterns are absent from less ductile metal surfaces, as shown by Fig. 3.17 for steel specimens. Micrograph (a) was obtained from commercial AISI 1020 steel, while micrograph (b) was taken from

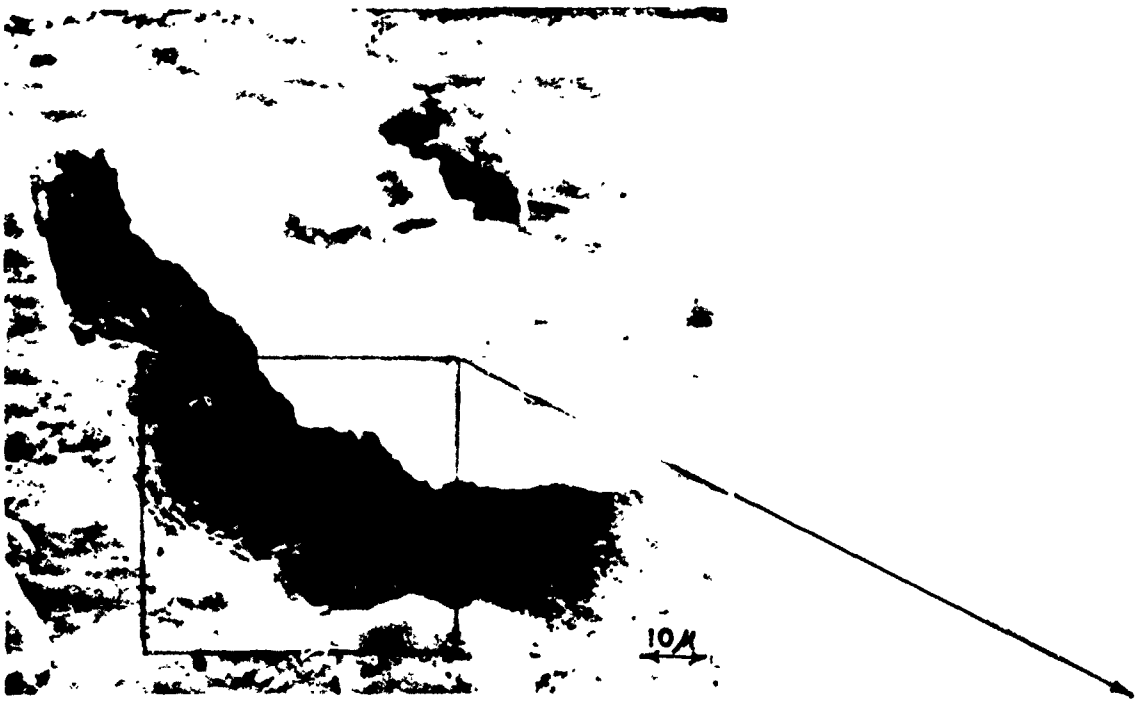

(a)

(b)

(c)

Figure 3.16 Worn surface of pure iron (Test No. 6)
a) Wear sheet formation
b) Shear dimples beneath the wear sheet in (a)
c) Dimpled appearance of a wear crater

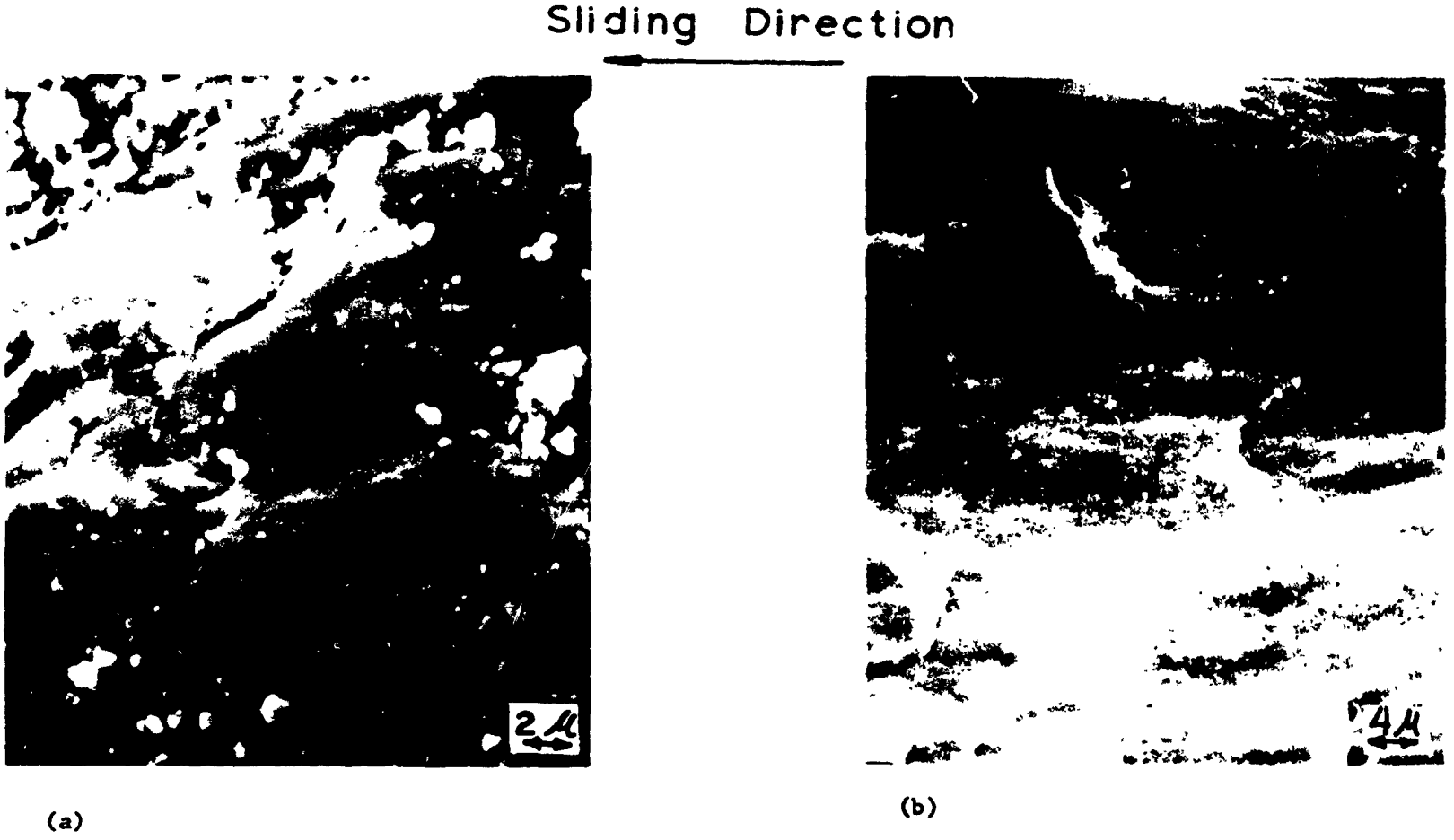

(a) (b)

Figure 3.17 Surface of wear craters in steel
a) Commercial AISI 1020 (Test No. 43)
b) Doped AISI 1020 (Test No. 41).

specially doped AISI 1020 steel (the bright areas in (a) are believed to be oxide particles). Both of these surfaces appear to be relatively smooth as compared to Fig. 3.16 c, which is for pure iron. This an indication that the subsurface cracks in this two phase material form by crack propagation between the voids surrounding the carbides as opposed to the void growth and coalescence in iron solid solutions.

When the wear sheets become detached from the surface, shallow craters are produced on the worn surface, as shown by Fig. 3.18. This specimen which had been sectioned, polished and etched, before the wear track examination, reveals that the ductile fracture patterns are absent. This is attributed to the removal of the dimple patterns by the etchant.

3) Shape of the Wear Particles

Wear particles which were suspended in lubricating oils used in various applications were collected using the Ferrograph technique [27]. These wear particles were first observed using the bichromatic microscope developed by Trans-Sonics, Inc. in order to identify the general characteristics of wear particles. These examinations revealed that, in general, bronze particles are thicker and bigger than the steel particles collected in the same experiment. The thickness of the bronze particles was in the neighborhood of 5 microns, whereas the steel particles were thinner than 1 to 2 microns. There were also some helical wear particles.

These wear particles were then examined using a scanning electron microscope. Some of the typical wear particles are shown in Figs. 3.19 through 3.24 in stereo pairs. It was astonishing to see that in all cases most of

Figure 3.18 Wear crater in iron solid solution (Test No. 18).

Figure 3.19 A stereo picture of typical wear particles collected from the lubricating oil used in gun mounts. Although there are a variety of shapes, most of the wear particles are flat.

Figure 3.20 A stereo picture of small wear particles. Note that the small particles on the right is a thin curved sheet.

the wear particles were thin sheets! Fig. 3.19 shows the wear particles collected from the oil used to lubricate gun mounts. Most of the wear particles are steel, although some of the bigger particles are bronze. There are many different shaped wear particles including a spherical one near the lower left-hand corner. However, it should be noted that most of them are flat. Fig. 3.20 shows a greatly magnified view of small wear particles collected from the same oil. The wear particle on the right is a slightly curved sheet. Fig. 3.21 shows the stereo pictures of wear particles from another lubricating oil sample collected from a gun mount. In this figure the large wear particles are bronze. Again, it should be noted that most of the wear particles are flat. The large particles at the bottom appear as if they are being rolled into even bigger ones. One of these particles is magnified in Fig. 3.22, showing that a large number of thin sheets are agglomerating together into one large particle. These extremely thin particles are steel. The large flat particles on the left-hand side are bronze. All the samples shown in Figs. 3.19 through 3.22 were collected from the oil samples which lubricated sliding contacts.

Figs. 3.23 and 3.24 show the wear particles collected from the oil that lubricated gear teeth. Even in this case many wear particles are thin sheets, as shown in Fig. 3.23. Although it is not clear what they are, the small rough particles located between the thin sheets appear as if they are in the process of being rolled into larger particles. Fig. 3.24 shows a typical large wear particle collected from the lubricating oil for gear teeth. The particle appears to be a laminate consisting of a large number of thin sheets.

Figure 3.21 A stereo picture of typical wear particles collected from the lubricating oil for gun mounts. The large flat particles are bronze.

Figure 3.22 A stereo picture of a large particle shown in Fig. 3.21. Note the agglomeration of many thin sheets into a large particle. The large sheet particles on the left are bronze and the small particles are steel.

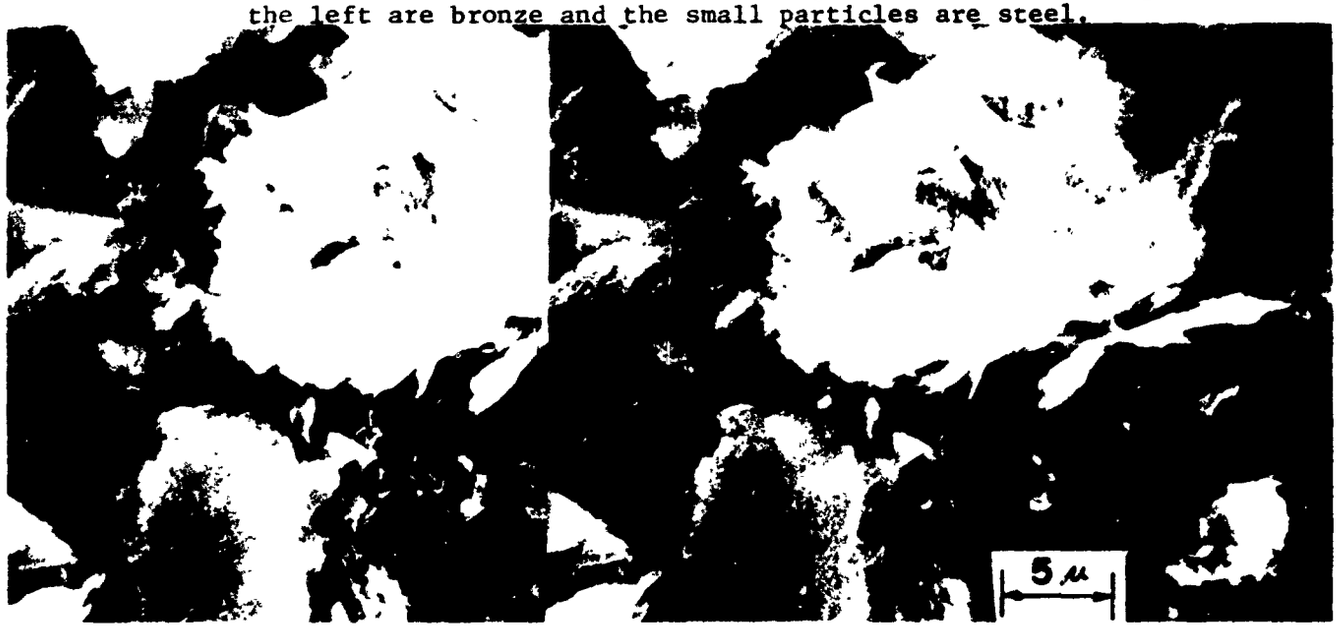

Figure 3.23 A stereo picture of wear particles collected from the lubricating oil for gear teeth.
Figure 3.24 A typical large wear particle from the gear lubricating oil. Note that the particle looks as if a large number of thin sheets are pressed together.

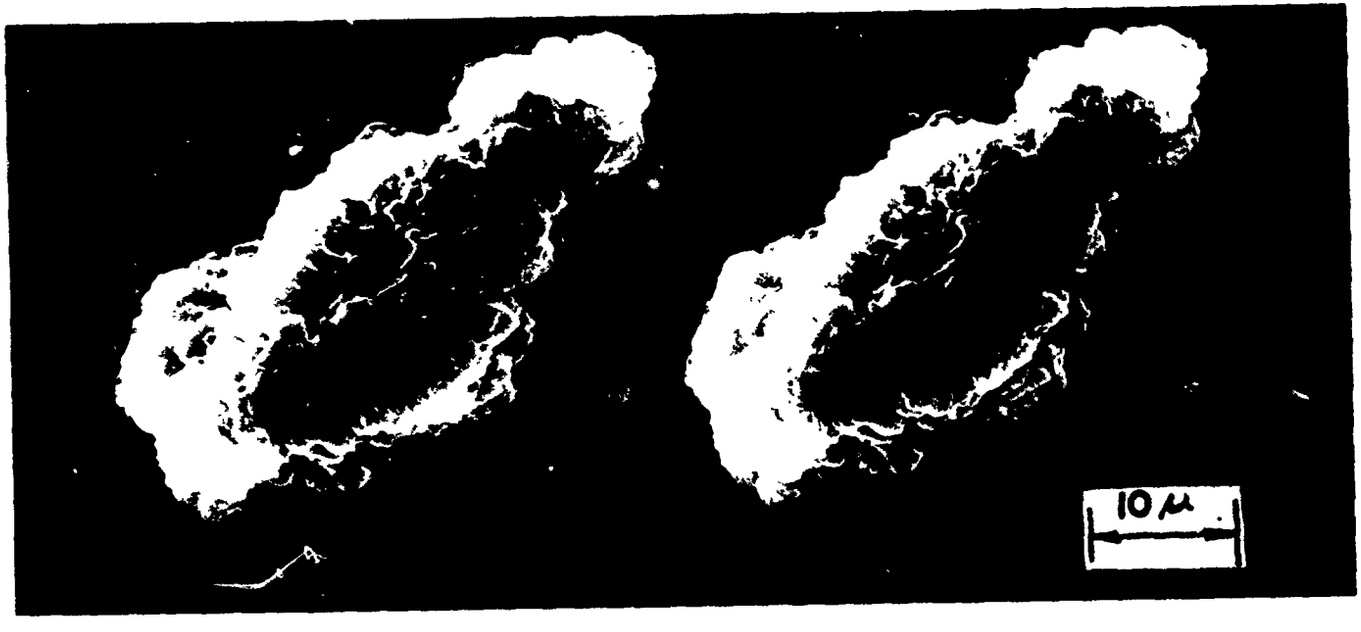

It may also be that it is a single large wear particle, each thin sheet representing the cracks partly grown at different depths from the surface.

4) Measured Size of Wear Particles and Wear Rates

One of the implications of the delamination theory of wear is that the thickness of the sheet is thicker in f.c.c. metals due to their lower friction stress than in b.c.c. metals. Certain h.c.p. metals such as cadmium, zinc and magnesium should also form thick sheets due to their large c/a ratios in comparison to other h.c.p. metals such as titanium and beryllium which have small c/a ratios. This also implies that the metals with low friction stress may wear faster than those with high friction stress. This situation is further accentuated by the fact that the soft metals which in general have low friction stress undergo large shear deformation when sliding against a hard metal. The fact that soft metals in contact with harder wear faster is a well known experimental fact.

In figures 3.21 and 3.22 it was shown that bronze particles were indeed bigger than steel particles. The compilation of wear particle sizes given by Rabinowicz [14] also indicates that the particle size of ductile metals is larger than the less ductile ones.

5) Fretting Wear

One of the conclusions of the delamination theory of wear was that when the amplitude of displacement along a given direction is less than a critical value, the wear coefficient may depend on the displacement amplitude. Although the experimental results have been questioned [28], Halliday and Hirst [29], Charner [30], and Akoi [31] found that the wear per unit

distance of sliding falls drastically when the amplitude is less than a critical value. According to the delamination theory, the critical displacement amplitude should depend on the density and distribution of hard particles as well as the surface topography. Recently Waterhouse [32] has shown that, in fact, fretting occurs by delamination.

6) Minimum Load for Loose Particle Formation

Rabinowicz [14] found that no wear particles are produced between gold sliding against gold when the normal load is less than 5 grams. He has explained this phenomenon in terms of the surface energy concept. This explanation may further be strengthened by the fact that the image force on dislocations is affected by the surface energy [33]. However, it is also probable that the absence of wear in gold may be related to the absence of hard oxide particles. In the absence of inclusions and at such low loads, the surface deformation is likely to occur over a long period of time, longer than the duration of tests.

7) Wear of Metals Sliding Against Graphite Fiber Reinforced Epoxy

Hauser [34] showed that there is almost no wear when metals such as nickel, cobalt, chrome, 52100 steel and tungsten are sliding against graphite fiber reinforced epoxy. When the surface of the metal specimens were examined, it was also found that there was no gross plastic deformation at their surface. On the other hand, the worn metals such as zinc, copper and 316 stainless steel showed evidence of substantial plastic deformation. This is an indication that plastic shear deformation is needed for appreciable wear.

C) DEVELOPMENT OF THE WEAR EQUATION

For the delamination theory of wear to be fully effective it must be able to predict the wear rate quantitatively without relying on experimentally determined coefficients. However, this cannot be done at present since there are many unresolved questions. The formation and joining of voids, in spite of the extensive work done in fracture mechanics, is still difficult to predict theoretically. Even the problem of relating the surface traction to the shear deformation of the surface layer has not been solved. Although these problems are currently being investigated at M.I.T., it will be sometime before these questions can be answered definitively.

In this section two simplified wear equations are derived primarily to show that this theory is consistant with the phenomenological wear behavior. For this purpose, consider a circular wear track produced in a pin-on-disk type of wear tests. An isolated view of the metal under the wear track is illustrated in Fig. 3.25. It shows the process of the metal being removed layer by layer, similar to the removal of skin from an onion. Each layer consists of a large number of wear sheets.

There are two possible sets of assumptions which can be made to build a model of wear by the delamination process. In one case it may be assumed that the metal is sheared until a wear sheet is formed, i.e., a wear sheet is created by interaction of one set of asperities. In the other case, it may be assumed that the creation of a wear sheet is a cumulative process which results from the metal being sheared a small amount by each passing asperity, but the creation of a wear sheet will occur only after

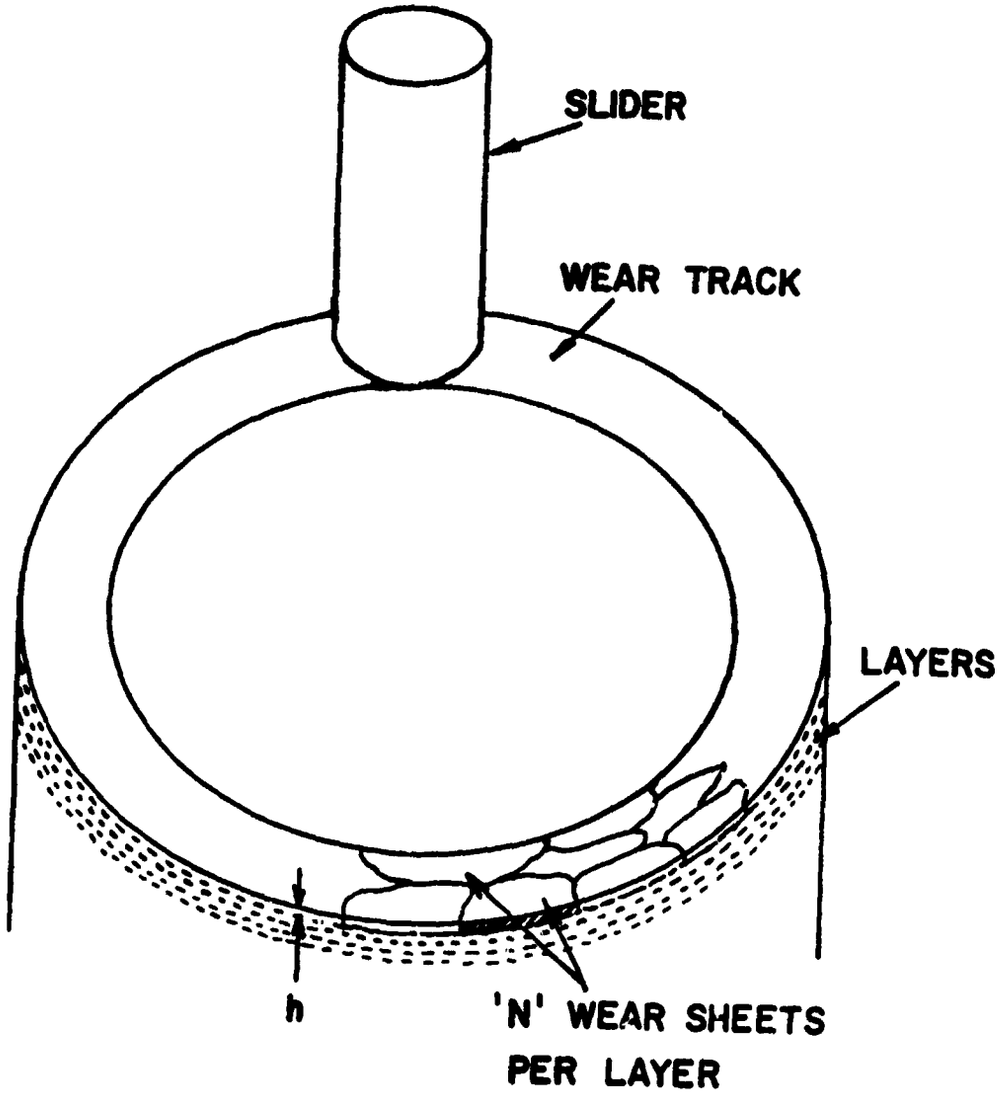

Figure 3.25 An isolated view of the metal being removed under a circular wear track in pin-on-disk type wear tests.

a large number of asperities have passed each point on the surface.

In order to derive a wear equation based on the first assumption, the following suppositions will be made about the wear process:

a) Metals wear layer by layer, each layer consisting of N wear sheets.

b) The number of the wear sheets per layer is proportional to the average number of asperities in contact at any instance between the slider and the disk.

c) The rate of void and crack nucleation and the critical degree of shear deformation for loose particle formation can be expressed in terms of a critical sliding distance S_o for a given sliding situation. S_o is defined as the critical sliding distance required for removal of a complete layer (i.e. N wear sheets).

Using these assumptions, the total wear for the case of a hard surface sliding against a soft surface may be expressed as

$$W = N_1 \left(\frac{S}{S_{o_1}}\right) A_1 h_1 + N_2 \left(\frac{S}{S_{o_2}}\right) A_2 h_2 \qquad (1)$$

where A is the average area of the delaminated sheet, h is the thickness of the delaminated sheet, and S is the distance slid. The subscripts 1 and 2 refer to the soft and hard metals sliding against each other. The ratio (S/S_o) is equal to the number of layers removed. S_o is likely to be less when compatible materials are slid due to the greater shear stress established at the interface.

The thickness h will be assumed to be, to a first approximation, equal

to the depth of the low dislocation density zone (see Appendix B), i.e.,

$$h = \frac{Gb}{4\pi(1-\nu)\sigma_f} \tag{2}$$

where G is the shear modulus, σ_f the friction stress, b the Burgers vector, and ν Poisson's ratio. The average surface area of each delaminated sheet may be assumed to be proportional to the real area of contact per asperity A_r as

$$A = C\, A_r \tag{3}$$

where C is a proportionality constant. Gupta and Cook [12, 13] showed that the real area of contact per asperity A_r and the number of asperities in contact are proportional to the applied load L as

$$\begin{aligned} A_r &\propto L^{0.09} \\ n &\propto L^{0.91} \end{aligned} \tag{4}$$

By the second assumption $n \propto N$

The substitution of Eqs. (2), (3) and (4) into Eq. (1) yields

$$W = \frac{k}{4\pi}\left[\frac{b_1 G_1}{\sigma_{f_1} S_{o_1}(1-\nu_1)} + \frac{b_2 G_2}{\sigma_{f_2} S_{o_2}(1-\nu_2)}\right] \cdot LS \tag{5}$$

where R is a constant which depends primarily on the surface topography. Eq. (5) states that the wear rate is proportional to the normal load and the distance slid. According to Eq. (5), in order to minimize wear rate (G/σ_f) must be small and S_o large. In most commercial grade metals, σ_f is proportional to G (see Appendix B). However, σ_f can change drastically at constant G, if the metal is extremely pure initially with few dislocations and/or impurities. In general, the ratio G/σ_f decreases with an

increase in solid solution hardening and with hardening by secondary phase particles, but increases with overaging. S_o is expected to increase when incompatible materials are slid against each other and when lubricants are used. S_o should decrease with an increase in the density of hard particles and dislocation density. Therefore, increasing the hardness by formation of solid solution is likely to reduce the wear rate, while hardening by inclusion of secondary phase particles may or may not reduce the wear rate, depending on the distribution of the hard particles. Eq. (5) may be written as

$$W = \kappa \cdot LS \tag{6}$$

where κ is a wear factor given by

$$\kappa = \frac{k}{4\pi} \left[\frac{b_1 G_1}{\sigma_{f_1} S_{o_1} (1-\nu_1)} + \frac{b_2 G_2}{\sigma_{f_2} S_{o_2} (1-\nu_1)}\right] \tag{7}$$

Eq. (6) differs from Archard's wear equation in that it does not depend directly on hardness.

A second wear equation* may be derived by considering that the generation of a wear sheet is a cumulative process which results from the metal being sheared a small amount by each passing asperity, but the generation of a wear sheet will occur only after a large number of asperities have passed each point on the surface. It will be assumed that metal under the slider wears layer by layer and each layer consists of many sheets. It will

*This was done by Dr. A.P.L. Turner, formerly a member of the faculty at M.I.T. and now with Argonne National Laboratory.

further be assumed that a loose wear sheet is formed when a critical plastic displacement, d_c, has occurred at the surfaces and that the plastic displacement, d_p, which has occurred at a point on the surface is proportional to the total distance slid and the percentage of time that any point on the surface has been in actual contact. If A_r is the total real area of contact at any time and A_T is the actual area of the wear track on the wearing surface, each point on the wear track should be in actual contact with the mating surface for a fraction of the total time equal to the ratio A_r/A_T. Therefore, the plastic displacement is given by

$$d_p = \frac{BSA_r}{A_T} \tag{8}$$

where B is a proportionality constant and S is the distance slid. When d_p reaches its critical value d_c, a layer of loose wear particles will be formed. The total area of the layer will be equal to the wear track area A_T. The thickness of the layer, h, is assumed to be determined by the structure and mechanical properties of the material and to be independent of the normal load, L. The critical sliding distance for producing a layer of loose particles is found by setting $d_p = d_c$ and solving Eq. (8) for S, giving

$$S_c = \frac{d_c A_T}{BA_r} \tag{9}$$

where the subscript c denotes the critical values. When the total sliding distance S is greater than S_c, the ratio $S/S_c = N$ is the total number of layers removed.

The volume of material worn away, W, is then given by

$$W = N_1 h_1 A_{T_1} + N_2 h_2 A_{T_2} = \frac{S}{S_{c_1}} h_1 A_{T_1} + \frac{S}{S_{c_2}} h_2 A_{T_2} \qquad (10)$$

where the subscripts 1 and 2 refer to the two materials of the contacting pair. Substituting for S_c using Eq. (9) gives

$$W = \frac{B_1 h_1 A_r S}{d_{c_1}} + \frac{B_2 h_2 A_r S}{d_{c_2}} \qquad (11)$$

Since the real area of contact is proportional to the normal load, L, according to $A_r = CL/H$, (11) can be written as

$$W = \frac{B_1 h_1}{d_{c_1} H} LS + \frac{B_2 h_2}{d_{c_2} H} LS = \kappa \cdot LS \qquad (12)$$

where $B = BC$ is a new constant and H is the hardness of the softer material.

The above equation depends on a number of material parameters in addition to the hardness, H. The way in which the thickness of the layer removed, h, depends on the material structure was discussed in the preceding section. The critical plastic displacement to form loose particles, d_c, should be qualitatively related to the ductility of the material in shear. Increasing hardness is usually accompanied by decreasing ductility, especially when the hardness is achieved by introducing second phase particles. Thus the two constants in the denominator often have compensating behavior.

Equations (6) and (12) were derived primarily to show that the delamination theory is consistant with the experimentally observed results that the worn volume is proportional to the sliding distance and the normal load. These equations are very elementary and further refinements are required.

Chapter 4

DELAMINATION IN VARIOUS METALS

It was shown in the preceeding chapter that slow sliding wear occurs primarily by the process of delamination initiating from the deformed subsurface. It was also dicussed that the presence of hard second phases or inclusions accelerate the process of subsurface void nucleation and delamination. This phenomenon was checked for different materials ranging from an extremely soft and pure bi-crystal of cadmium to fully hardened AISI 4340 steel. The results of these investigations are reported in the present chapter. The wear tests were carried out with different materials under various conditions as listed in Table 1. The materials and the experimental variables are discussed in detail in the Appendices C and D, respectively. Table 1 also includes the wear rates and friction coefficients.

A) Cadmium

Wear tests were conducted on bi-crystals of cadmium (Test Nos. 1-3) to study the mechanism of deformation during sliding. The experimental condition and results are given in Table 1. Since this material was extremely soft, a very low load of 10 gm. was used. Even under such a low load, material was built up at the wear track edge as shown in Fig. 4.1 a. The wear track of test #3, Fig. 4.1 b, indicates some structure around the wear track. This is believed to be grain structure generated by recrystalization of the deformed material at the edges of the tracks. Even though this material was very pure and did not contain any inclusions, many indications of delamination were observed. Fig. 4.2 shows a wear sheet on the wear track of one crystal. It is interesting to note that the wear sheet lies opposite to the direction

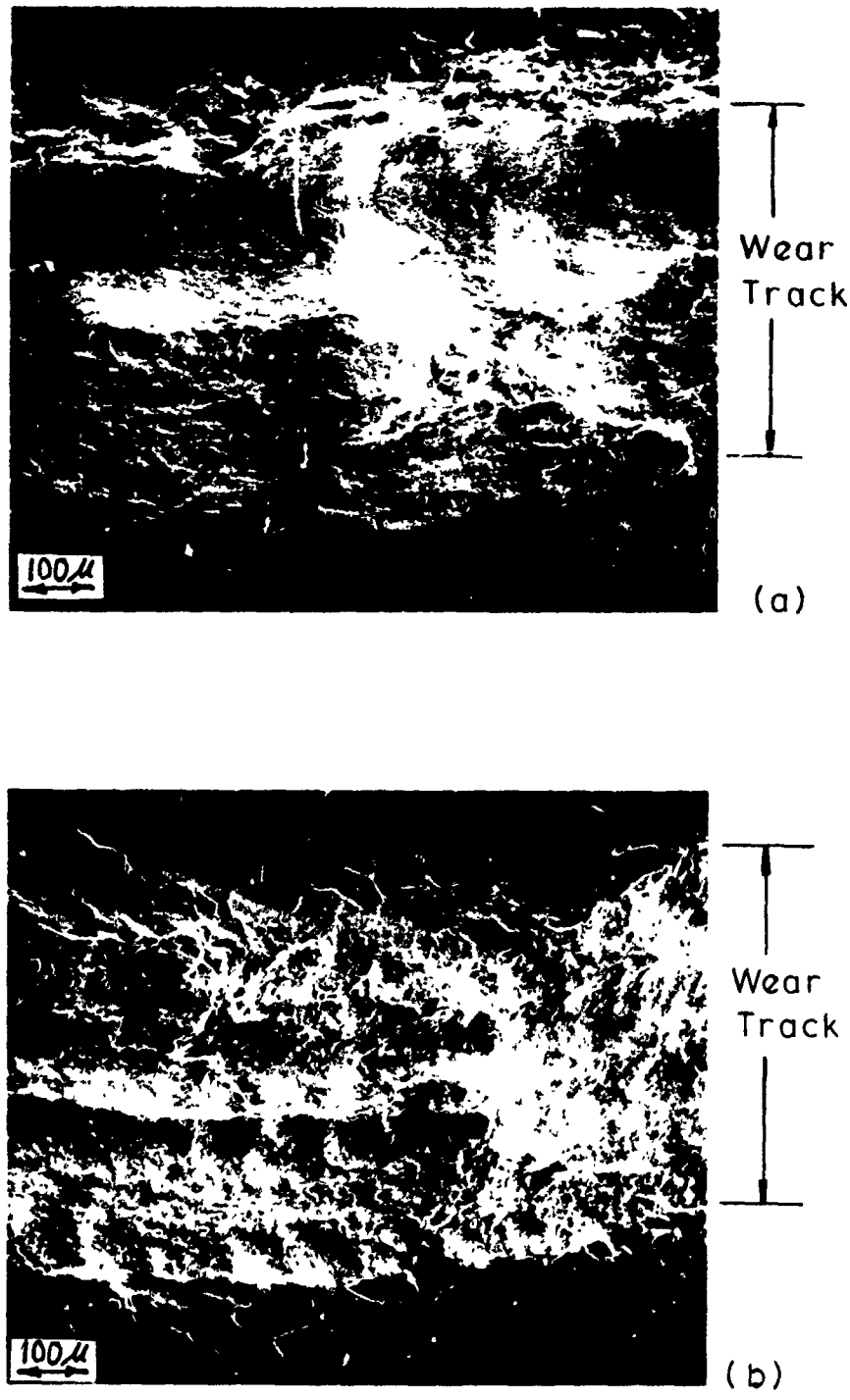

Figure 4.1 Wear tracks of Cd bi-crystal showing extensive deformation and recrystalization.
a) Test No. 2
b) Test No. 3

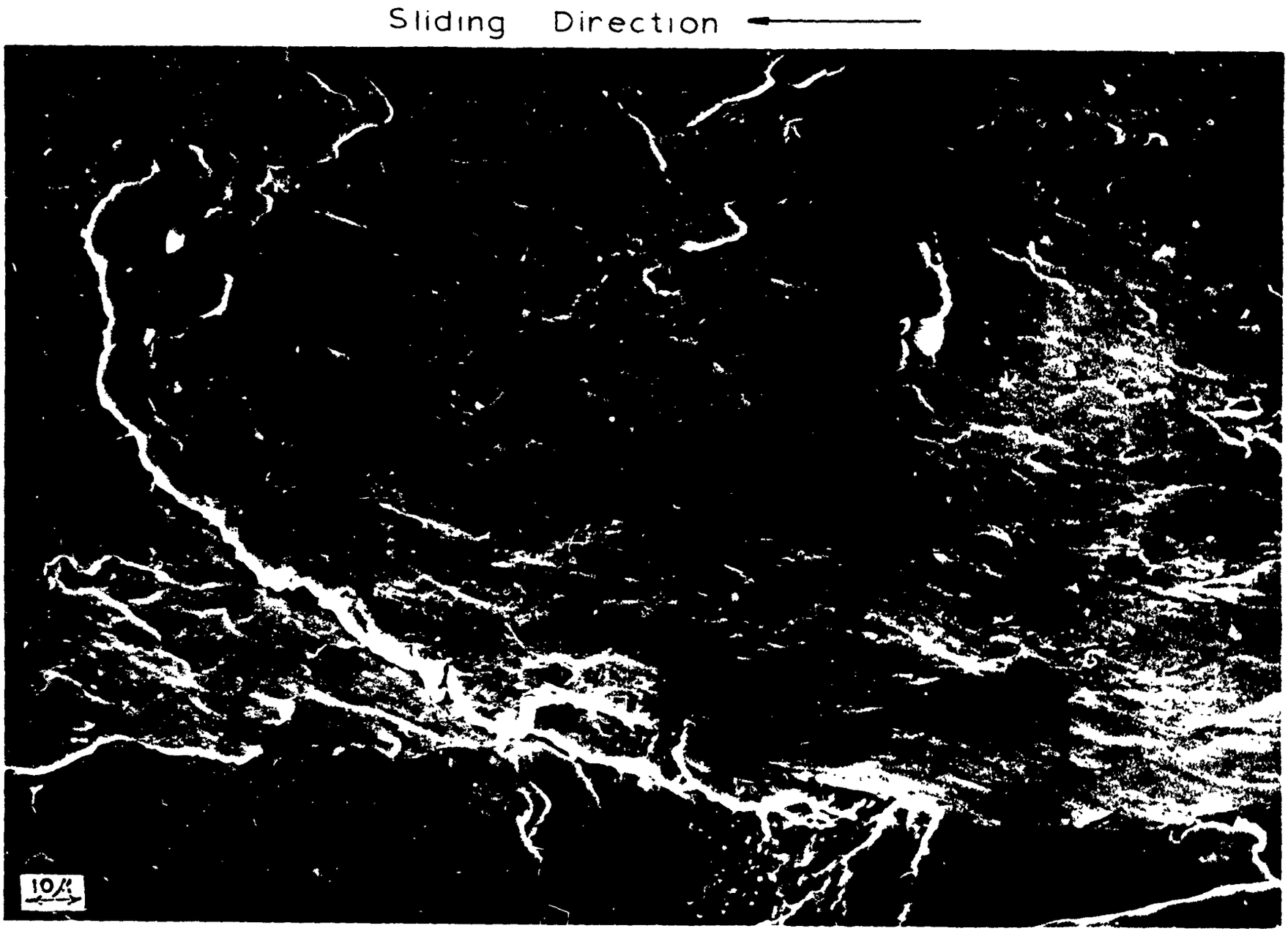

Figure 4.2 Wear sheet on the wear track of Cd bi-crystal (Test No. 1).

of (sliding) deformation.

B) Zinc

Two tests were carried out on annealed pure zinc (Test Nos. 4 and 5). Since this material contained no observable inclusions, it was expected to have a low wear rate. However, the wear was moderate and most of the wear particles were generated from material built-up at the edge of the wear track. These test which were under different loads showed that the wear rate of zinc depends sensitively on the normal load.

C) Pure Iron and Iron Solid Solutions

A series of wear tests were carried out on pure iron, iron-tungsten and iron-molybdenum solid solutions (Test Nos. 6 through 25). The pure zone refined iron (Test No. 6) had a moderate wear rate similar to the zinc sample. Less material was built-up at the wear track edge and delamination was often observed, Fig. 3.1 b.

In order to investigate the effect of alloy concentration on wear behavior, a set of inclusion-free iron-tungsten solid solutions were carefully prepared. Tungsten was added in different amounts to the pure iron by zone levelling. The results of wear tests on this material (Table 1 Test Nos. 6 through 19) showed no significant effect of alloying on the wear behavior, probably because the amount of alloying was very low (500 to 8800 ppm). Delamination was prevalent on the wear tracks of these samples (Figs. 3.10-3.16), even though the material did not contain any inclusions. The subsurface deformation and void nucleation in a Fe-500 ppm W specimen is shown

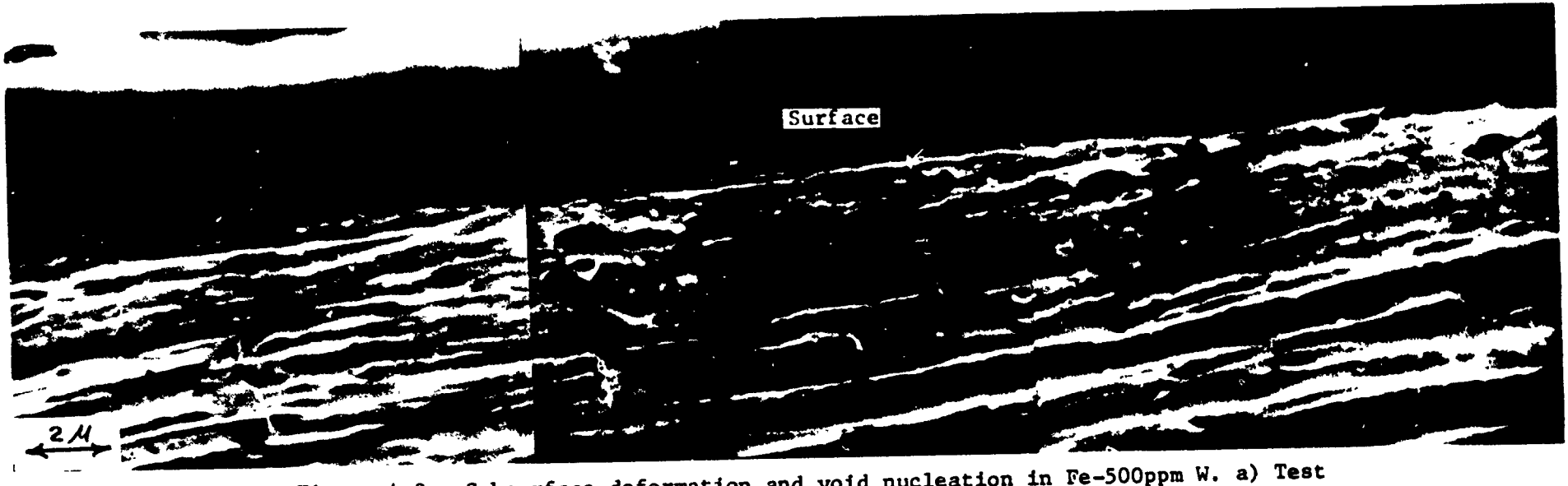

Figure 4.3 Subsurface deformation and void nucleation in Fe-500ppm W. a) Test No. 8 b) Test No. 7.

in Fig. 4.3. The micrograph indicates many subsurface voids and cracks. However, the number of voids and cracks is much less than steel since this material contains no inclusions or second phase particles. The mechanism of subsurface void and crack formation in this material has not been determined. It is clear that in metals with hard second phase particles or inclusions, voids nucleate around these particles by matrix/particle separation. However, in metals without hard particles, voids may nucleate by dislocation interactions or vacancy coalesence, among other possible mechanisms.

All of the wear tests were carried out with AISI 52100 slider pins, except Test No. 9. In that case a Fe-3000 ppm W slider was used on Fe-500 ppm W specimen. The results show that the test with the iron slider had a much higher wear rate than Test No. 10 where a AISI 52100 steel slider was used, even though the friction coefficient was the same. The wear track of the specimen in Test No. 9 is shown in Fig. 4.4. The micrograph indicates that delamination occurs irrespective of the slider material.

Wear tests were also performed on iron-molybdenum solid solution with 1.3 to 5.8% Mo. (This material contained many oxide inclusions, whereas the Fe-W specimens were free of inclusions.) The wear rate did not change significantly (Test Nos. 20 through 25) by increasing the molybdenum content. The wear rate of the specimen with 1.3% Mo (Test Nos. 20 and 21) was considerably higher than the specimens with 2.7 and 5.8% Mo (Test Nos. 22 through 25). Metallographic sectioning of the samples revealed that the material with 1.3% Mo contained many more oxide inclusions than the specimens with higher Mo concentration. The higher wear rates of Fe-1.3% Mo specimens was therefore

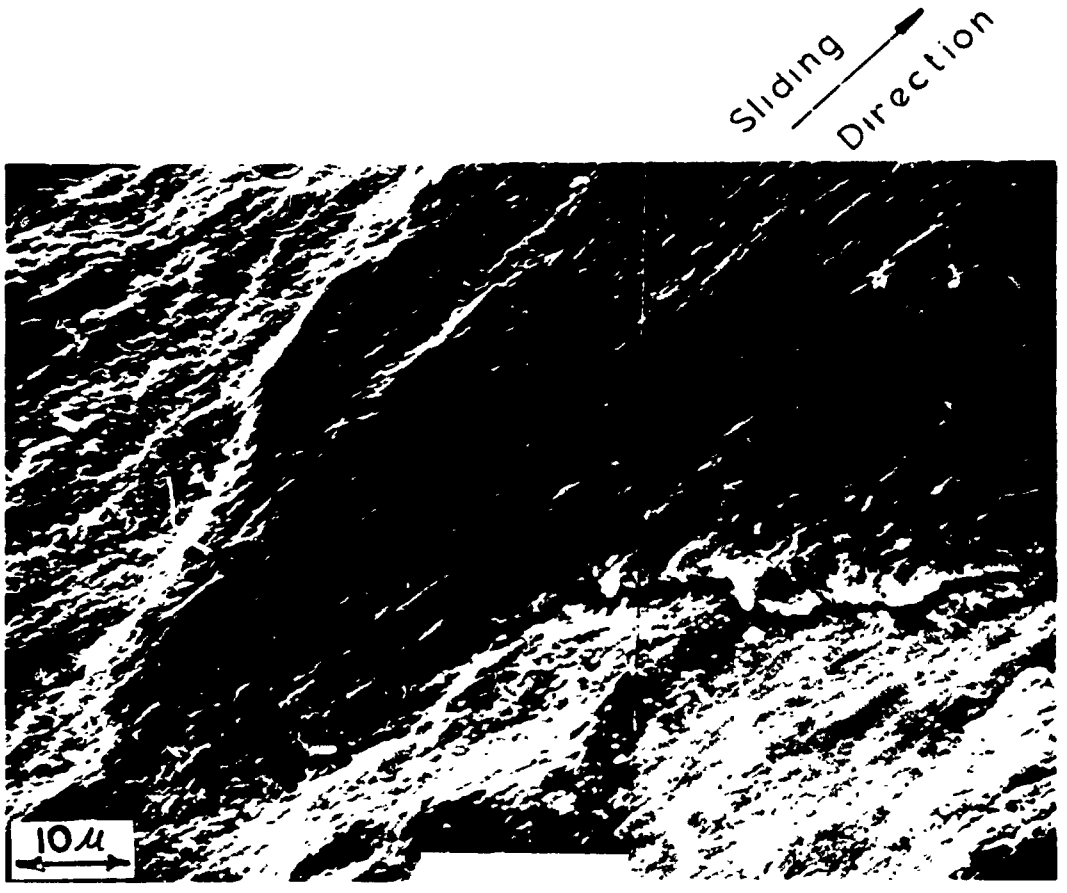

Figure 4.4 Wear sheet on the wear track of Fe-500ppm W (Test No. 9).

attributed to the higher inclusion content, as these have been shown to be the sites for void nucleation (Fig. 3.3).

D) Steel

The steel specimens tested included spheroidized AISI 1010 (Test Nos. 26 through 28) spheroidized AISI 1018, (Test Nos. 29 and 30), specially doped AISI 1020 (Test Nos. 31 through 42), pearlitic AISI 1020 (Test No. 43), pearlitic AISI 1095 (Test No. 44) and fully heat treated AISI 4340 steel. The wear rates of the steels (Test Nos. 41 and 43)* were higher than that of Fe-W and Fe-Mo specimens (Test Nos. 7, 8, 10, 11, 13-19, and 22-25) by a factor of 5 to 12 despite the markedly higher hardness of the steels. This is attributed to the presence of carbide particles.

The effect of inclusions on wear rate is more evident from the tests on AISI 4340 steel. Test Nos. 45 and 46 were conducted on an ESR AISI 4340 steel, whereas Test No. 47 was conducted on a conventionally melted AISI 4340 steel. It is clear that the slag-melted specimen, with fewer inclusions, has a wear rate approximately one-fifth of that of the conventional material.

The subsurface deformation and void formation in a spheriodized AISI 1020 steel is shown in Fig. 4.5. One can observe the nucleation of voids around the carbide particles increasing as the surface is approached. This material had a 5 μm grain size and showed no long subsurface cracks. Under the same test conditions, a commercial spheroidized AISI 1020 steel having a

*Other tests on steels were conducted under different experimental conditions than the tests with iron solid solutions.

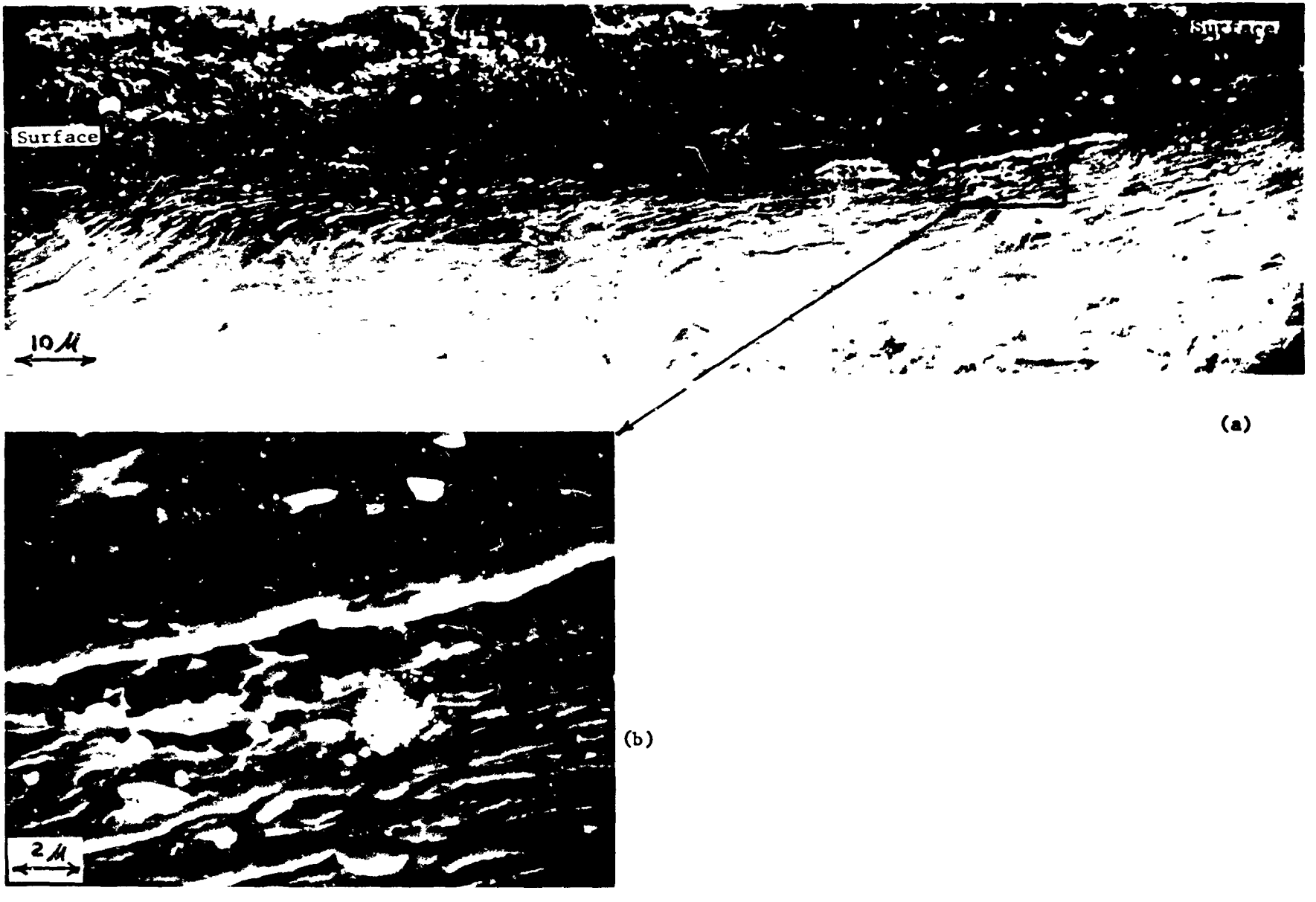

Figure 4.5 Subsurface deformation and void formation in annealed, doped AISI 1020 steel (Test No. 36).

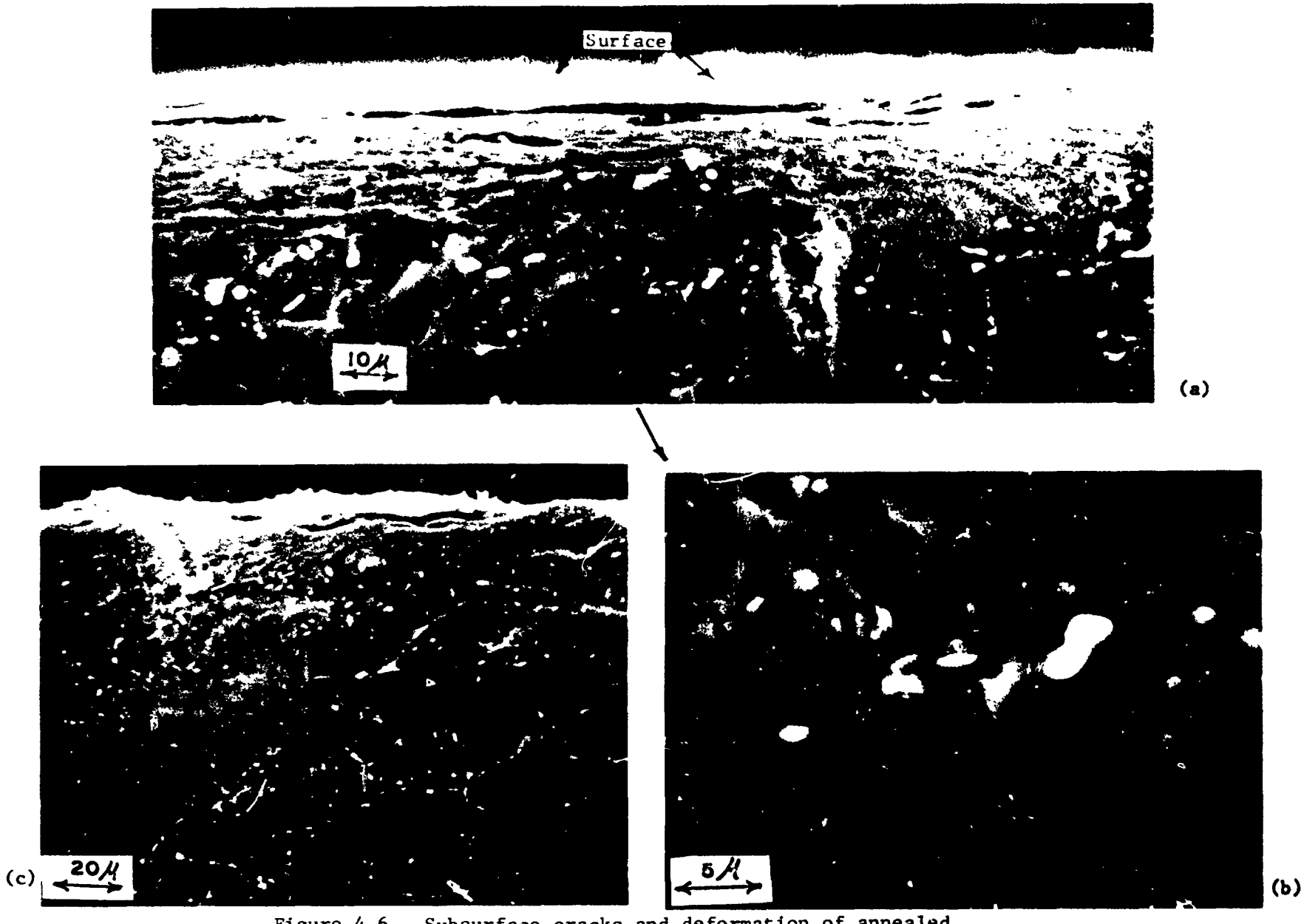

Figure 4.6 Subsurface cracks and deformation of annealed AISI 1020 steel (Test No. 29).

35 μm grain size had many long cracks, as shown in Fig. 4.6. This suggests that grain size may be one of the controlling factors for the rate of delamination.

The morphology of second phase particles has an effect on void formation. In the case of a pearlitic steel, voids may also form by the fracture of the Fe_3C plates, c.f. Fig. 4.7. When a series of these small cracks join, a long subsurface crack will form, Fig. 4.8.

In Fig. 4.7 a, one can see the extensive deformation of the brittle Fe_3C plates. Plastic deformation of brittle materials has only been observed in the presence of a large hydrostatic pressure (35), suggesting that such is the case for the subsurface of a wear track.

Examination of the deformed subsurface of free machining AISI 1020 steel, containing lead, indicated that voids and cracks also form at the interface between the steel and the soft lead, as shown in Fig. 4.9. Since the lead particles do not wet the steel matrix, the particles can be visualized as large voids, after some deformation, generate subsurface cracks.

E) Discussion of the Experimental Results

The experimental results agree with the delamination theory postulation indicating that the process of wear is controlled by void formation, coalescence or shearing of voids to form microcracks, growth of these cracks beneath the wear track to a critical length, and finally shearing to the surface to form a delaminated wear sheet. It has been shown that the rate at which this delamination occurs is controlled by the microstructure. In metals with voids

(a)

(b)

Figure 4.7 Subsurface of AISI 1095 pearlitic steel (Test No. 44)
a) Deformation of pearlite plates
b) Void formation by pearlite fracture

Figure 4.8 A long subsurface crack in AISI 1095 steel (Test No. 44).

Figure 4.9 Subsurface crack formation from Pb particles in AISI 1020 steel under a load of 2.25 kg in argon.

and inclusions, the rate at which void formation will occur is directly dependent upon hard second phase particles and/or voids.

It is clear that inclusions are the sites for crack nucleation and propagation. Figs. 3.3-3.5 and 4.5-4.8 are, among others, are a qualitative demonstration of crack nucleation and propagation from the site of inclusions. Voids form around inclusions due to plastic deformation. The additional shear deformation tends to spread the voids into cracks around the particles. With further deformation, these cracks then develop parallel to the shear strain direction. When the inclusion is not spherical but rather an elongated sheet, cracks may form when the total shear force at the inclusion surface exceeds the cohesive strength of the inclusion, c.f. Fig. 4.7 b. The process of void and crack nucleation from second phase particles is not yet clearly understood, even for a metal undergoing general bulk plastic deformation [36,37]. However, the complex state of loading near the surface is more involved than the corresponding problem in the bulk and no known solution exists for the problem.

The experimental results show that voids existing in a matrix aid the process of wear sheet formation. For bulk deformation of metal it has been generally established that voids can be expanded plastically under various states of shear and normal stresses [36]. McClintock and his coworkers showed that cylindrical voids in an infinite viscous body deform into elliptical voids, its major axis reaching a steady-state eccentricity when subjected to tension and shear and that the voids close under pressure and shear [25]. Even for voids near the surface where severe plastic strain gradient exists,

it can be shown experimentally that a spherical void deforms into a relatively ellopsoidal shape under certain loading conditions. Preliminary experimental results with plasticine show that cracks may develop from these elongated holes [38].

The results obtained with essentially pure iron and iron solid solutions without any voids and inclusions clearly indicate that voids form during the deformation of the subsurface layer, the void density increasing toward the surface. The rate of void formation and the wear rate however, is much slower than when there are large second phase particles and inclusions. In single phase metals voids may nucleate through the coalescence of microvoids and vacancies during plastic deformation of the subsurface layer. The density of voids will then be controlled by the subsurface stresses and strains.

The experimental results with the soft metals show that hardness is not necessarily a good measure for wear resistance, since these metals had low wear rates despite their softness. An ideal metal for low wear applications should be one which does not have any inclusions or voids and yet have high flow stress. Argon, et al. [39] showed theoretically that when the inclusion diameter is less than about 400 Å, there is insufficient elastic energy stored around the surronding matrix of the inclusion to form a stable crack. Therefore, a high flow stress may be achieved, without imparing the wear characteristics, by having a metal with second pahse particles less than 400 Å in diameter.

Table 1 Experimental Condition and Results

Test No.	Material	Hardness Kg/mm^2	Test Geometry	Normal Load Kg	Sliding Speed cm/Min	Sliding Distance m	Friction Coeff.	Wear Rate $gm/cm \times 10^{-7}$	Wear Factor $cm^3/Kg.\ m \times 10^{-8}$
1 ≠a	Cd Bi-crystal	20	Pin-on-disk	0.01	95	47	-	-	-
2	"	"	"	"	"	30	-	-	-
3	"	"	"	"	"	47	-	-	-
4	Zn	34	Cylinder-on Cylinder	2.25	180	54	0.5	2.6	1.7
5	"	"	"	1.15	"	126	"	0.3	0.4
6	Fe	34	"	2.25	"	54	0.7	4.8	2.7
7	Fe-500ppm W	35	"	"	"	18	0.5	1.1	0.6
8	"	"	"	"	"	90	0.6	0.7	0.4
9*	"	"	"	"	"	54	"	22.3	12.4
10	"	"	"	"	"	"	0.5	3.3	1.8

≠Tests No. 1-5 were run in air, others in an argon atmosphere unless specified.

[a]The slider was AISI 52100 steel in all tests except test No. 9.

*The slider used was Fe-3000ppm W.

Table 1 (Cont.)

Test No.	Material	Hardness Kg/mm^2	Test Geometry	Normal Load Kg	Sliding Speed cm/Min	Sliding Distance m	Friction Coeff.	Wear Rate $gm/cm \times 10^{-7}$	Wear Factor $cm^3/Kg.cm \times 10^{-8}$
11	Fe-3000ppm W	35	Cylinder-on-Cylinder	2.25	180	54	0.5	2.2	1.2
12**	"	"	"	"	"	"	'	6.7	3.7
13	Fe-4000ppm W	"	"	"	"	90	0.6	2.3	1.3
14	"	"	"	"	"	54	"	0.7	0.4
15	"	"	"	"	"	"	0.7	0.7	0.4
16	"	"	"	"	"	90	0.6	2.1	1.2
17	Fe-8800ppm W	56	"	"	"	"	0.5	1.1	0.6
18	"	"	"	"	"	"	"	1.8	1.0
19	"	"	"	"	"	"	0.6	1.9	1.1
20	Fe-1.3% Mo	80	"	"	"	21	0.7	9.6	5.3
21	"	"	"	"	"	"	"	4.8	2.7
22	Fe-2.7% Mo	84	"	"	"	54	0.6	1.9	1.1
23	Fe-5.8% Mo	116	"	"	"	21	0.8	1.4	0.8
24	"	"	"	"	"	"	0.9	1.4	0.8
25	"	"	"	"	"	105	0.7	2.1	1.2

**This is the slider used for Test No. 9.

Table 1 (Cont.)

Test No.	Material	Hardness Kg/mm^2	Test Geometry	Normal Load Kg	Sliding Speed cm/Min	Sliding Distance m	Friction Coeff.	Wear Rate gm/cm x 10^{-7}	Wear Factor $cm^3/Kg.cm$ x 10^{-8}
26	AISI 1010 Steel	120	Pin-on-flat reciprocating	1.8	76	45	0.7	2.7	1.9
27	"	"	"	"	"	"	"	1.6	1.1
28	"	"	"	"	"	"	0.8	4.0	2.8
29	AISI 1018	80	"	"	"	69	"	3.3	2.3
30	"	"	"	"	"	"	"	1.4	1.0
31	Doped AISI 1020 Steel	120	"	"	"	45	0.9	5.6	3.9
32	"	"	"	"	"	"	1.0	6.2	4.3
33	"	"	"	"	"	"	0.9	4.9	3.4
34	"	"	"	"	"	"	"	4.7	3.3
35	"	"	"	"	"	"	1.0	4.5	3.1
36	"	98	"	"	"	"	"	3.5	2.4
37	"	"	"	"	"	"	"	3.1	2.2
38	"	"	"	"	"	"	"	3.3	2.3
39	"	110	"	"	"	69	0.7	2.2	1.5
40	"	"	"	"	"	"	"	2.2	1.5

Table 1 (Cont.)

Test No.	Material	Hardness Kg/mm^2	Test Geometry	Normal Load Kg	Sliding Speed cm/Min	Sliding Distance m	Friction Coeff.	Wear Rate gm/cm $\times 10^{-7}$	Wear Factor $cm^3/kg.cm \times 10^{-8}$
41	Doped AISI 1020 Steel	83	Cylinder-on-Cylinder	2.25	180	54	0.5	10.8	6.0
42	"	"	"	0.42	"	"	"	2.0	6.0
43	AISI 1020 Steel	145	"	2.25	"	"	"	8.5	4.7
44	AISI 1095 Steel	240	Pin-on-Cylinder	1.8	430	65	-	-	-
45	AISI 4340 Steel Slag-melted		Cylinder-on-Cylinder	1.6	230	69	0.5	0.7	0.5
46	"	"	"	"	"	"	0.4	0.5	0.4
47	AISI 4340 Steel	"	"	"	"	"	0.5	2.2	1.7
48	Doped AISI 1020 Steel*	184	Pin-on-Flat reciprocating	1.8	76	45	0.3	1.3	0.9
49	"	"	"	"	"	"	0.3	2.0	1.4
50	"	"	"	"	"	"	0.4	1.5	1.0
51	OFHC Copper	35	Cylinder-on-Cylinder	2.25	180	81	1.0	0.4	0.2
52**	"	40	Pin-on-Flat reciprocating	1.8	76	15	0.9	5.3	3.3
53	"	35	Cylinder-on-Cylinder				-	-	

*Cold Worked Condition.

**Tested at 120°C.

Chapter 5

THE EFFECT OF SLIDING DISTANCE ON WEAR AND WEAR PARTICLES

The adhesion theory states that the worn volume depends linearly on the sliding distance [9], which has some experimental support [14,40]. However, practical experience and laboratory investigations have shown that this dependence is not general and, under most conditions, the weight change is not a linear function of the sliding distance [41-45]. Since the wear rate varies with the sliding distance, one may conjecture that the morphology and the mechanism of wear particle formation also changes with the sliding distance. This phenomenon is described in the present chapter in terms of the delamination theory of wear; and it is supported by some preliminary experimental evidence.

A) Review of Earlier Work

On the initiation of sliding, a large weight change is observed; eventually, the weight loss decreases to a steady state value [41]. This phenomenon, known as the "run-in", is generally observed in most machines [42]. Sasada et al. [43,44] attributes this behavior to the transfer of particles from one surface to the other and oxidation of both surfaces to reduce the wear rate. This explanation can only be true in air and could not occur under lubricated conditions, yet "run-in" is also observed when the surfaces are lubricated. Queener, et al. [42] correlated the "run-in" behavior to the removal of the original surface asperities. Their study showed that under lubricated conditions the "run-in" wear depended on the original surface roughness. Dorinson and Broman [45] have shown that following the steady

state wear regime, the weight change increases drastically if the sliding is continued. This catasrophic state of wear was found to depend on the normal load, i.e., the transition to the severe wear occured at shorter sliding distances for higher loads.

B) Experimental Results and Discussion

Cylinder-on cylinder type of wear tests were conducted on OFHC copper specimens annealed at 350°C for one hour in vacuum. (Please refer to the Appendix D for details of the experimental set-up and procedure.) The tests were run without lubricant under a normal load of 1.15 Kg. at a surface speed of 180 cm/min in argon, for different sliding durations. The specimens were degreased and weighed before and after the tests to an accuracy of 0.05 mg. The wear particles were collected and observed by scanning electron microscopy.

The result of the weight change as a function of sliding distance is shown in Fig. 5.1. It is observed that the weight change is large initially, but it is reduced to a steady value after about 10×10^3 cm of sliding. During this initial stage, wear particles form from the deformed asperities and/or the material build-up at the edge of the wear track c.f. Fig. 5.2. When the slider passes over the asperities, a plowing action occurs and the asperities smear to fill the valley, Fig. 5.3. Eventually the deformed and smeared asperities separate to form plate-like wear particles, such as the one shown in Fig. 5.4 a. Wear particles in this stage may also be generated from the material build-up at the edges of the wear track. These particles, are generally elongated as shown in Fig. 5.4 b.

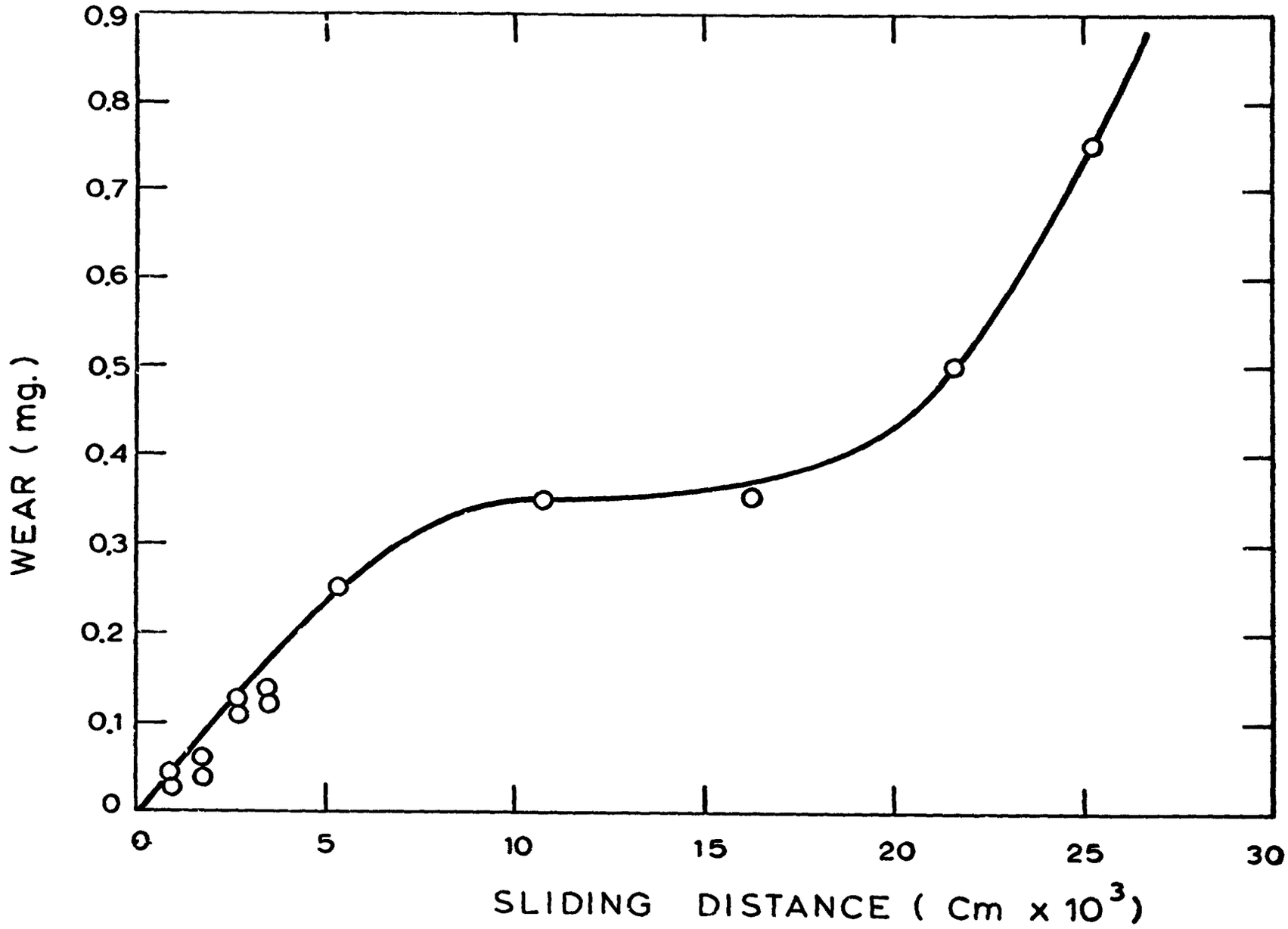

Figure 5.1 Weigh loss as a function of sliding distance for OFHC copper sliding under a load of 1.15 kg in argon.

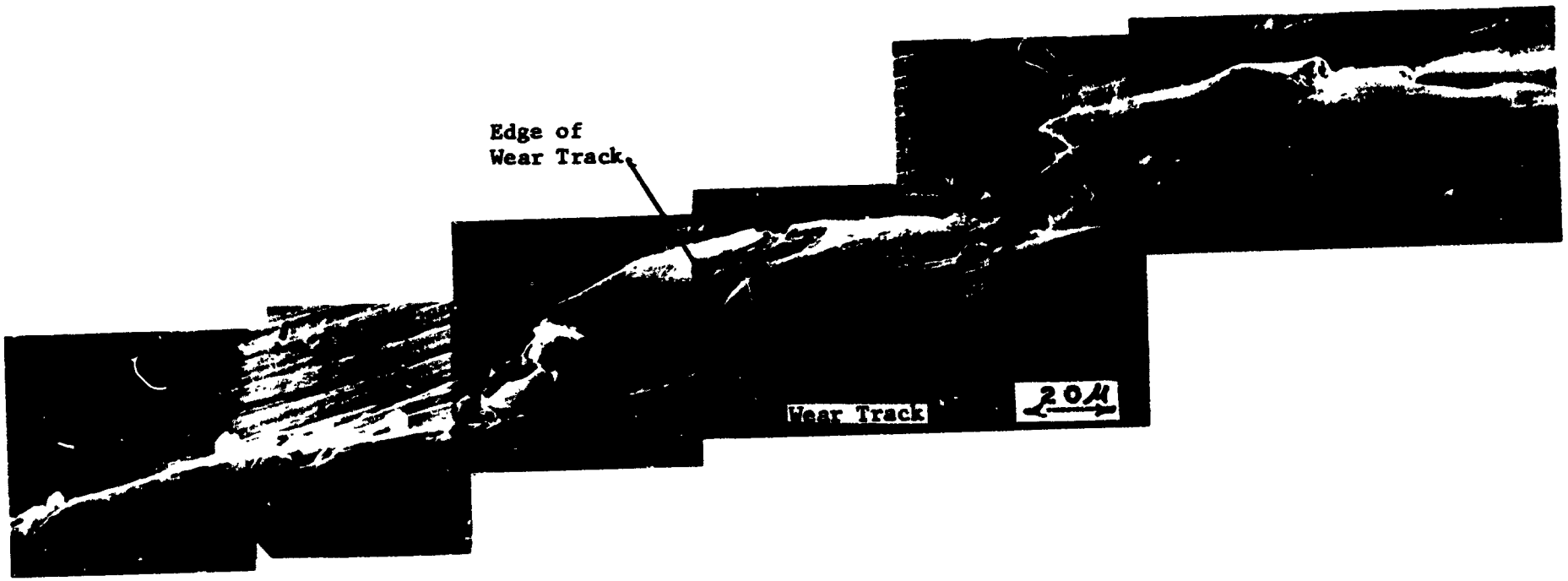

Figure 5.2 Pile-up at the edge of wear track in OFHC copper.

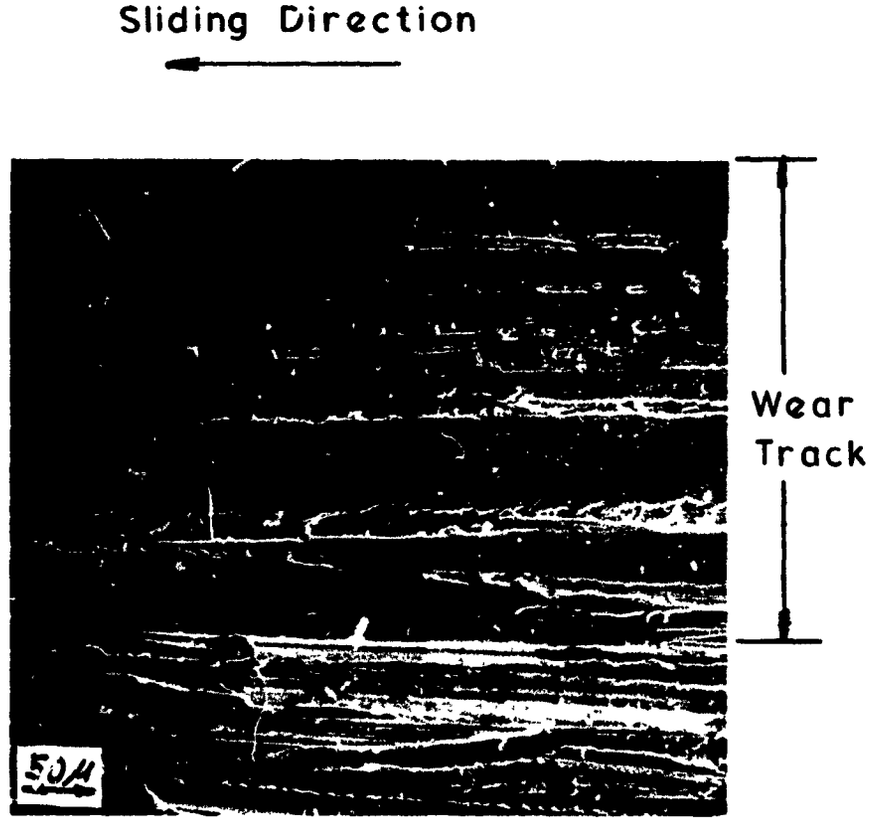

Figure 5.3 Initial smoothing of the wear track; after 36 cm of sliding.

(a)

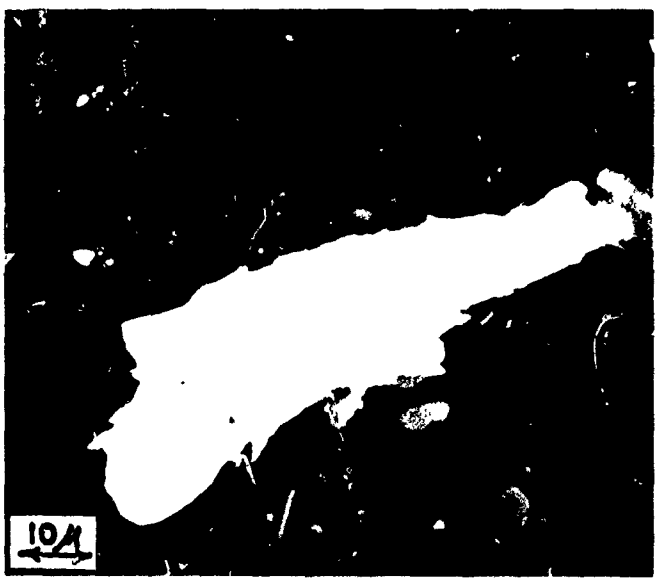

(b)

Figure 5.4 Wear particles in the transient stage, after 9×10^3 cm of sliding.
a) From the deformed asperities
b) From edge of wear track

After the origianl asperities have been deformed and separated, a smooth surface will be produced containing furrows in the sliding direction, Fig. 5.5 a. There is little perceptible change in weight during this stage. However, subsurface deformation continues, generating subsurface voids. With continued sliding, the subsurface cracks reach the critical length and shear to the surface, as shown in Fig. 5.5 a. Further sliding leads to the wear sheet generation, Fig. 5.5 b, which is the beginning of the catasrophic wear regime.

The fact that the transition between the three regimes depends on the normal load [45], is consistent with the above results and discussion. The higher the normal load the greater will be the asperity and subsurface deformation, thus shortening the first two regimes of wear and hastening catastrophic wear.

The proposed correlation between the weight change and the wear particle formation mechanism will be investigated more completely in the next phase of this program, and will be extended to other materials.

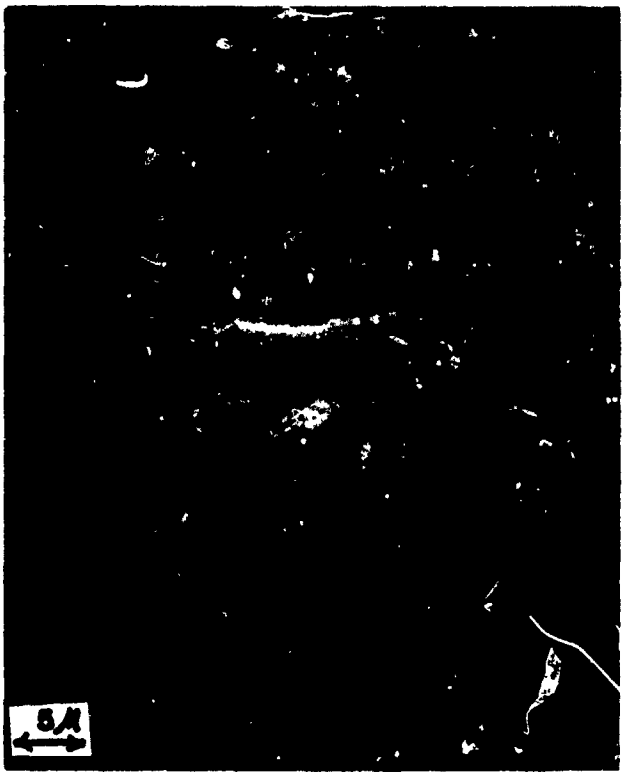

(a)

Sliding Direction

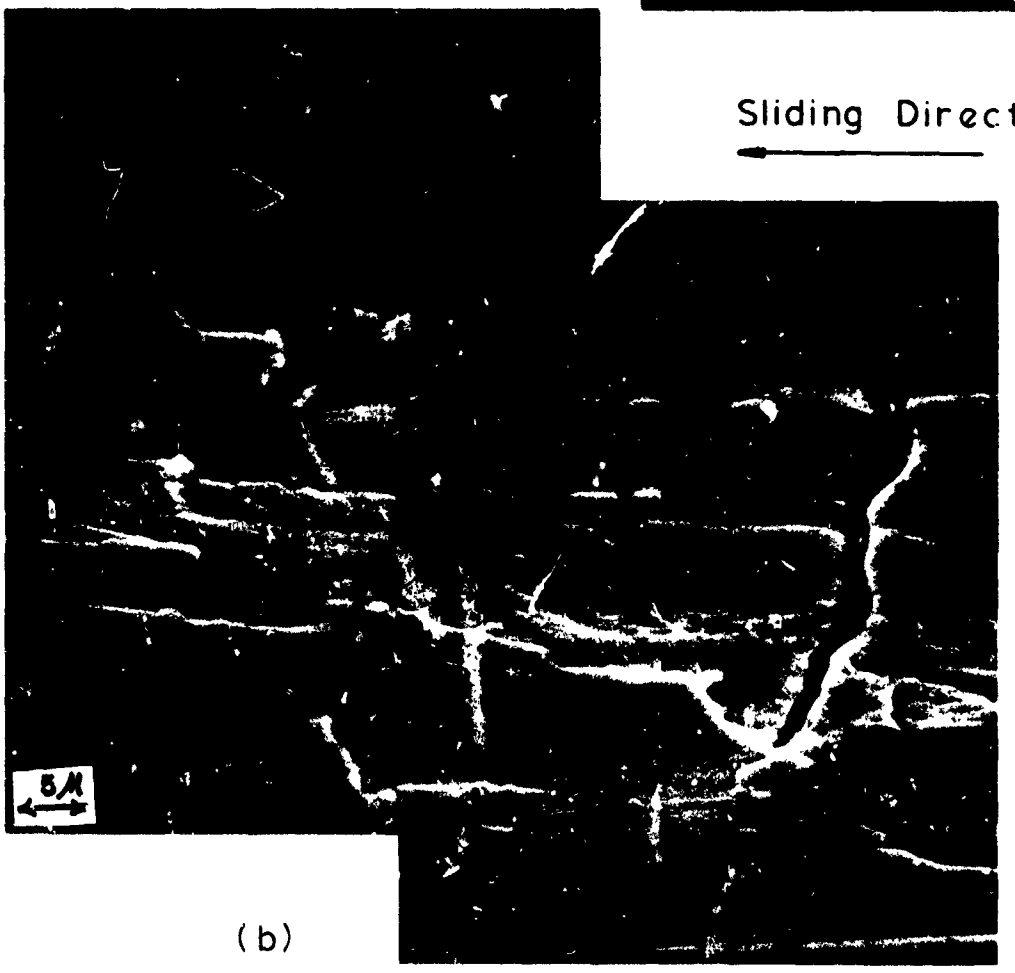

(b)

Figure 5.5 Wear surface topography at the end of steady state regime.
a) Subsurface crack reaching the surface
b) Wear sheet formation

Chapter 6

PREVENTION OF WEAR

The experimental evidence of the preceeding chapters has shown that sliding wear of metals does occur by the delamination process. It was also shown that wear occurs only at a surface layer and that the presence of the inclusions or incoherent second phase particles accelerates the wear process by increasing the rate of delamination. Therefore, the best material for sliding wear situations must be single phase material with no inclusions and yet have a high flow stress to support the normal stress at the point of contact. However, the production of such a material will be costly, if it is technically possible, and may not be economical for many sliding applications.

Therefore, one alternative procedure is to produce a composite surface of a pure, soft metal on a relatively hard, but economical material. The soft layer must be very thin in order that it will not delaminate within itself through dislocation accumulation. This chapter describes the results with cadmium plated steel.

A) Application of the Delamination Theory of Wear to Composite Metal Surfaces

The delamination theory of wear postulates the existance of a soft, low dislocation-density zone at the outer surface of the wear track. This layer would be softer than the subsurface and could deform continuously without much work hardening. Therefore, if a composite metal surface is created by depositing a thin layer of a softer metal on a harder substrate, heavy plastic deformation and delamination of the substrate may be prevented.

This is based on the fact that dislocations are not stable in very thin layers of metals having a low flow stress.

In a conventional homogeneous material the dislocations pile up and tangle beneath the soft layer. When the dislocations are generated in a composite material with an extremely soft outer layer and a much stronger substrate, they pile up at the interface between the deposited metal and the substrate. As the slider moves on, these dislocations escape through the surface of the wear track if the deposited soft metal is very thin. The forces acting on dislocations in metals with low shear modulus are such that these dislocations are repelled from the interface [46]. In the case of very high stresses there will be some transfer to and generation of dislocations in the substrate material. However, the dislocation transfer will be considerably less than would be observed on an uncoated material because of the lower tangential force transmitted. Thus the composite surface will markedly delay delamination of the substrate material.

Following the development of this method to prevent wear, a review of the literature indicated that others had tried coatings to reduce wear. However, without the benefit of a theoretical foundation, their results were for relatively thick coatings or for coatings on one surface only.

B) Review of the Earlier Work on the Wear of Composite Metal Surfaces

Tsuya and Takagi [47] electroplated one of their copper sliding surfaces with 6 to 75 μm lead. They found that under a stress of 10 kg/cm^2, in air, the lead film was subjected to wear until a stable layer of 2 μm remained on the surface. Some of this lead was transferred to the unplated copper surface

and formed a stable film of 2 μm thick. The wear tracks of these samples were very smooth containing fine parallel lines in the sliding direction. This investigation was extended by Takagi and Liu [48] to AISI 440C stainless steel and AISI 52100 steel and 0.1 μm of gold electrodeposits on one of the sliding surfaces. The best results occurred for the AISI 440C stainless steel sliding on 0.1 μm gold plated AISI 52100 steel or 440C stainless steel. However, the wear was only reduced by a factor of 2 to 3. Takagi and Liu [49] extended this investigation by considering two gold alloys, silver, copper, and nickel electroplating on AISI 52100 and 440C steels. In these tests only the rotating surface was plated and the normal load used was 60 kg. They found that a 20 μm gold, copper or silver plate on AISI 52100 steel was needed for wear rate reduction. The thicker coating required in this series of tests was attributed by Takagi and Liu to the higher normal load, but it has been found [7] that the optimum thickness of the plate does not depend on the normal load. Therefore, the thicker coat which was required in the tests conducted by Takagi and Liu may be due to the fact that only one surface was plated, resulting in abrasive wear of the coating.

Solomon and Antler [50] investigated the effect of load and thickness of gold, silver-gold and nickel-gold alloys electroplated on both sliding copper surfaces. They found that beyond a critical thickness (depending on load and the substrate material) resistance to wear increased dramatically. These results were improved if a very thin nickel plate was used on copper before the gold and gold alloy electrodeposition. It may be speculated the hard nickel layer prevented the subsurface deformation of copper.

Kuczkowski and Buckley [51] coated nickel and AISI 440C stainless steel with 25 μm of various binary and ternary alloys of gallium and indium. A ternary alloy of gallium, indium, and tin reduced the wear rate of AISI 440C stainless steel in vacuum by four orders of magnitude. The wear rate of nickel was reduced by the same amount when the surface was coated with a binary alloy of gallium and indium. However, they did not investigate the influence of the plating thickness on the wear rate.

The process of electroplating the sliding surfaces with precious metals has been applied to ball bearings [52-55], and gears [56-57] operated in a vacuum. Even though the life was increased in these applications, the components still exhibited a high degree of wear. This is probably due to the thick (30-75 μm) coatings used.

In a previous paper by the authors [7], it was found that thickness of the deposited layer is one of the primary factors, if any major improvements in wear characteristics are to be achieved. This phenomenon is discussed in the chapter for cadmium electrodeposited on steel.

C) Experimental Investigation on the Application of the Delamination Theory

1) Procedure

Wear tests were carried out on a lathe by employing a cylinder on cylinder geometry. The specimens were rotated at a surface speed of 180 cm/min and the stationary pins were pushed against the specimens by a normal load of 2.25 kg. The normal and friction forces were measured by a dynamometer and a Sanborn recorder. A more complete discussion of the experimental set-up can be found in Appendix D.

The material tested was AISI 1018 steel, commercially electroplated with cadmium to various thicknesses ranging from 0.05 to 10 μm. The specimens were 0.63 cm in diameter by 7.6 cm long with a 16RMS ground finish prior to plating. All steel specimens were annealed at 670°C for 10 hours in $5x10^{-5}$ torr vacuum before plating.

The slider pins were prepared of the same material as the specimens using similar procedure. They were 0.63 cm in diameter and 3.8 cm long. The sliders were electroplated to the same thickness as the cadmium on the mating specimens.

Prior to testing, the specimens were degreased and weighed to an accuracy of 0.05 mg. The wear tests were carried out dry, both in air and in argon gas. A chamber was constructed around the mating surfaces and argon entered at a rate of 5 lit/min. All tests were performed at room temperature for a sliding distance of 54 meters. Some wear tests were also conducted under boundary lubrication in air. Gulftex 39 or a pure mineral oil (Nujol) was gravity fed to the contact at a steady rate.

Following the tests, the specimens were carefully brushed to remove the loose wear particles and weighed. The wear tracks were observed with the scanning electron microscope. The specimens were then sectioned parallel to the wear track metallographically polished and etched with 1% Nital to reveal the structure. The scanning electron microscope was then used to observe the subsurface damage.

2) Results

The results of the wear tests in argon and in air are presented in Fig.

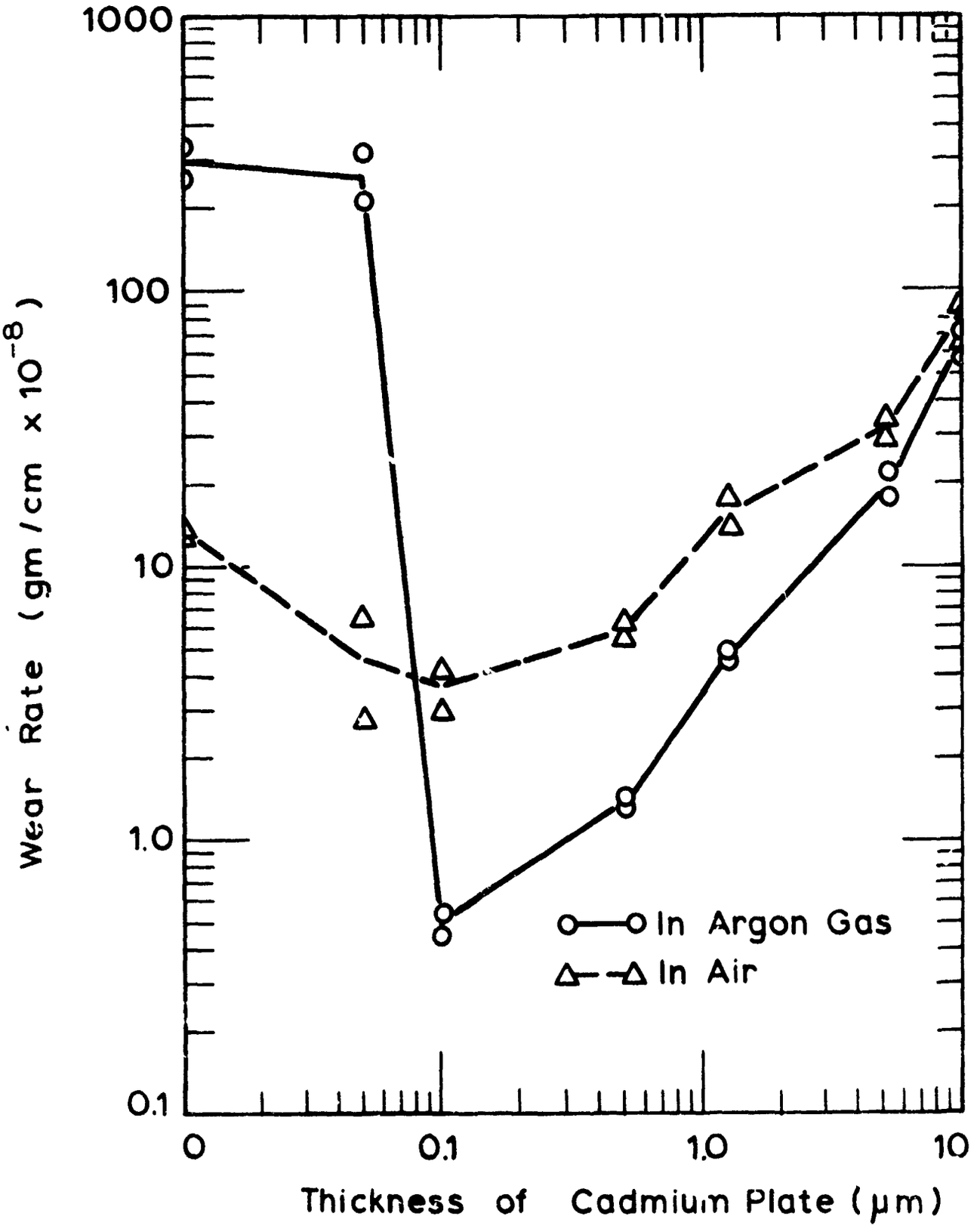

Figure 6.1 The effect of cadmium plate thickness on the wear rate.

6.1. The graph indicates that the wear rate in argon decreases by nearly three orders of magnitude when both sliding members are electrodeposited with 0.1 μm of cadium. For plates thinner than 0.1 μm, the cadmium wears off at the beginning of the test and the wear rate is nearly equal to that of the unplated steel. Conversely, when the thickness of the cadmium layer is larger than 0.1 μm, the cadmium layer is subjected to wear by delamination until a thin layer of Cd remains on the surface for steady state wear. This is quite consistent with the previous results of the authors [7].

In order to make sure that these results were not limited to the experimental geometry employed in these tests, a series of annular wear tests were conducted in argon on similar materials. An annular specimen of 2.5 cm OD, having 5.3 cm^2 contact area was pressed under a load of 22.5 kg, on another annular sample rotating at 60 RPM for 15 minutes. Similar results were obtained both for the 0.1 μm Cd plated steel and for the thicker coatings.

The wear tracks of the unplated samples appeared to be very rough when compared with that of 0.1 μm cadmium plated steel tested in argon, as shown in Fig. 6.2 a and 6.2 b, respectively. The cratered appearance of the unplated steel indicates that many wear sheets have been separated from the wear track. The wear track of the plated sample, on the other hand, is much smoother with parallel furrows in the sliding direction. Only a few indications of delamination were observed on the 0.1 μm Cd plated steel specimens.

In a previous paper [7], it was observed that thicker Cd plates wear by delamination until a thin layer (probably 0.1 μm) remains for steady state wear. This was further substantiated by an extended test on the thicker

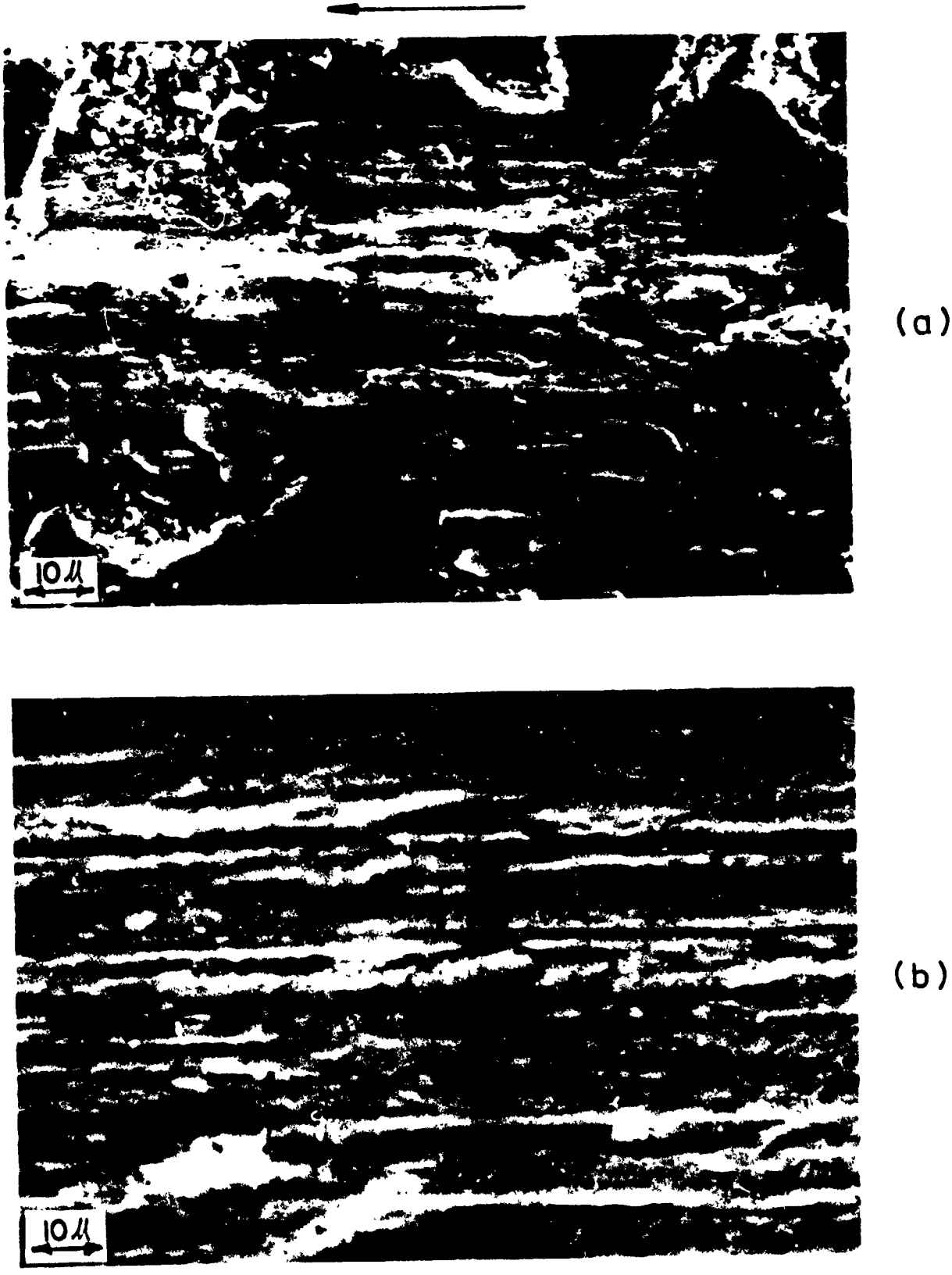

Figure 6.2 Wear tracks in argon gas under a load of 2.25 kg after 45m sliding distance.

a) Unplated steel
b) 0.1 μm Cd plated steel

coatings. The results showed no increase in weight loss after the thin layer was attained. Fig. 6.3 shows the smooth wear track of 10 μm Cd plated steel in the steady state. The micrograph shows no evidence of delamination initiated from the substrate, and only a few indications of delamination were observed over the wear track.

Figure 6.4 compares the subsurface damage and deformation of the unplated steel (Fig. 6.4 a) and the 0.1 μm Cd plated steel (Fig. 6.4 b) tested in argon. In both cases the normal stress exceeded the yield strength of the substrate, (hardness of the specimen, 84 kg/mm^2; contact stress based on Hertzian stress analysis, 130 kg/mm^2). The plated sample has undergone less deformation and contains a smaller number of subsurface voids and cracks. The depth of subsurface deformation in the unplated sample is 30-35 μm while the deformation depth in the plated steel is only 25-30 μm. The fact that the plated samples have some voids and cracks in the steel substrate indicates that the cadmium layer will eventually be removed when the steel subsurface delaminates. An extended test in argon with a 0.1 μm Cd plated specimen exhibited subsurface delamination after 86 m of sliding. The unplated steel specimen tested for the same distance of sliding had a weight loss greater than the Cd plated specimen by a factor of 5000.

The results in Fig. 6.1 indicate that a much smaller wear rate reduction was achieved by cadmium plating when the tests were carried out in air. However, the lowest wear rate is still obtained with the 0.1 μm Cd plating. Fig. 6.1 also shows that the wear rates are higher in air than in argon when the cadmium layer is thicker than 0.1 μm. The poor performance of Cd plated steel

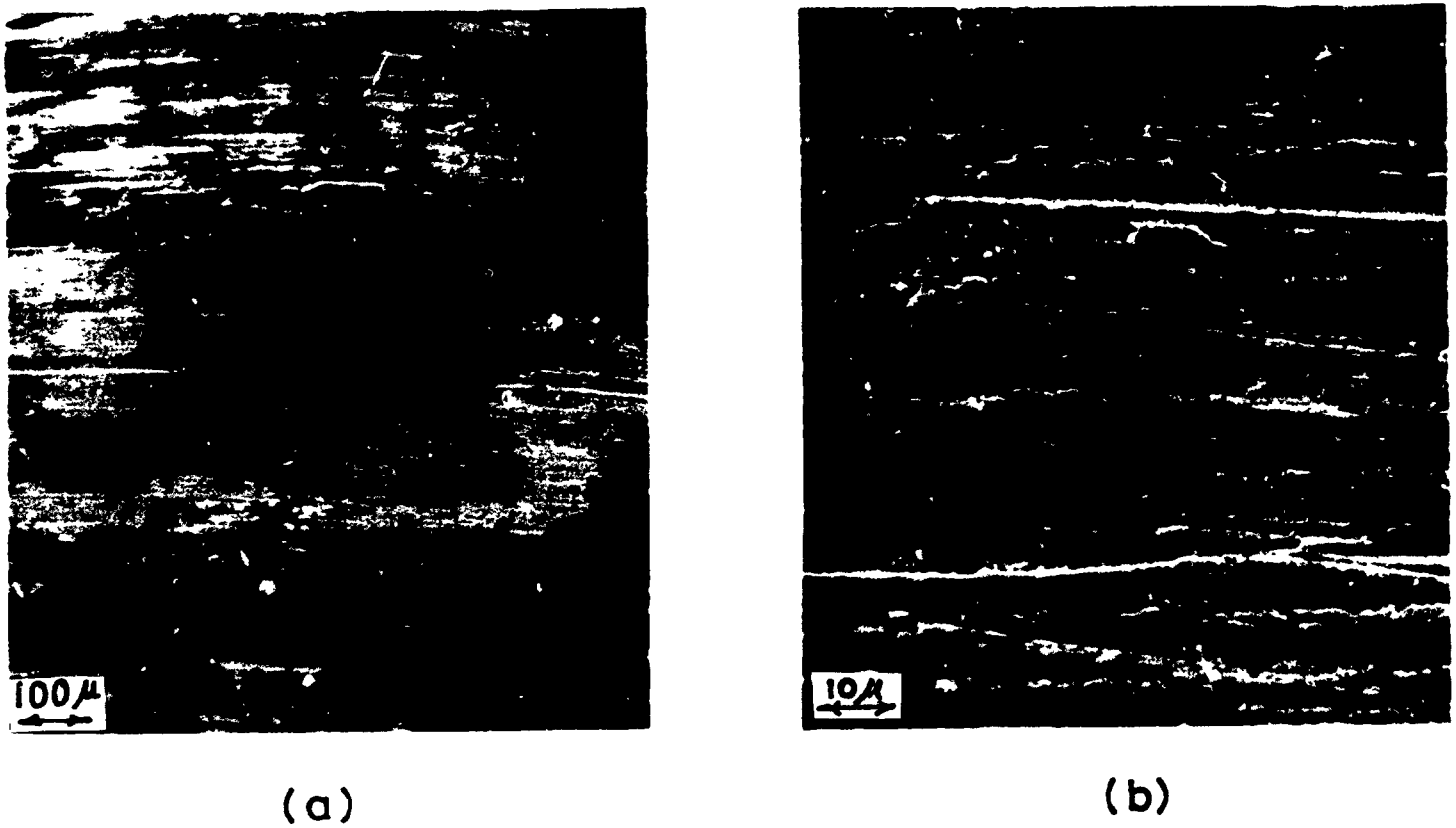

Figure 6.3 Smooth wear track of 10 μm Cd plated steel tested in argon. b) Is a higher magnification of an area in (a).

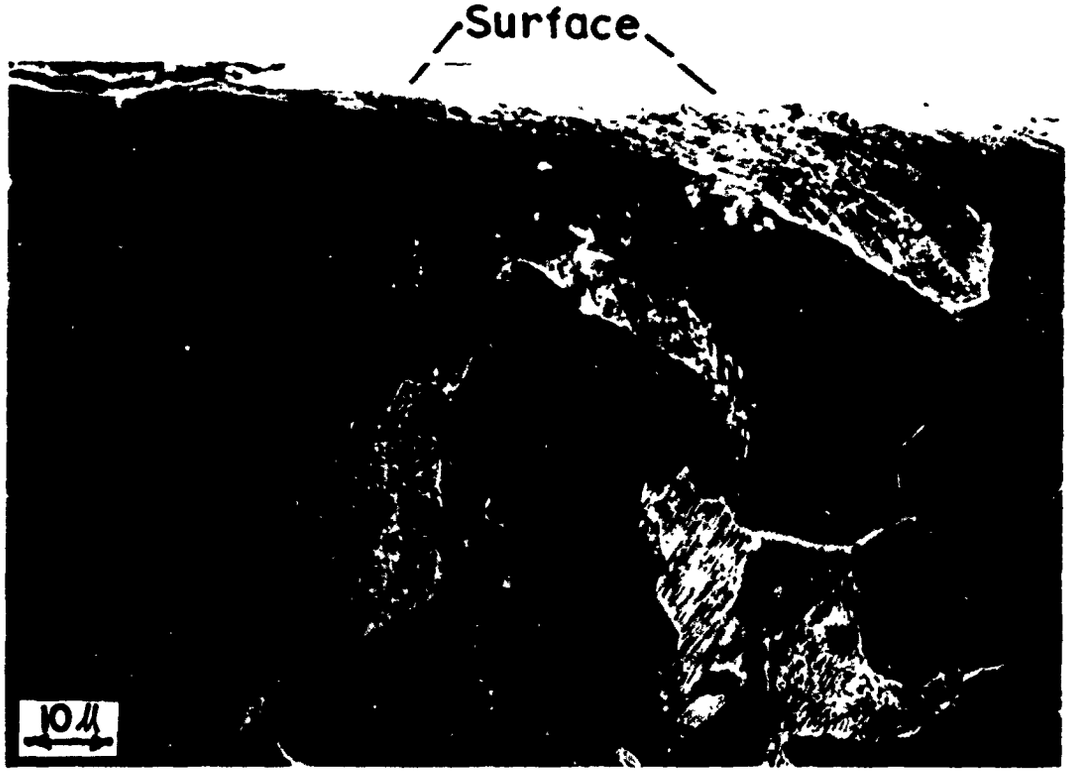

(a)

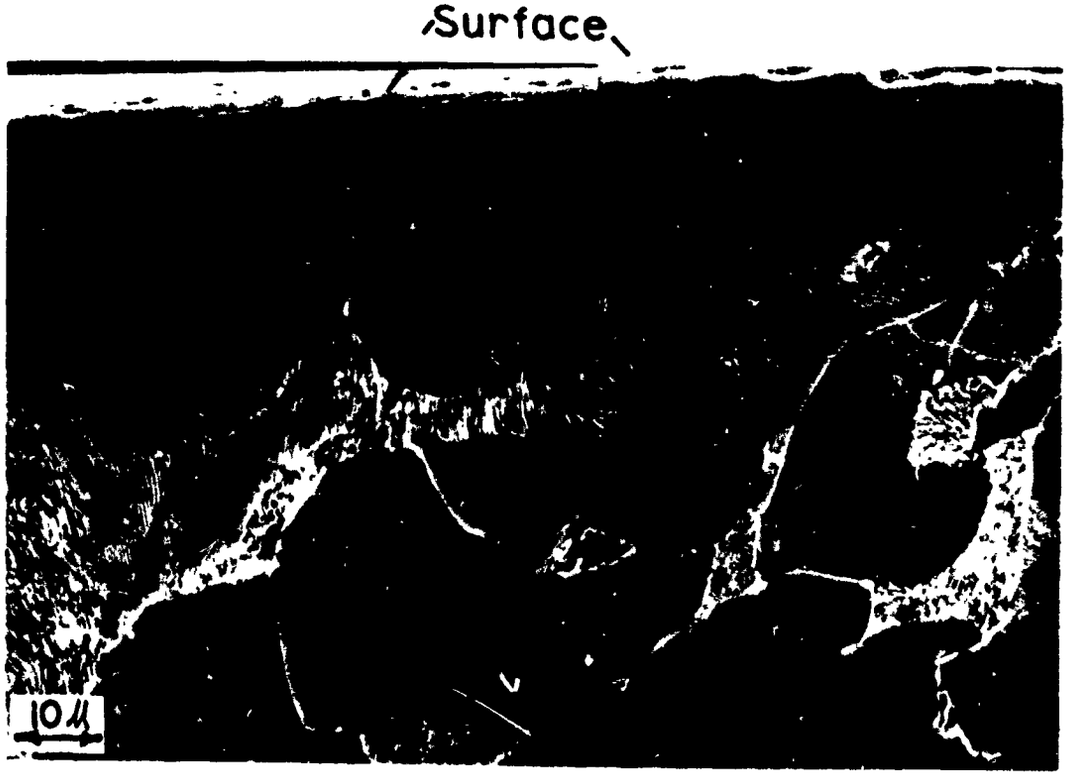

(b)

Figure 6.4 Subsurface damage and deformation in argon under a load of 2.25 kg after 54m sliding distance.
a) Unplated steel
b) 0.1 μm Cd plated steel

in air may be caused by oxidation, since the wear tracks of all the specimens tested in air were covered by a dark oxide.

The wear track of 0.1 μm Cd plated steel tested in argon (Fig. 6.5 a) is compared with the wear track in air (Fig. 6.5 b). The micrograph indicates that delamination has occurred quite extensively in air. The subsurface deformation in air (Fig. 6.6) indicates a smaller depth of deformation in air than in argon. The deformation zone for the unplated steel in air is 25-30 μm (Fig. 6.6 a), while for the 0.1 μm Cd plated steel it is only 15-20 μm (Fig. 6.6 b).

Since the poor performance of Cd plated steel in air was believed to be caused by oxidation, a series of tests were conducted under boundary lubrication to minimize oxidation. The first set of tests were run with Gulftex 39 under a load of 2.25 kg for 216 m sliding distance. The unplated steel and 0.1 μm Cd plated steel exhibited a similar wear rate of 4.6×10^{-9} gm/cm. The wear track of both specimens had become dark, indicating that the Gulftex oil had reacted with the specimens and caused the high wear rate of Cd plated steel. Therefore, for the next set of tests a pure mineral oil (Nujol) was used. Under the same conditions as the tests with Gulftex 39, the unplated steel had a wear rate of 3.2×10^{-9} gm/cm when lubricated with mineral oil, whereas, the 0.1 μm Cd plated steel had experienced such low wear that no weight change could be detected. Therefore, the test duration was tripled (648m). After the tests the unplated steel had a wear rate of 7×10^{-9} gm/cm, while the wear rate of 0.1 μm Cd plated steel was only 0.5×10^{-9} gm/cm It is believed that longer tests will result in larger wear rate reductions, similar

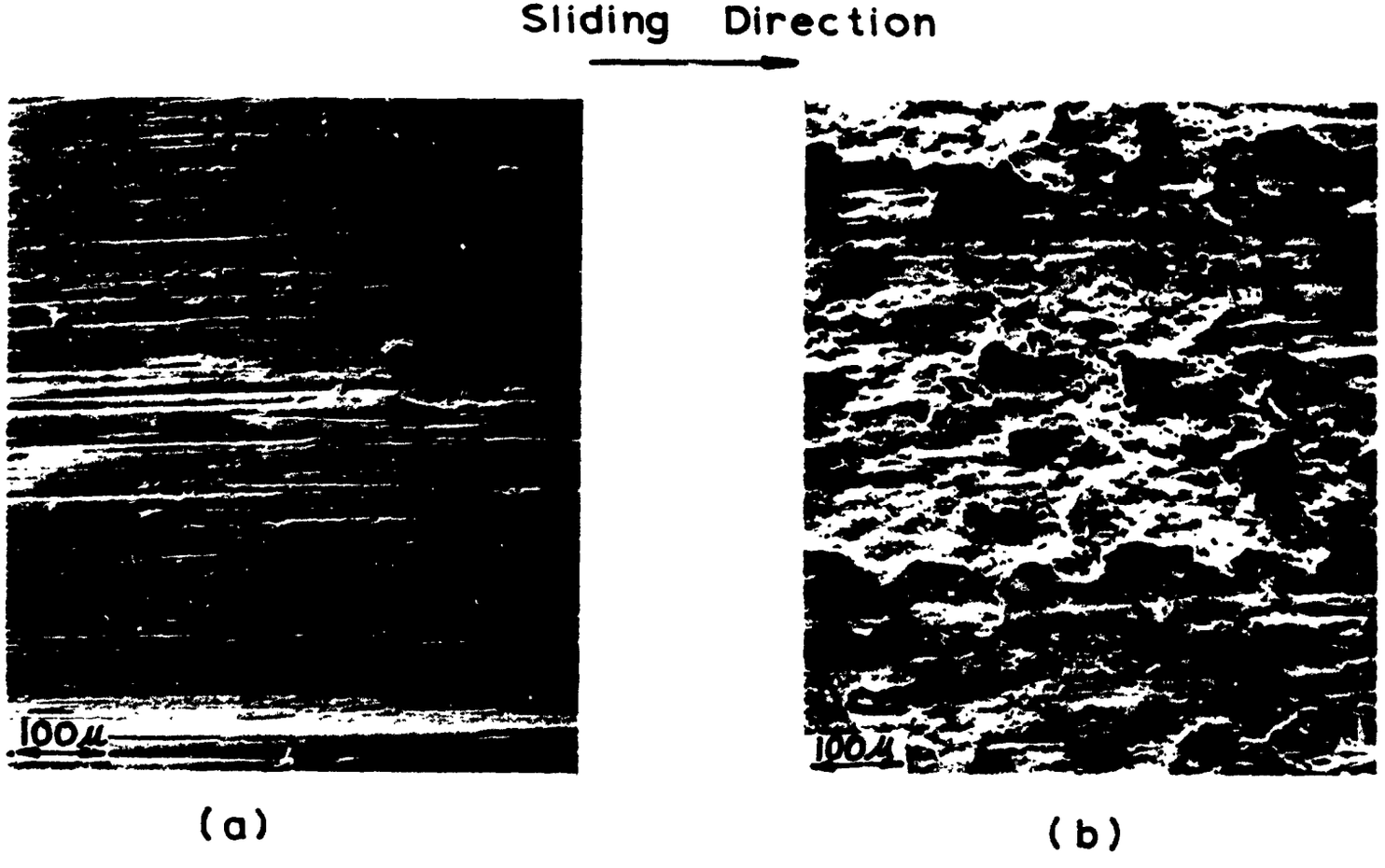

Figure 6.5 Wear track of 0.1 μm Cd plated steel
a) Tested in argon
b) Tested in air

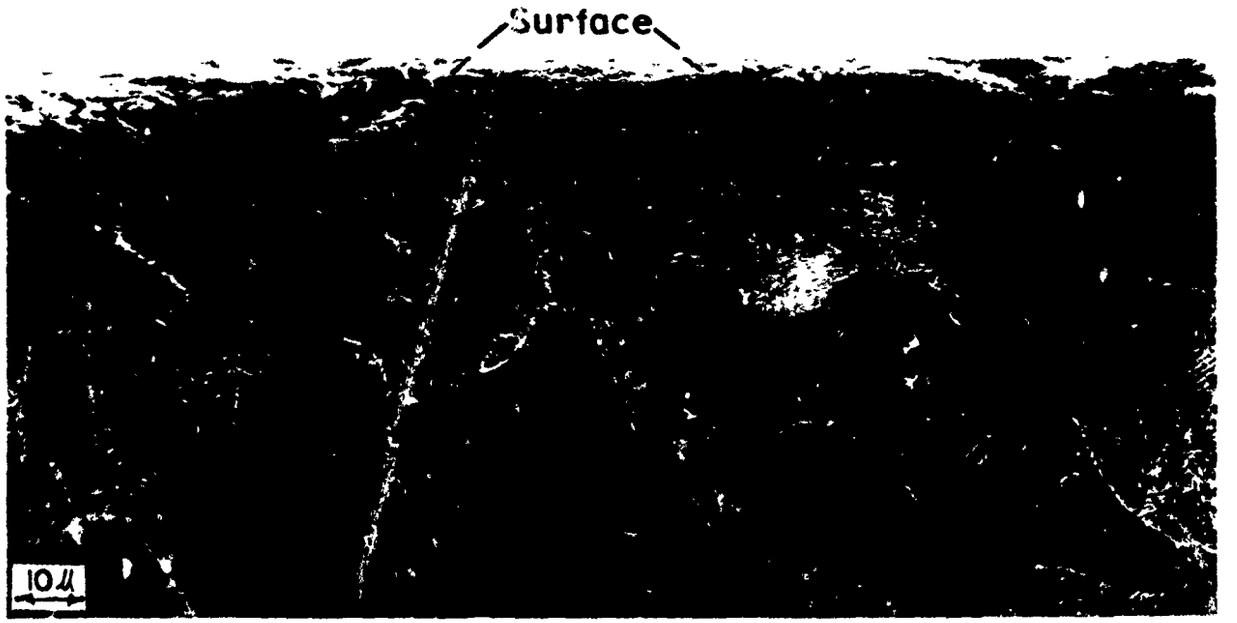

(a)

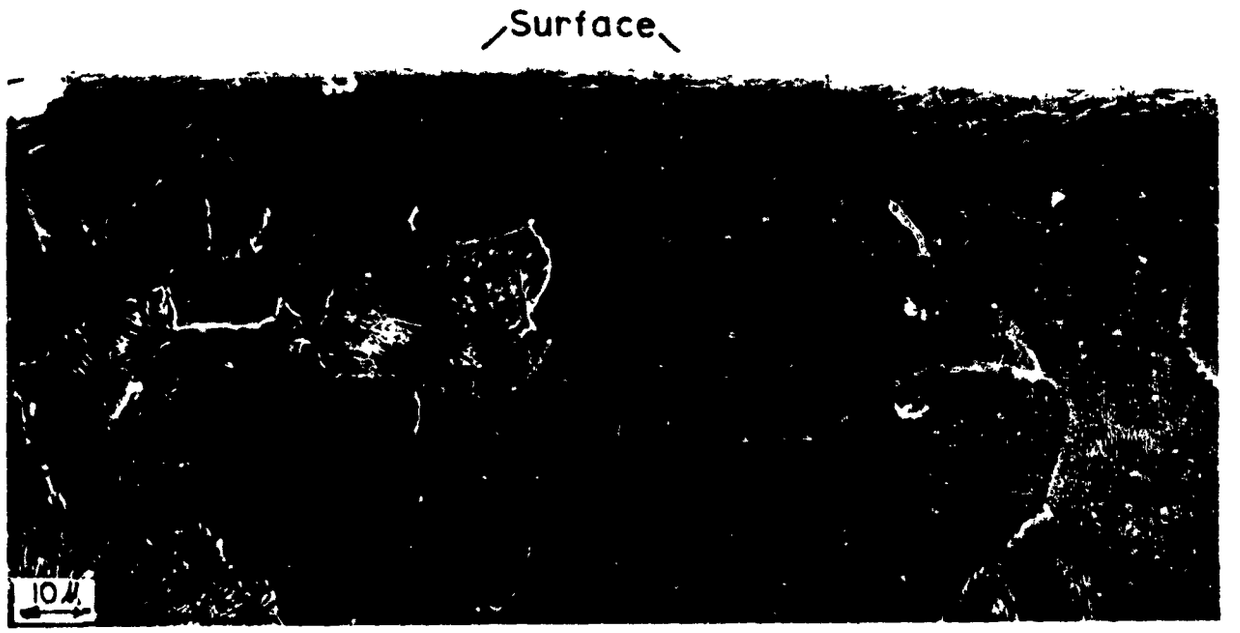

(b)

Figure 6.6 Subsurface deformation in air
a) Unplated steel
b) 0.1 μm Cd plated steel

to the tests performed in argon.

The data on the frictional coefficient of the Cd plating wear tests are presented in Fig. 6.7. It is interesting to note that the coefficient of friction changes as a function of the plate thickness in a manner very similar to the wear rate vs. plate thickness data (Fig. 6.1). The figure shows that the 0.1 μm Cd plating reduces friction by more than a factor of 3 in argon and approximately by a factor of 2 in air. The 0.1 μm Cd plating also decreased friction in the lubricated tests. The friction coefficient was reduced from 0.18 to 0.11 in the Gulftex oil, while it decreased from 0.16 to 0.10 in the mineral oil.

3) Discussion

The results presented here show that the delamination theory of wear may be applied to a composite surface to reduce wear by more than three orders of magnitude. The best result was obtained in an argon atmosphere when 0.1 μm Cd was plated on annealed AISI 1018 steel.

In these experiments we have a composite material: an extremely soft outer layer and a much stronger substrate. When the dislocations are generated they pile up at the coating-substrate interface. As the slider moves on, some of these dislocations escape through the surface of the wear track if the coating is very thin. The forces acting on dislocations in metals with a low shear modulus bonded to metals with a higher shear modulus are such that the dislocations are repelled from the interface. These dislocations are then pulled out of the surface by the image force created by the free surface. In the case of high stresses there will be some transfer to and generation of

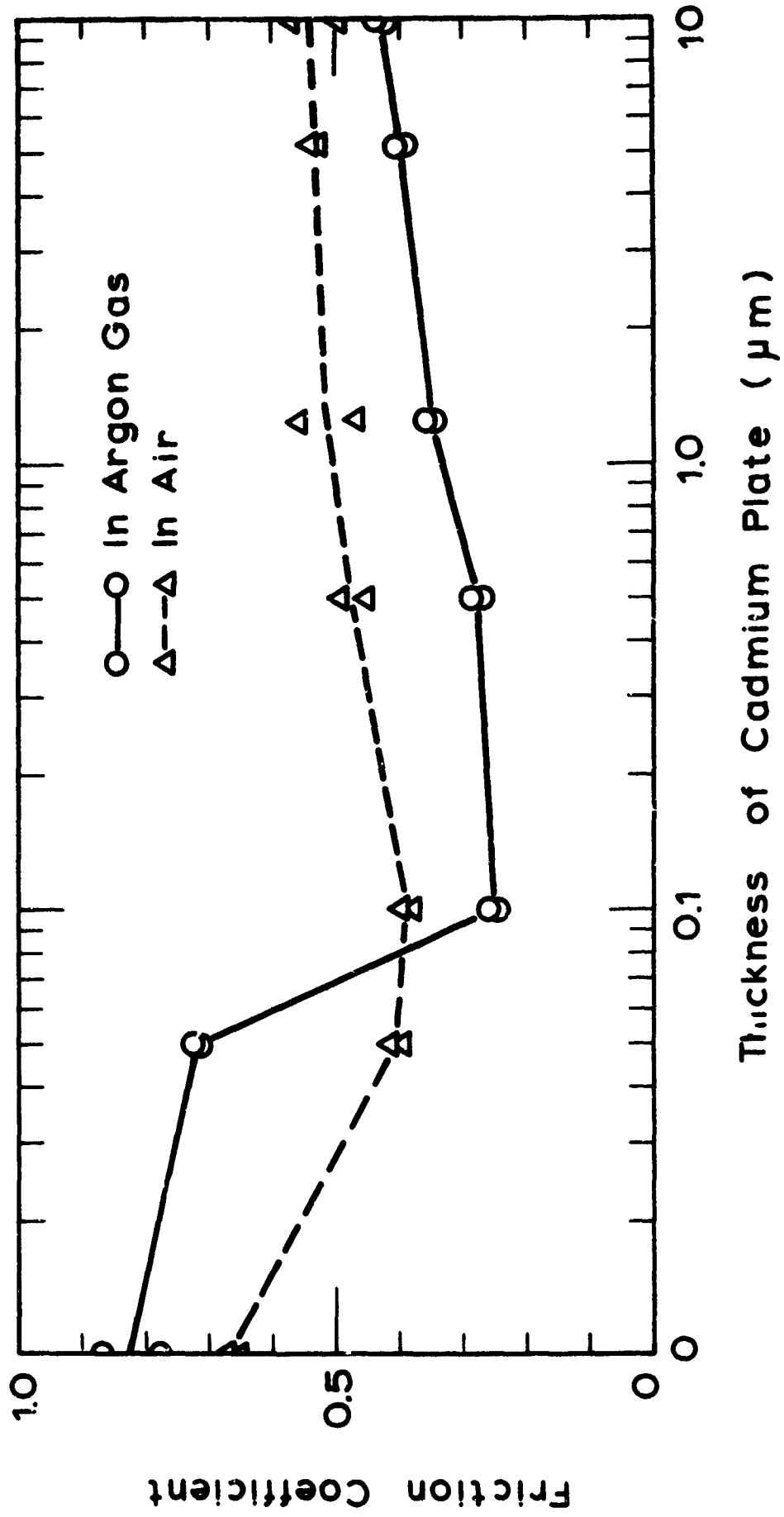

Figure 6.7 The friction coefficient of Cd plated steel as a function of plate thickness.

dislocations in the substrate material. However, the subsurface damage will be considerably less than would be observed on an uncoated material because of the lower tangential force transmitted. Thus the coating-substrate interface will markedly delay delamination of the substrate material.

In the case of thick coatings of cadmium, there is sufficient thickness for dislocation pile-up in the cadmium below the low dislocation layer at the immediate surface. This leads to delamination of the cadmium coating until the thickness is reduced to a stable level. After this is attained there should be no further wear, as in the case of the very thin coatings.

The poor performance of the Cd plated steel in air as compared with the tests in argon, is attributed to the oxidation of the Cd layer. The cadmium oxide, which is probably much harder than the cadmium itself, would impede the escape of the dislocations through the free surface and allow the delamination process to occur. Furthermore, these hard oxides, once removed, will cause abrasive wear of the soft cadmium layer. When oxidized, the thin Cd layer will undergo strain-hardening since dislocations cannot escape from the free surface. This is supported by the evidence that the coefficient of friction is increased in air, which results in an increase in the rate of delamination. Wear rate reduction may be obtained with 0.1 μm Cd plating only in atmospheres such as inert gas or non-corrosive lubricants, where thin and hard oxides or corrosion products will not form on the cadmium.

The friction coefficient data for Cd plating wear tests indicated that the frictional force of 0.1 μm cadmium plated steel in argon and in the lubricated tests was one-half or one-third that of unplated steel. This is

probably related to the non-work hardening nature of the thin Cd layer. Since the tangential force required for sliding is smaller than that for the unplated steel, the friction force will be less.

The subsurface examination of the wear tracks for the tests in air or in argon showed that the depth of the deformed zone is less in the Cd plated samples than in the unplated samples. The subsurface deformation is also less in air than in argon for both Cd plated and unplated specimens. This may be attributed to the decrease in the coefficient of friction.

Chapter 7

FUTURE RESEARCH PROGRAM

The result of this investigation on the delamination theory of wear has shown that in fact wear occurs by delamination in various metals and that the rate of delamination can be reduced effectively by a soft metal coating. However, many aspects of the theory and it's application still need to be clarified and extended to actual sliding situations such as bearings, cams and gears. The tentative program for future investigations is presented in this chapter in an outline form. It should be noted that this list is not complete by any means, and it is included in this report only to indicate the extent of the necessary work in the area of sliding wear.

A) Mechanism of Delamination

a) Depth of deformation and its dependence on the sliding distance, normal and frictional loads.

b) The increment of subsurface strain and the effect of normal and frictional forces.

c) The strain at which subsurface voids nucleate around inclusions in a specified material.

d) Void nucleation in "inclusion-free" metals.

e) Void elongation and crack propagation as a function of sliding distance.

f) Critical crack length in various materials.

g) The effect of metallurgical variables such as grain size, cold working, second phase, etc. on delamination.

B) Wear Rates and Wear Particles

a) Mechanism of transient wear particle formation from the deformed asperities.

b) Correlations between wear rates, wear particles and subsurface damage.

C) Wear Rate and Friction Coefficient Equations

a) Elastoplastic stress and strain distribution below the wear track.

b) Stress distribution due to plowing.

c) Wear rate equation based on the stress distribution, mechanics of crack propagation and the obtained experimental results.

d) Relationship between the friction coefficient and the wear rate.

D) Wear Rate Reduction

a) Single phase, inclusion-free metals with high flow stress.

b) Extension of the soft metal coating to other substrates and coating materials.

c) Extension of wear prevention to fretting and fretting fatigue.

d) Other surface treatments possible for wear reduction.

REFERENCES

1) National Academy of Science, Committee on the Survey of Materials Science and Engineering, "Materials and Man's Needs", (1974).

2) N. P. Suh, "The Delamination Theory of Wear", Wear, 25 (1973) 11-124.

3) N. P. Suh, S. Jahanmir, E. P. Abrahamson, II and A. P. L. Turner, "Further Investigation of the Delamination Theory of Wear", J. Lub. Tech., Trans. ASME, (1974).

4) S. Jahanmir, N. P. Suh and E. P. Abrahamson, II, "Microscopic Observations of the Wear Sheet Formation by Delamination", Wear, 28 (1974) 235-249.

5) E. P. Abrahamson, II, S. Jahanmir, D. A. Colling and N. P. Suh, "Failure by Delamination During Wear", Proc. Scanning Electron Microscopy Conf., (1974) part IV, 889-894.

6) N. P. Suh, S. Jahanmir, D. A. Colling and E. P. Abrahamson, II, "The Delamination Theory for Wear of Metals Slidng at Low Speeds", Proc. 2nd North American Metalworking Research Conf., (1974) 117-127.

7) E. P. Abrahamson, II, S. Jahanmir, N. P. Suh and D. A. Colling, "Application of the Delamination Theory of Wear to a Composite Metal Surface", Proc. Int. Conf. on Production, (1974).

8) S. Jahanmir, N. P. Suh and E. P. Abrahamson, II, "The Delamination Theory of Wear and the Wear of a Composite Metal Surface", Wear, (1975), submitted for publication.

9) J. F. Archard, "Contact and Rubbing of Flat Surfaces", J. Appl. Phys., 24 (1953) 981-993.

10) H. Ernst and M. E. Merchant, "Surface Friction of Clean Metals - A Basic Factor in the Metal Cutting Process", Proc. Special Summer Conf. on Friction and Surface Finish, M.I.T.,(1940) 76-101.

11) A. P. Green, "The Plastic Yielding of Metal Junctions Due to Combined Shear and Pressure", J. Mech. Phys. Solids, 2 (1954) 197-211.

12) P. K. Gupta and N. H. Cook, "Junction Deformation Model for Asperities in Sliding Interaction", Wear, 20 (1972) 73-87.

13) P. K. Gupta and N. H. Cook, "Statistical Analysis of Mechanical Interaction of Rough Surfaces", J. Lub. Tech., Trans. ASME., (1972) 19-26.

14) E. Rabinowicz, Friction and Wear of Materials, Wiley, London (1965).

15) P. Sridharan and N. P. Suh, unpublished results, (1974).

16) J. H. Dautzenberg and J. H. Zaat,"Quantitative Determination of Deformation by Sliding Wear", Wear, 23 (1973) 9-19.

17) G. Agustsson, "Strain Field Near the Surface Due to Surface Traction", S.M. Thesis, M.I.T. (1974).

18) H. Koba,"Wear Particle Formation Mechanism", S.M. Thesis, M.I.T. (1974).

19) K. B. Savitskii, cited in V. I. Kragel'skii, Friction and Wear, Butterworth Washington (1965).

20) F. A. McClintock and A. S. Argon, Mechanical Behavior of Materials, Addison-Wesley, Reading (1965).

21) C. Zener, Fracturing of Metals, ASM, Novelty, Ohio (1949) 3-31.

22) A. N. Stroh, "The Formation of Cracks as a Result of Plastic Flow", Proc. Royal Soc. London, A223 (1954) 404-414.

23) A. N. Stroh, "The Formation of Cracks as a Result of Plastic Flow, II" Proc. Royal Soc. London, A232 (1955) 548-560.

24) F. A. McClintock,"On the Mechanics of Fracture From Inclusions", Ductility, ASM, Metals Park, Ohio (1968) 255-277.

25) F. A. McClintock, S. M. Kaplan and C. A. Berg, "Ductile Fracture by Hole Growth in Shear Bands", Int. J. Fract. Mech., 2(1966) 614-627.

26) C. D. Beachem, "An Electron Fractographic Study on the Influence of Plastic Strain Conditions Upon Ductile Rupture Processes in Metals Trans. ASM, 56(1963) 318-326.

27) W. W. Seifert and V. C. Westcott, "A Method for the Study of Wear Particles in the Lubricating Oil", Wear, 21 (1972) 27-42.

28) I. F. Stowers and E. Rabinowicz, "The Mechanism of Fretting Wear", J. Lub. Tech., Trans. ASME, (1973) 65-70.

29) J. S. Halliday and W. Hirst, "The Fretting Corrosion of Mild Steel", Proc. Royal Soc. London, A236 (1956) 411-425.

30) H. Charney, "Fundamentals of Interfacial Slip Damping", S. M. Thesis, M.I.T. (1970).

31) S. Akoi, T. Fujiwara and I. Furukawa, Bul. Jap. Soc. Prec. Engr., 2 (1947) 238-245.

32) R. B. Waterhouse and D. E. Taylor, "Fretting Debris and the Delamination Theory of Wear", Wear, 29 (1974) 337-344

33) A.R.C. Westwood, "Enviromental Sensitive Mechanical Properties", Ind. Eng. Chem., 56 (1964) 15-25.

34) W. M. Hauser, "Wear of Carbon Fiber Composites", Ph.D. Thesis, M.I.T., (1973).

35) B. I. Bresnev, "Some Problems of Large Plastic Deformation of Metals at High Pressures, McMillan, New York, 1963.

36) A. R. Rosenfield. "Criteria for Ductile Fracture of Two Phase Alloys," Met. Rev., Vol. 13 No. 121. (1968) 29-42.

37) K. E. Easterling, H. F. Fishmeister and E. Navara, "The Particle-to-Matrix Bond in Dispersion - Hardened Austenitic and Ferritic Iron Alloys", Powder Met., 16 (1973) 128-145.

38) N. P. Suh and G. Agutsson, unpublished results (1973).

39) A. S. Argon, J. Im and R. Safoglu, "Cavity Formation from Inclusions in Ductile Fracture", Trans. AIME (1974).

40) J. T. Burwell and C. D. Strung, "On the Empirical Law of Adhesive Wear", J. Appl. Phys., 23 (1952) 18-28.

41) T. Sata, "Transience of the State of Wear by Repeated Rubbing", Wear, 3 (1960) 104-113.

42) C. A. Queener, T. C. Smith and W. L. Mitchell, "Transient Wear of Machine Parts", Wear, 8 (1965) 391-400.

43) T. Sasada, H. Ohmura and S. Nororse, "The Wear and Mutual Transfer in Cu/Fe Rubbing", Proc. 15th Japan Cong. on Mat. Res., (1972) 1-6.

44) T. Sasada, S. Norose and K. Sugimoto, "The Mutual Metalic Transfer at Friction Surfaces in Lubricating Oil", Proc. 17th Japan Cong. on Mat. Res. (1974) 32-35.

45) A. Dorinson and V. E. Broman, "Contact Stresses and Load as Parameters in Metalic Wear", Wear, 4 (1961) 93-110.

46) J. P. Hirth and J. Lothe, Theory of Dislocations, McGraw-Hill, New York (1968).

47) Y. Tsuha and R. Takagi, "Lubriating Properties of Lead Films on Copper", Wear, 7 (1964) 131-143.

48) R. Takagi and T. Liu, "The Lubrication of Steel by Electroplated Gold", ASLE Trans., 10 (1967) 115-123.

49) R. Takagi and T. Liu, "Lubrication of Bearing Steels with Electroplated Gold Under Heavy Loads", ASLE Trans., 11 (1968) 64-71.

50) A. J. Solomon and M. Antler, "Mechanisms of Gold Electrodeposits", Palting, Aug. (1970) 812-816.

51) T. J. Kuczkowski and D. H. Buckley, "Friction and Wear of Low Melting Binary and Ternary Gallium Alloy Films in Argon and in Vacuum", NASA TN D-2721 (1965).

52) H. E. Evans and T. W. Flatley, "Bearings for Vacuum Operations, Retainer Material and Design", NASA TN D-1339 (1962).

53) H. E. Evans and T. W. Flatley, "High Speed Vacuum Performance of Gold Plated Miniature Ball Bearings with Various Retainer Materials and Configurations", NASA TN D-2101 (1963).

54) T. W. Flatley, "High Speed Vacuum Performance of Miniature Ball Bearings Lubricated with Combination of Barium, Gold and Silver Films", NASA TN D-2304 (1964).

55) P. E. Brown, "Bearing Retainer Material for Modern Jet Engines", ASLE Trans., 13 (1970) 225-239.

56) T. L. Ridings, "Operational Evaluation of Dry Thin Film Lubricated Bearings and Gears for Use in Aerospace Environmental Chambers", AEDC-TR-65-1 (1965).

57) R. E. Lee, Jr., "Lubrication of Heavily Loaded, Low Velocity Bearings and Gears Operating in Aerospace Environmental Facilities", AEDC-TR-65-19 (1965).

Appendix A*

QUANTITATIVE DETERMINATION OF SHEAR STRAIN

When two materials slide against each other under pressure without any lubricant, substantial plastic deformation takes place at the surface. Dautzenberg and Zaat** have introduced methods to determine this deformation by measuring the geometrical alteration of the metal grains and calculating the equivalent plastic strain. This method is based on the fact that when an ideal spherical grain is deformed under pure shear it becomes an ellipsoid. Therefore, when a cut is made in the material parallel to the sliding direction and perpendicular to the sliding surface, the undeformed ideal spherical grains will appear as circles and the deformed grains as ellipses. The equivalent plastic strain can then be determined by observing the geometrical deformation of the grains when they change from spheres to ellipsoids.

1) Mathematical Derivation of the Equivalent Plastic Strain

The equivalent plastic strain at the subsurface is derived by Dautzenberg and Zaat by considering the change in the grain shape. The deformation is approximated by assuming a plane strain condition and a state of pure shear stress. It was assumed that each grain is spherically shaped before deformation and deforms into an ellipsoidal shape. Under these conditions the incremental equivalent plastic strain is reduced to:

---

*This appendix is a summary of G. Agustsson's S.M. Thesis entitled, "Strain Field Near the Surface Due to Surface Traction", MIT, 1974.

**J.H. Dautzenberg and J.H. Zaat, "Quantitative Determination of Deformation by Sliding Wear", Wear, 23 (1973) 9-20.

$$d\bar{\varepsilon} = \frac{d\gamma_{xy}}{3} \quad , \tag{1}$$

or

$$d\bar{\varepsilon} = \frac{1}{3} \left(\frac{d\ell_x}{\ell_y} \right) \quad , \tag{2}$$

if the only non-zero strain increment is $d\ell xy$. The equivalent plastic strain can be found from (2) by integration,

$$\bar{\varepsilon} = \frac{1}{3\,\ell_y} \int_0^{\ell_x} d\ell = \frac{1}{3} \frac{\ell_x}{\ell_y} \quad . \tag{3}$$

Fig. A-1, which schematicly represents the deformation of an ideal spherical grain to an ellipsoid, indicates that $\ell_y = OA$ and $\ell_x = AB$. Therefore,

$$\tan \gamma = \frac{\ell_x}{\ell_y} \quad ; \tag{4}$$

substitution in equation (3) gives the equivalent plastic strain in terms of the shear angle γ,

$$\bar{\varepsilon} = \frac{\tan \gamma}{3} \quad . \tag{5}$$

To determine $\bar{\varepsilon}$ as a function of grain thickness, the shear angle, γ, must be related to the grain thickness. This can be derived from geometry alone. If we consider a point (x,y) on the circle and its new position (x',y') on the ellipse after deformation, it can be shown that

$$x'^2 + y'^2(1 + \tan^2\gamma) - 2x'y' \tan\gamma - y'D = 0. \tag{6}$$

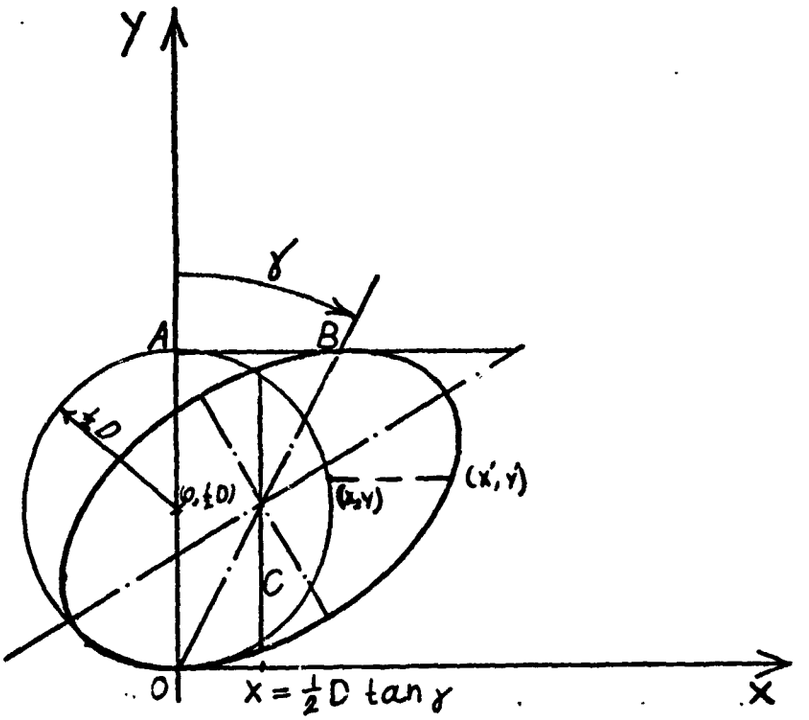

Figure A-1 Deformation of an ideal shperical grain under pure shear.

This can be done by substituting the geometric relation between (x,y) a. (x',y') into the equation for the circle of Fig. A-1.

It will be observed later that the best methods of measuring the change in grain shape will be by measuring the length of the line C passing through the center of the ellipse and relating it to the original size of the sphere (ideal grain). Therefore, we proceed to find a relation between C and D. This may be done by substituting the equation for the line C, i.e.,

$$x' = \frac{1}{2} D \tan \gamma \qquad (7)$$

into equation (6), solving for y' and substracting the smaller y' value from the larger one; it is found that

$$C = D \cos \gamma \quad . \qquad (8)$$

By changing, cos γ into tan γ, using a trigonometric relation between $\cos^2 \gamma$ into $\tan^2 \gamma$, and substituting the resulting equation into (5) we obtain the final relation between the equivalent strain, $\bar{\varepsilon}$, and the relative change in the grain shape, D/C,

$$\bar{\varepsilon} = \left[\frac{\left(\frac{D}{C}\right)^2 - 1}{3} \right]^{1/2} \qquad (9)$$

The equivalent plastic strain, therefore, could be calculated approximately by measuring the diameter before deformation and the C value after deformation.

2) Experimental Evaluation of the Model

The derived relation between the equivalent plastic strain and the grain shape change was tested experimentally on plasticine specimens before applying the method to metals. For this purpose, a test instrument was made to

impose a pure shear deformation on a plasticine sheet under plane strain conditions.

The plasticine sheet was marked with evenly spaced circles of diameter 0.254 in. by a digitally controlled "Tap-O-Matic" drill press A known shear deformation was then imposed on the specimen which deformed the circles into ellipses, Fig. A-2. The length of the lines passing through the centrum of the ellipses (C in Fig. A-1) was then measured by making a slide from the deformed plasticine and observing the shape change of the circles at 10x on an optical comparator.

Equation (9) was then used to calculate the equivalent plastic strain. The calculated strain was lower than the applied strain by 2%. Since this difference is within reasonable limits, the project was continued to measure the subsurface equivalent plastic strain in a worn metal specimen.

3) The Effective Plastic Strain in Metals

Since metal grains never have the ideal spherical shape and are not usually uniform in size, a new method should be devised to measure the grain shape change. Dautzenberg and Zaat incorporated the linear intercept method in their calculations. Linear intercepts are lines parallel to the y-axis which intersects the grain circumference (Fig. A-3). It was shown that the equivalent plastic strain will be approximated by

$$\bar{\varepsilon} \approx \left[\frac{\left(\frac{\bar{D}}{\bar{C}}\right)^2 - 1}{3} \right]^{1/2} , \qquad (10)$$

where $\bar{D}$ and $\bar{C}$ are the average linear intercepts of the virgin grains and the

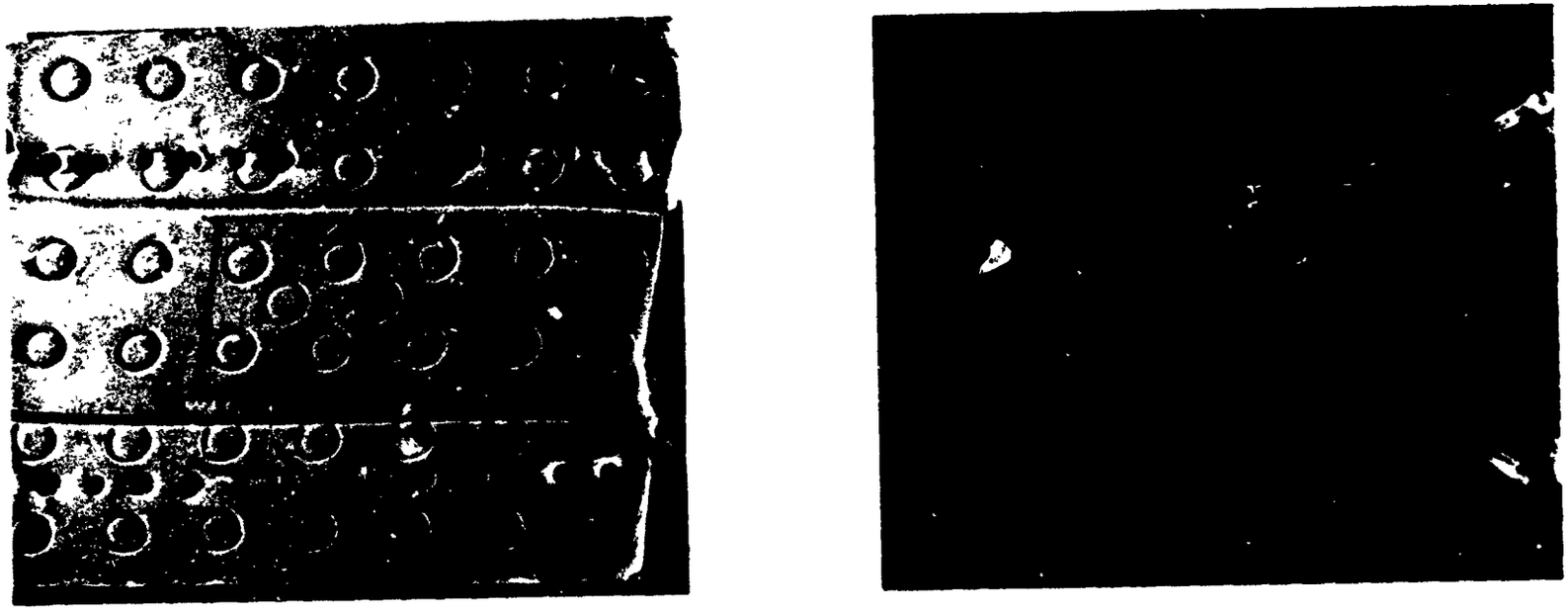

(a) (b)

Figure A-2 Plasticine specimen
a) Before deformation
b) After deformation

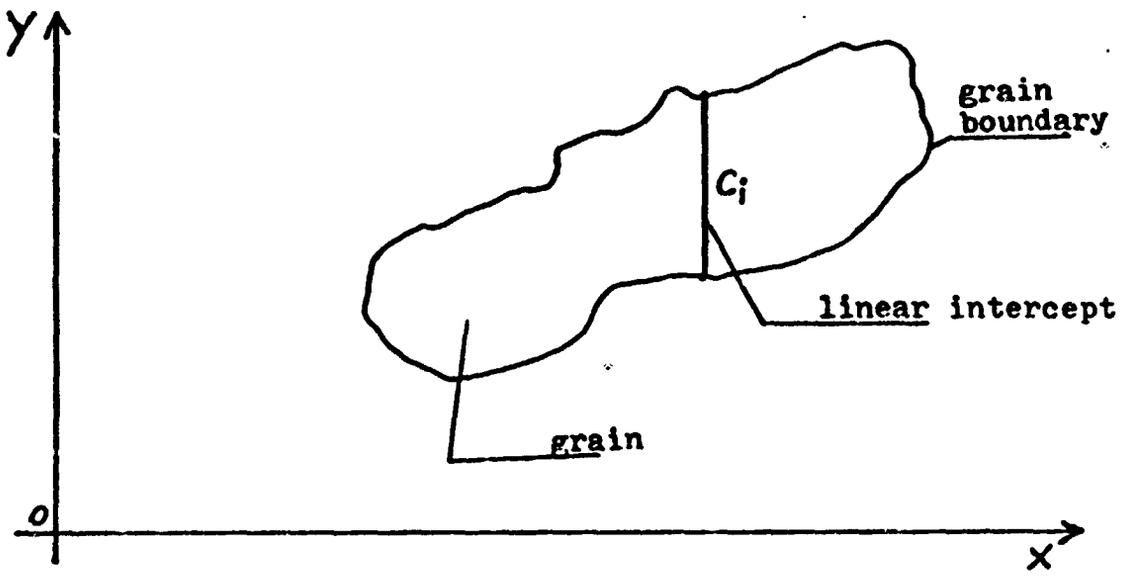

Figure A-3 Linear intercept representation.

deformed grains, respectively.

4) Experimental Procedure

Wear tests were performed on steel and copper and the subsurface strain field was calculated using equation (10). The chemical composition, heat treatment and hardness of the specimens is given in Table A-1. The tests were conducted on a lathe with a cylinder-on-cylinder geometry. (Please refer to Appendix D for details of experimental arrangements.) An AISI 52100 steel slider was used. The tests were run in an argon flow of 10 lit/min at room temperature. The normal load, friction force sliding distance and speed are included in Table A-2.

After the wear tests, the specimens were sectioned paralell to the sliding direction and normal to the wear surface. They were then metallographically polished and etched. A 2% Nital solution was used for steel, whereas the copper was etched electrolytically in a solution of orthophosphoric acid (Table A-1). In order to obtain good quality micrographs at high magnifications, the etched surfaces were vapor deposited with 50-100 Å of gold.

The subsurface deformation was then observed by SEM and recorded on polaroid film. The micrographs were reproduced on slides; an optical comparator was used to measure the average linear intercepts as a function of the depth below the wear surface. The subsurface equivalent strain was then calculated from equation (10) for a number of positions below the surface.

5) Subsurface Equivalent Plastic Strain Due to Wear

The subsurface deformation of the steel and copper specimens are shown in Figs. A-4 and A-5, respectively. The micrographs indicate that the grains

Table A-1 Specimen Material

Metal	Chemical Composition %	Annealing Treatment	Brinell Hardness Kg/mm^2	Etching Reagent
Doped AISI 1020 Steel	0.17 C 0.60 Mn 0.50 W 0.25 Zr Bal. Fe	$680^{o}C$, 17 hrs $600^{o}C$, 14 hrs	159	2% Nital
Copper	0.25 Cr 0.10 Ti 0.08 Cb Bal. Cu	$250^{o}C$, 3 hrs.	76	Electrolytic etching in 70% orthophosphoric acid solution

Table A-1 Experimental Condition

Specimen	Normal Load Kg	Friction Coef.	Sliding Distance cm x 10^3	Sliding Velocity cm/min
Steel	2.4	0.8	18.1	603
Copper	2.1	0.6	6.8	228

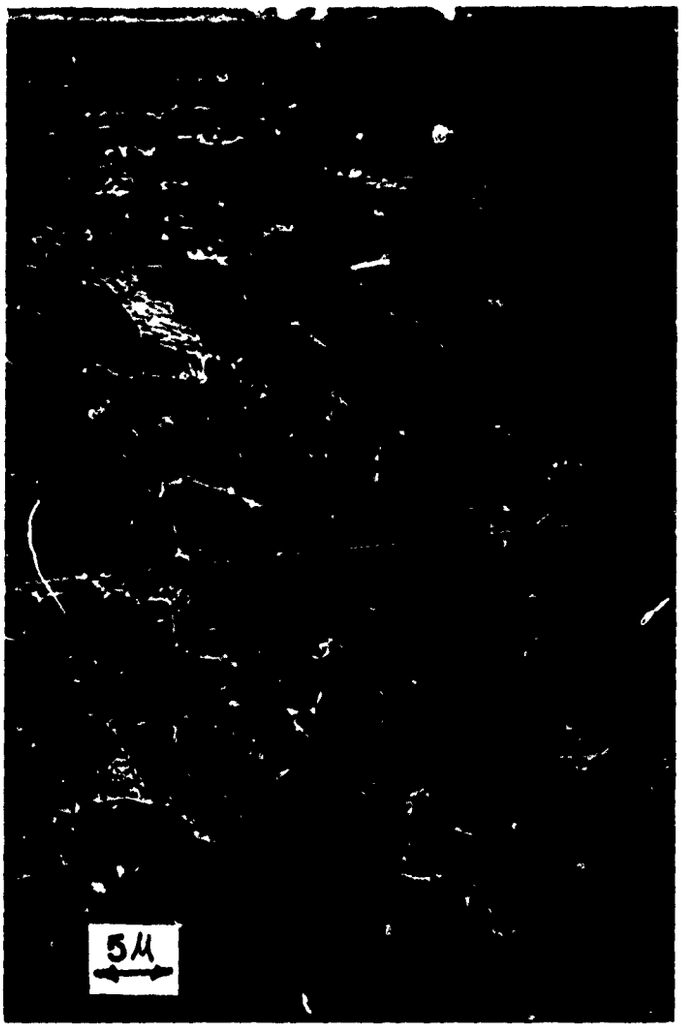

Figure A-4 Subsurface deformation in AISI 1020 steel.

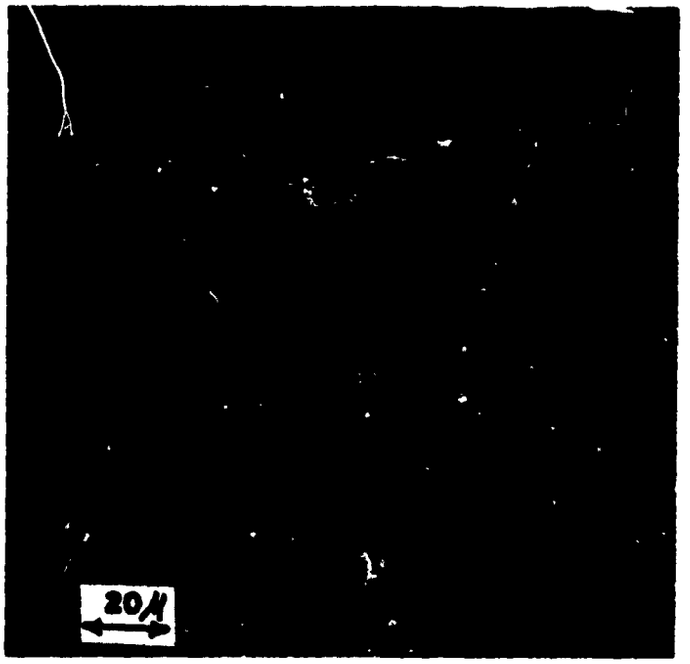

Figure A-5 Subsurface deformation in copper.

very close to the surface have deformed extensively and have become paralell to the surface. The line which is drawn on the micrograph to measure the linear intercepts indicates the distance below the surface.

Results from the calculation of the effective strain at different distances using equation (10), is represented in Fig. A-6 for steel where the effective strain is plotted versus distance from the surface. This graph shows that at a distance 1 μm from the surface the strain is as high as 14.3 and that from the surface down to 15 μm there is a region of very high strain gradient. It was technically impossible to determine the strain very close to the surface because the grains had deformed so much that no intercept measurements could be made. In order to extrapulate the shear strain at the very surface, three data points closest to the surface were assumed to lie on a straight line. This approximation indicated that the effective strain at the surface is 16.5.

The equivalent plastic strain in copper is shown in Fig. A-7 as determined from the micrograph of Fig. A-5. It is observed from Figs. A-6 and A-8 that deformation in copper extends to a depth of 100 μm. The effective strain could only be calculated for positions deeper than 10 μm because the grains very near the surface are so deformed (Fig. A-5) that no intercept measurements could be made. However, if the curve is extrapolated to the surface, it could be observed that the strain at the surface is approximately 100.

Figs. A-6 and A-7 indicate that subsurface deformation is not uniform, but a large strain gradient exists very near the surface. The thickness of the layer in which this gradient occurs is approximately 8 μm for AISI 1020 steel whereas it is 25 μm for the copper alloy.

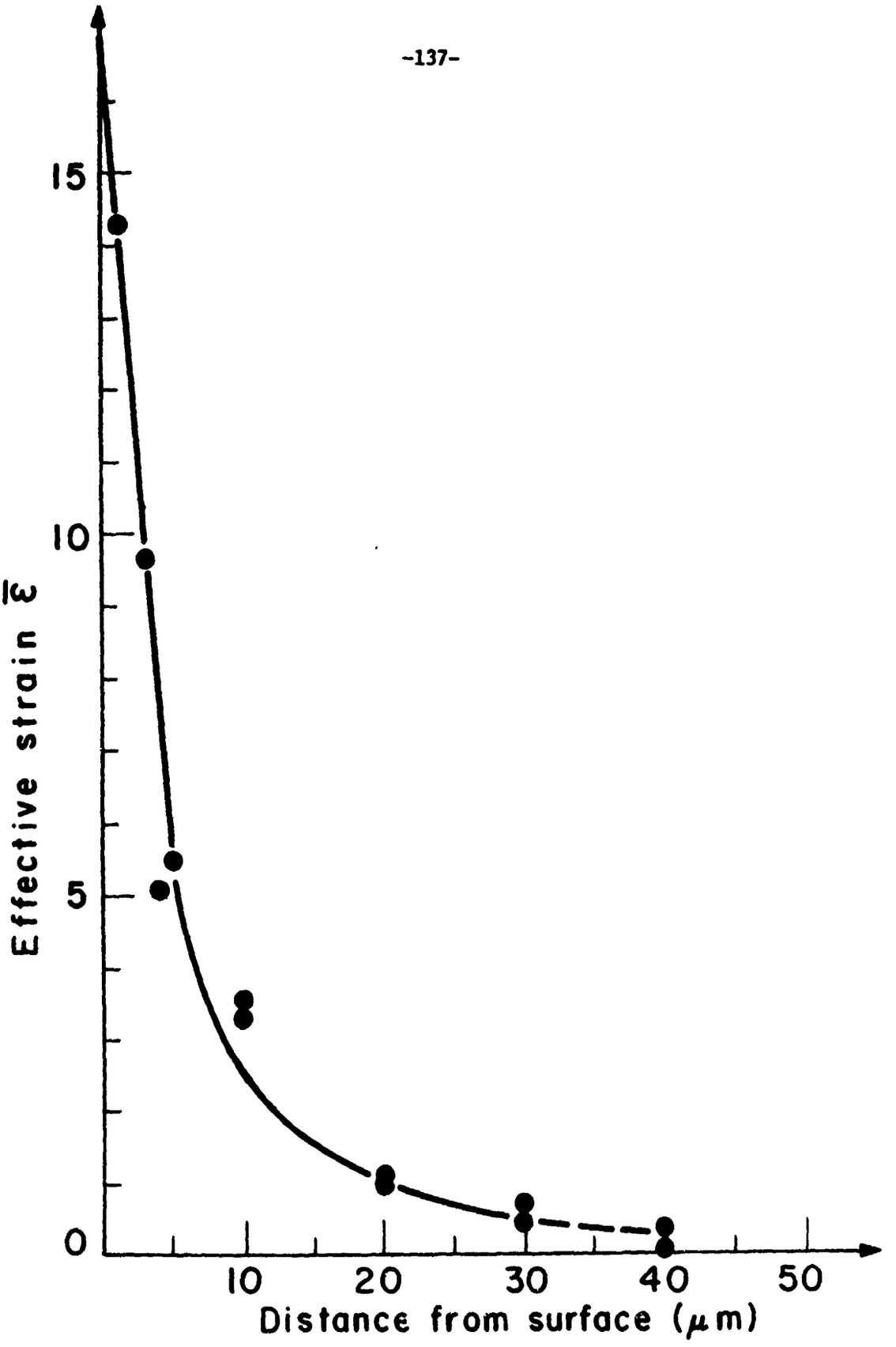

Figure A-6 Subsurface strain distribution in AISI 1020 steel.

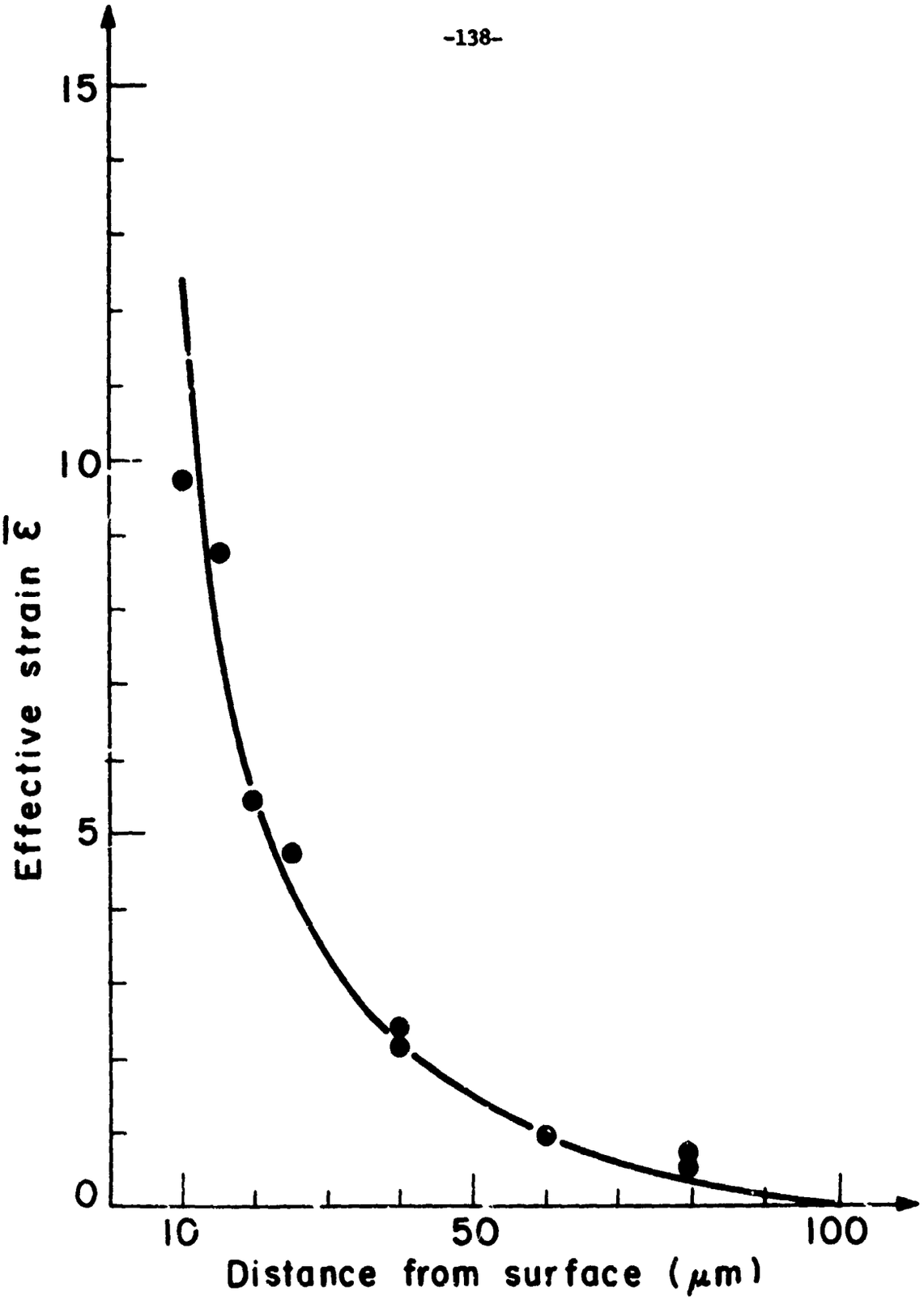

Figure A-7 Subsurface strain distribution in copper.

Appendix B

ESTIMATION OF THE LOW DISLOCATION DENSITY ZONE

A rough estimate of the image shear stress acting on a dislocation parallel to the surface may be made by*

$$\sigma_{xy} = \frac{Gb}{4\pi(1-\nu)h} \tag{1}$$

This force is opposed by the friction stress and the change in the surface energy as the dislocations emerge from the surface.** It will be assumed that the friction stress dominates.

Equating Eq. (1) to the friction stress σ_f and solving for h, Eq. (1) becomes

$$h = \frac{Gb}{4\pi(1-\nu)\sigma_f} \tag{2}$$

The friction stress in the low dislocation zone may be approximately expressed for solid solutions, precipitation hardened alloys and overaged alloys as**

$$\begin{aligned} \sigma_f &= G\epsilon^2 C \qquad \text{(Solid Solution)} \\ \sigma_f &= 2G\epsilon C \qquad \text{(Precipitation hardened alloy)} \\ \sigma_f &= \frac{Gb}{\lambda} \qquad \text{(Overaged)} \end{aligned} \tag{3}$$

where ϵ is the misfit strain, C the atomic concentration of substitutional

---

*J.P. Hirth and J. Lothe, Theory of Dislocations, McGraw-Hill, 1968.

**A.H. Cottrell, Dislocation and Plastic Flow in Crystals, Oxford (Clarendon) 1953.

atoms, and λ the spacing between hard particles.

In the case of 3% silicon iron, σ_f = 1500 kg/cm^2, G = 3.9 x 10^6 kg/cm^2, ν=0.3, and b = 2 to 5 $\mathring{A}$, h comes to be about $\frac{1}{10}$ of a micron. For pure copper with extremely low dislocation density σ_f = 4 kg/cm^2, G = 2.2 x 10^6 kg/cm^2, ν=0.3 , h is equal to about 10 to 20 microns. These values represent the maximum thickness of the low dislocation zone attainable in these metals.

Appendix C

SPECIMEN PREPARATION FOR THE WEAR TESTS

A) Chemical Composition and Processing Methods

The specimens were selected to represent a wide variation in metallurgical properties. The materials used included f.c.c., b.c.c. and h.c.p. metals. These metals were: cadmium bicrystal, pure zinc, pure iron, iron-tungsten and iron-molybdenum solid solutions, different grades of steels and copper.

1) Cadmium Bi-crystal

The 99.999% pure cadmium bi-crystal was in the as-cast condition. The wear surface was orientated to be perpendicular to the grain boundary for Test Nos. 2 and 3, whereas the wear surface was oriented at 30° to the grain boundary for Test No. 1. The wear surfaces were metallographically polished before testing.

2) Pure Zinc

After casting, the 1/2" rods of the 99.999% pure zinc were swaged to 1/4". The specimens were then prepared for cylinder-on-cylinder wear tests. A final anneal was given, after machining, at 85°C for 1 hour in vacuum.

3) Pure Iron and Iron-tungsten Solid Solutions

The high purity iron was specially prepared to achieve an inclusion free structure. The iron was zone refined and had a final impurity content of 2 ppm of O, 1 ppm of N and 2 ppm of C. Tungsten was added by zone levelling to give several concentrations of tungsten in solid solution. This material was then machined to 1/4" diameter and cut into 1 1/2" length. A final heat

treatment was given at 630°C for Test Nos. 6-16 and at 750°C for Test Nos. 17-19, for one hour in vacuum of 2×10^{-6} mm of Hg.

4) Iron-molybdenum Solid Solution

Three different concentrations of molybdenum in iron were selected, mainly 1.3 wt%, 2.7 wt% and 5.8 wt%. This material was prepared to achieve a clean solid solution structure. However, the polished and etched sections showed some inclusions. The chemical composition of these inclusions was determined by x-ray analysis, and it is believed that they are either iron oxides or iron carbides. The inclusion concentration in the 1.3% Mo was higher than the 2.7% and 5.8% Mo, by an order of magnitude.

This material was prepared by alloying 99.5% pure iron containing 0.02 wt% O, 0.004 wt% C and 0.001 wt% N. The molybdenum used for alloying was 99.9 wt% pure. The alloys were arc melted six times and cast into 400-gm ingots under an argon atmosphere. They were then hot pressed and rolled at 500°C . This was followed by a swaging to 1/2" diameter rods. A final vacuum anneal for one hour was given at 575°C for Test Nos. 20 and 21 and at 650°C for Test Nos. 22-25.

5) Steel

Different grades of steels with spheriodized or pearlitic microstructures were used. These were AISI 1010, 1018, 1020, 1095, and 4340 steels.

a) AISI 1010 Steel

This steel was rolled from a thickness of 3" to 3/4" at 930°C, followed by a water quench. Specimens for reciprocating tests were prepared by machining. Then the specimens were annealed at 650°C for 1 hour in vacuum.

b) AISI 1018 Steel

This material was commercially available as hot rolled bars. The specimens were annealed at 700°C for 48 hours in vacuum after machining to obtain a spheroidized structure.

c) AISI 1020 Steel

Two types of AISI 1020 steel were used; commercially available hot rolled bars and specially doped steel to control the grain growth during annealing. The specimen which was made from the commercial AISI 1020 steel (Test No. 43) was not annealed before testing and it had a pearlitic structure.

The doped steel had the same carbon concentration as the AISI 1020 steel. The additional alloying elements were 5.0% W and 0.25% Zr to inhibit grain growth and raise the recrystallization temperature of the iron.

The doped steel was vacuum melted and cast as a 100 lb ingot. The ingot was trisected and the pieces were forged at 1375°F to flat bars of 1" x 1" cross section and 3/4" rods. The bars were then cold rolled to 3/16" thickness, and the rods were swaged to 3/8". A final vacuum anneal was given after machining at 658°C - 22 hours for Test Nos. 31-35, at 680°C - 17 hours for Test Nos. 36-38, at 625°C - 20 hours for Test Nos. 39 and 40 and at 690°C - 1 hour for Test Nos. 41 and 42.

d) AISI 1095 Steel

The specimens from this material were prepared from 1" diameter AISI 1095 steel and were fully heat treated to result in a pearlitic structure.

e) AISI 4340 Steel

The commercially available AISI 4340 steel bars were used to prepare

3/8" in diameter specimens for cylinder-on-cylinder wear tests. The specimens were then heat treated at 810°C for 1 hour, followed by water quenching. They were then tempered at 200°C for 1 hour. Some specimens were also made from an ESR (electroslag remelted) AISI 4340 steel with a low inclusion density. These specimens were given the same heat treatment as the regular AISI 4340 steel.

6) Copper

High purity, oxygen free, high conductivity copper (99.96% pure) was used for the copper specimens. The specimen which was prepared for the reciprocating Test No. 52, was cold rolled by 90% reduction before machining and it was annealed at 235°C for 4 hours after machining. The specimen for Test No 51 was swaged by 66% RA and was annealed at 315°C for 4 hours after machining.

B) Specimen Preparation for Wear Tests

The specimens were prepared for the sliding wear tests by the following procedure:

1) Specimens for Reciprocating Tests

The specimens which were tested by a reciprocating friction and wear machine had dimensions of 2 3/8" x 1 1/8" x 1/8". The surface on each face was ground to assure flatness and to remove hot or cold working marks. The samples were polished on grade 1 emery paper to remove the grinding marks. A final polish was then performed perpendicular to the sliding direction of the wear machine. These specimens were washed with soap and water, rinsed with alcohol and dried by a jet of air.

The clean specimens were annealed in a high vacuum furnace (2×10^{-5} -

2×10^{-6} mm Hg) to minimize oxidation and decarburization. Annealing times and temperatures were given in the last section. After this annealing treatment, the specimens were stored in a dessicator. Before the wear tests, the specimens were immersed in trichloroethylene for at least 10 minutes, dried and weighed to an accuracy of 0.1 mg. It should be emphasized that no mechanical work was done on the sliding surface after annealing and prior to wear tests.

2) Specimens for Cylinder-on-Cylinder Tests

These specimens were machined to 1/4" diameter, ground and then polished by silicon carbide paper grit size 120 and 600, respectively. The Fe-W specimens were received as polished had a surface finish of 2 RMS. Fe-Mo specimens were not polished after grinding and they had a surface finish of 16 RMS. The specimens were then cleaned, annealed and stored by a procedure similar to the one used for reciprocating specimens.

3) Specimens for Annular Tests

The annular specimens were 1" in outside diameter and 0.8 $in.^2$ in contact area. The wear surface of these specimens were ground to 16 RMS surface finish before annealing.

4) Preparation of the Sliders

The sliders used in most of the wear tests were AISI 52100 (560 Kg/mm^2 Brinell hardness). Pins of 1/4" diameter and 2 1/2" length were selected which had a 1/4" radius of curvature at both ends. The curved ends were used as the sliding surfaces for reciprocating tests, while the cylindrical surfaces were used for unidirectional sliding tests. Before testing, the sliders were

degreased by immersion in trichloroethylene. After the reciprocating wear testing, the curvature at the sliding end was polished on grade 1 and 4/0 emery papers respectively, and the pin was reused. However, for the unidirectional tests, the used pin was simply rotated to expose a new surface for sliding.

Appendix D

WEAR TESTING INSTRUMENTS AND PREPARATION OF THE SPECIMENS FOR SEM OBSERVATION

A) Wear Testing Equipments

Wear tests were performed on three different machines with different sliding geometries to show that the experimental results did not depend on sliding geometry and the type of equipment used.

1) Reciprocating Wear Testing

The basic sliding geometry of this equipment was that of a pin-on-flat reciprocating motion (Fig. D-1 a). The specimen was stationary and the slider was moved by a variable speed motor and a cam. Normal load was applied to the specimen from below by a lever and a dead weight. The friction force was measured by recording the bending stresses set up on the shaft connected to the specimen holder. A Sanborn 150 Recorder was used to record the data. Argon gas was flushed over the specimen and the slider at a flow rate of 4 liters per minute, with the exception of the reciprocating tests on copper Test No. 52.

2) Unidirectional Wear Testing

A cylinder-on-cylinder sliding geometry (Fig. D-1b) was used on a lathe. The specimen was rotated by the spindle and the slider was stationary. The pin was placed in a special holder and was connected to a lathe tool dynamometer. The dynamometer was attached to the carriage of the lathe. The normal force was applied to the pin by transverse motion of the carriage and was monitored on a Sanborn 321 Recorder through the dynamometer. The friction force was measured by the bending stress in the pin-holder bar and was recorded

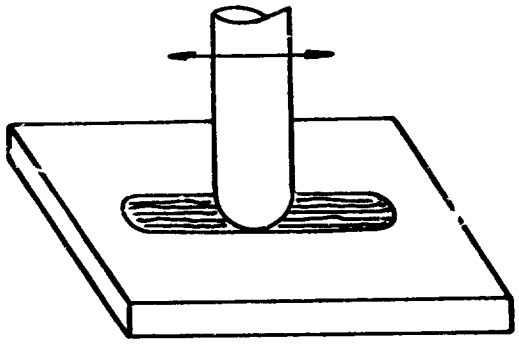

(a)

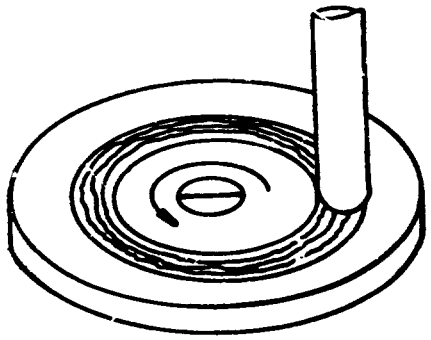

(c)

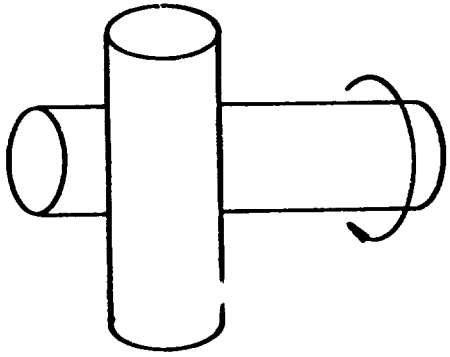

(b)

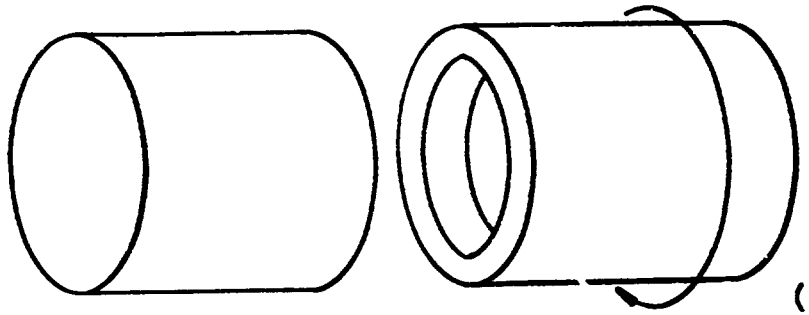

(d)

Figure D-1 Wear testing geometries.
a) Reciprocating
b) Cylinder-on-cylinder
c) Pin-on-disk
d) Annular

on the Sanborn.

The sliding interface was flooded with argon gas at a flow rate of 10 liters perminute during wear testing with the exception of Test Nos. 45-47 and 52. For these tests a plexiglas chamber was built around the contacting surfaces and argon entered at a rate of 5 lit/min.

3) Pin-on-Disk Wear Testing

A Cd bi-crystal was tested by a pin-on-disk geometry of Fig. D-1 c. The specimen was rotated by a variable speed motor and the slider pin was stationary. The normal load was applied to the pin by a dead weight. The tests were performed in air.

4) Annular Wear Testing

This type of geometry which is shown in Fig. D-1 d was used for one set of tests on the Cd plated steel (Chapter 7). One of the samples was rotated by a lathe and the stationary annulous was pushed against it. The normal contact load and the friction torque were measured by a dynamometer built in the tail-stock of the lather. A plexiglass chamber was constructed around the samples and was filled with argon gas at a steady flow of 5 lit/min.

B) Specimen Preparation After Wear Tests

After the wear tests, the specimens were gently brushed to remove the loose wear debris. Then, they were degreased in trichloroethylene, dried and weighed to an accuracy of 0.1 mg.

1) Wear Track Observations

The specimens were placed in a scanning electron microscope to examine the wear tracks. The flat specimens were located so that the flat surface

containing the wear tracks were perpendicular to the electron beam. However, the cylindrical specimens were positioned so that the cylindrical axis was parallel with the electron beam. Then by tilting the specimen, the wear track on the cylindrical surface was observed. Tilting was very important to discern the shape and dimension of the wear sheets.

2) Sectioning and Observations

After observing the wear track, the specimen was cut by a hack saw approximately 1/8" away from the wear track, parallel to the sliding direction and perpendicular to the worn surface. Then it was placed in a special holder and abraded on grade 2 and 1 emery papers. The specimen holder was used to protect the edges during polishing. When a desired location in the wear track was reached, the section was metallographically polished.

After polishing, the specimens were etched to reveal the microstructure. A 2% Nital solution was used to etch the steel, Fe-Mo and Fe-W samples, while a 10% ammonium persulfate etch was used on copper specimens. The Fe-Mo specimens were etched by a solution prepared by mixing of 30 cc - 4% Nital, 30 cc 4% Picral, 10 cc - Zephrin and 180 cc ethyl alcohol.

The effectiveness of the etching procedure was checked by an optical microscope. The scanning electron microscope was then used to observe the microstructure and the subsurface damage due to wear.

3) Wear Particle Collection

The wear particles were collected in the plexiglass chamber which enclosed the specimens. After the wear tests, the chamber was flushed with alcohol

and the particles were precipitated on a polished aluminum flat. They were then observed by SEM.

Appendix E

PUBLISHED PAPERS ON DELAMINATION THEORY OF WEAR

1) N. P. Suh, "The Delamination Theory of Wear", Wear, 25 (1973) 11-124.

2) N. P. Suh, S. Jahanmir, E. P. Abrahamson, II and A. P. L. Turner, "Further Investigation of the Delamination Theory of Wear", J. Lub. Tech., Trans. ASME, (1974).

3) S. Jahanmir, N. P. Suh and E. P. Abrahamson, II, "Microscopic Observations of the Wear Sheet Formation by Delamination", Wear, 28 (1974) 235-249.

4) E. P. Abrahamson, II, S. Jahanmir, D. A. Colling and N. P. Suh, "Failure by Delamination During Wear", Proc. Scanning Electron Microscopy Conf., (1974) part IV, 889-894.

5) N. P. Suh, S. Jahanmir, D. A. Colling and E. P. Abrahamson, II, "The Delamination Theory for Wear of Metals Sliding at Low Speeds", Proc. 2nd North American Metalworking Research Conf., (1974) 117-127.

6) E. P. Abrahamson, II, S. Jahanmir, N. P. Suh and D. A. Colling, "Application of the Delamination Theory of Wear to a Composite Metal Surface", Proc. Int. Conf. on Production, (1974)

7) S. Jahanmir, N. P. Suh and E. P. Abrahamson, II, "The Delamination Theory of Wear and the Wear of a Composite Metal Surface", Wear, (1975), submitted for publication.

8)* R. B. Waterhouse and D. E. Taylor, "Fretting Debris and the Delamination Theory of Wear", Wear, 29 (1974) 337-344.

*At University of Nottingham (Gt. Britain)